Analysis of a Supercritical Hydrogen Liquefaction Cycle

by

Wayne Lawrence Staats, Jr.

B.S., Mechanical Engineering

University of Wisconsin-Madison, 2006

Submitted to the Department of Mechanical Engineering in partial fulfillment of the

requirements for the degree of Master of Science in Mechanical Engineering

at the

Massachusetts Institute of Technology

June, 2008

Signature of Author: _____

<div align="right">
Department of Mechanical Engineering

May 27, 2008
</div>

Certified by: _____

<div align="right">
John G. Brisson

Professor of Mechanical Engineering

Thesis Supervisor
</div>

Accepted by: _____

<div align="right">
Lallit Anand

Chairman, Department Committee on Graduate Students
</div>

Analysis of a Supercritical Hydrogen Liquefaction Cycle

by

Wayne Lawrence Staats, Jr.

Submitted to the Department of Mechanical Engineering on May 27, 2008 in partial fulfillment of the requirements for the degree of Master of Science in Mechanical Engineering

ABSTRACT

In this work, a supercritical hydrogen liquefaction cycle is proposed and analyzed numerically. If hydrogen is to be used as an energy carrier, the efficiency of liquefaction will become increasingly important. By examining some difficulties of commonly used industrial liquefaction cycles, several changes were suggested and a readily scalable, supercritical, helium-cooled hydrogen liquefaction cycle was proposed. A novel overlap in flow paths of the two coldest stages allowed the heat exchanger losses to be minimized and the use of a single-phase liquid expander eliminated the pressure reduction losses associated with a Joule-Thomson valve. A simulation program was written in MATLAB to investigate the effects of altering component efficiencies and various system parameters on the cycle efficiency.

In addition to performing the overall cycle simulations, several of the system components were studied in greater detail. First, the required volume of the ortho-para catalyst beds was estimated based on published experimental data. Next, the improvement in cycle efficiency due to the use of a single-phase liquid expander to reduce the pressure of the hydrogen stream was estimated. Finally, a heat exchanger simulation program was developed to verify the feasibility and to estimate the approximate size of the heat exchangers in the cycle simulation.

For a large, 50-ton-per-day plant with reasonable estimates of achievable component efficiencies, the proposed cycle offered a modest improvement in efficiency over the current state of the art. In comparison to the 30-40% Second Law efficiencies of today's most advanced industrial plants, efficiencies of 39-44% were predicted for the proposed cycle, depending on the heat exchange area employed.

Thesis Supervisor: John G. Brisson
Title: Professor of Mechanical Engineering

Acknowledgements

First, I thank Professor Brisson for his guidance and advice. I have learned a great deal working with him and he has always been available and helpful. Second, I am very appreciative of Professor Smith's assistance in this project. My discussions with Professor Brisson and Professor Smith have been educational, thought-provoking and memorable.

I thank Gas Equipment Engineering Corporation (GEECO) for providing funding for this research. I have enjoyed working with Martin Shimko of GEECO.

My fellow Cryogenic Engineering Laboratory graduate students (Gunaranjan Chaudhry, Rory Monaghan, Teresa Baker, Fritz Pierre, Malima Wolf, David Lopez, Barbara Botros, and Martin Segado) have provided valuable conversation, advice and camaraderie. I have appreciated Doris Elsemiller's astute administrative advice.

I am grateful to my parents and sisters for their continuing love, encouragement and friendship. Above all, my sincere thanks are due to my fiancée Brooke, who has been my greatest source of support and strength throughout this research.

Table of Contents

List of Figures

List of Symbols

Symbol	Meaning	Unit
A	Area	m^2
c_p	Isobaric specific heat	kJ/kg·K
D	Diameter	m
f	Frequency	1/s
g	Mass transfer conductance	kg/m^2·s
h	Specific enthalpy	kJ/kg
k	Reaction rate constant	1/h
L	Length	m
m	Mass	kg
$\dot{m}$	Mass flow rate	kg/s
P	Perimeter	m
p	Pressure	bar
Q	Heat	kJ
R	Gas constant	kJ/kg·K
Re	Reynolds number	-
S	Entropy	kJ/K
s	Specific entropy	kJ/kg·K
T	Temperature	K
t	Time	s, h
U	Heat transfer coefficient	W/m^2·K
v	Velocity	m/s
V	Volume	m^3
W	Work	kJ
x	Mass fraction	-
X	Heat exchanger hydrogen UA fraction	-
ΔT	Change in temperature	K
ε_v	Void fraction	-
η	Efficiency	-
μ	Dynamic viscosity	kg/m·s
ρ	Density	kg/m^3

Subscript	Meaning
amb	Ambient
c	Cross section
char	Characteristic
f	Final
H	High temperature
HP	High pressure
i	Initial
o	Orthohydrogen
L	Low temperature
LP	Low pressure
mix	Mixture
n	Normal hydrogen
p	Parahydrogen
P	Particle

CHAPTER 1. INTRODUCTION

Given the scale of current hydrogen liquefaction and likely future expansion, improvements in efficiency have the potential to effect large energy and economic savings. Clearly, current liquefaction cycles can be improved by developing more efficient components; however, it is not obvious that these cycles take full advantage of available technology. The objectives of this work are to examine currently available liquefaction cycle technology, to explore the potential energy savings of new and more efficient cycle configurations, and finally to propose a new liquefaction cycle that offers increased efficiency without the need for extensive component development.

This introduction will begin with a discussion of the societal importance, both present and future, of efficient hydrogen liquefaction. Next, a liquefaction issue unique to hydrogen – the ortho-para conversion – will be introduced. The ortho-para conversion's effect on hydrogen's thermodynamic properties, potential to be expedited with catalysis, and importance in liquefaction efficiency will be examined. Finally, current hydrogen liquefaction technologies will be briefly introduced.

1.1. Motivation

The notion of a "hydrogen economy" has been discussed widely since the oil crisis of the early 1970s and hydrogen is being examined as a potential alternative to petroleum-based fuels. In marked contrast to petroleum, hydrogen cannot be harvested from the earth – rather, energy must be supplied to liberate hydrogen atoms from a molecule. Thus, hydrogen is often referred to as an *energy carrier*.

Using hydrogen as an energy carrier has some advantages:

- Combustion of hydrogen in air can be designed to result only in water and nitrogen, eliminating the release of greenhouse gases at the point of use. Additionally, hydrogen has some desirable combustion properties including a high autoignition temperature and flame speed [1].

- Proton exchange membrane (PEM) fuel cells use hydrogen and have shown promise in achieving efficiencies of 50% or more [2], which is significantly higher than the efficiencies of modern internal combustion engines. Other desirable characteristics include low-temperature operation, compactness, and lightness [3].

- Hydrogen can be used to store energy derived from domestic sources and can be obtained from methane or water, both of which are abundant.

- Liquid hydrogen is a safe fuel that vaporizes and burns rapidly, minimizing heat exposure time [4]. In contrast to gasoline vapor, hydrogen gas is much lighter than air, eliminating its tendency to linger near a vehicle.

Governmental and commercial interest in hydrogen has been strong, potentially due to steadily rising fuel costs and political issues with oil-producing countries. In 2003, President Bush announced a Hydrogen Fuel Initiative that included the appropriation of $1.2 billion for its first five years [5]. The state of California has built over 20 hydrogen filling stations [6]. British Columbia is organizing a demonstration of various aspects of hydrogen technology including hydrogen production from solar electrolysis of water, hydrogen internal combustion engine (ICE) powered buses, and a fuel cell powered car wash [7]. Although not universally embraced, commercial demand for hydrogen as an energy carrier is growing. BMW has been researching ICE powered cars since the early 1980s [8] and is currently developing the Hydrogen 7, which can run on either hydrogen or gasoline [9]. Additionally, Ford developed the Model U hybrid electric vehicle, which is powered by a supercharged hydrogen ICE [10]. Toyota is also developing a fuel cell hybrid vehicle [11].

Although hydrogen has the highest amount of energy per unit mass of any fuel [12], it has a very low density. Consequently, a given volume of hydrogen contains very little energy in comparison to other fuels. The volumetric energy density can be improved by compression, but high-pressure storage containers cause concern about crashworthiness in automotive applications. Additionally, high-pressure

storage vessels add a substantial amount of weight to a vehicle's storage system. By liquefying hydrogen, these high-pressure storage conditions can be avoided while increasing the energy density. Furthermore, liquid hydrogen at ambient pressure has a higher energy density than compressed hydrogen at ambient temperature and 800 bar pressure (a practical limit imposed by current pressure vessel technology) [12]. A comparison of hydrogen's energy densities as a compressed gas and as a liquid is shown in Figure 1. Hydrogen's low normal boiling point requires a cryogenically-insulated container, and the inevitable boiloff rate associated with ambient pressure, passive liquid storage may be unacceptable in some applications. Still, several automakers are pursuing liquid hydrogen storage for consumer applications, including BMW and Renault [13]. Other storage methods include chemical hydrides and metal hydrides; however, these methods are not yet competitive in cost or in system weight.

Except for extremely large amounts of hydrogen, where pipelines sometimes become cost competitive, the most economical transportation method for hydrogen is via liquid hydrogen tanker trucks [14]. Additionally, economies of scale result in centralized hydrogen production being more cost and
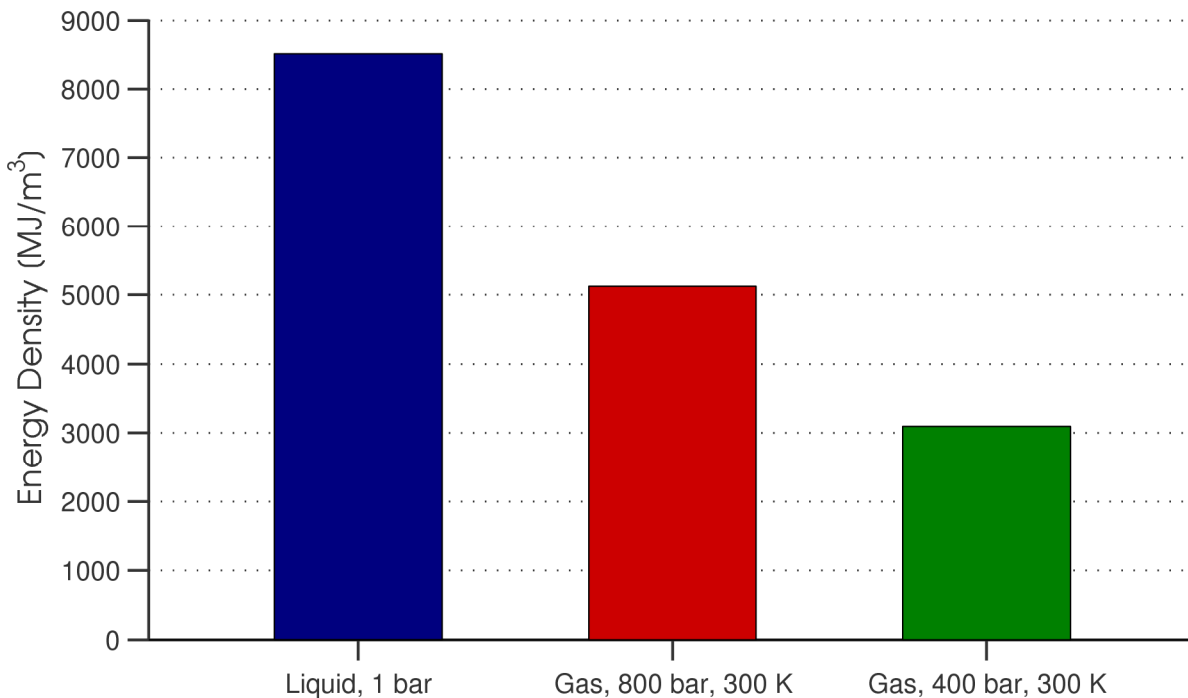
Figure 1: Energy density of hydrogen as liquid and as compressed gas.

energy efficient than distributed production. Gas liquefaction plants also tend to be more efficient as their size increases [15], and the lifetime cost of a large hydrogen liquefaction plant will be dominated by the cost of the input power [16]. Thus, improvement in the efficiency of these plants has potential to save significant amounts of energy and money.

As an example, consider replacing 1% of the 2006 US motor gasoline energy consumption with hydrogen. Assuming that all of the hydrogen required to meet this energy need is liquefied and that industrial electricity costs $0.06 per kilowatt-hour [17], an improvement from 35% to 40% in average hydrogen liquefaction plant efficiency would result in a savings of $125 million per year. As the fraction of hydrogen-powered transportation and the cost of electricity increase, the economic consequences of liquefaction efficiency grow. The details of this hypothetical scenario are summarized in Table 1.

Using hydrogen as an energy carrier implies that its production must experience as little loss as is

Table 1: Economic Savings Due to Improved Hydrogen Liquefaction Efficiency

Lower Heating Value of Hydrogen	120	[MJ/kg]
Ideal Work of Liquefaction	14.01	[MJ/kg]
Average Electricity Cost	0.06	[$/kW·h]
Liquefaction Plant Efficiency, base	0.35	[-]
Liquefaction Plant Efficiency, improved	0.40	[-]
2006 Motor Gasoline Use [18]	1.81E+13	[MJ]
1% of 2006 Motor Gasoline Use	1.81E+11	[MJ]
H_2 Required	1,508,554	[t/year][a]
H_2 Required	4,133	[t/day]
H_2 Required	47.84	[kg/s]
Ideal Liquefaction Power Input	670	[MW]
Actual Liquefaction Power Input, 35% Efficiency	1,915	[MW]
Actual Liquefaction Power Input, 40% Efficiency	1,675	[MW]
Liquefaction Power Cost, 35% Efficiency	$1,006,323,923	[$/year]
Liquefaction Power Cost, 40% Efficiency	$880,533,432	[$/year]
Savings Effected by Liquefaction Plant Improvement	$125,790,490	[$/year]

[a] 1 t = 1,000 kg

possible. Liquefaction of hydrogen constitutes a loss: the work of the liquefaction process adds to the total energy invested in each delivered unit of hydrogen. Often the liquefaction work cannot be recovered, but sometimes a portion of the liquefaction energy can be recouped by taking advantage of the properties of the liquid in a subsequent process. Parrish discussed several liquefaction work recovery techniques, including (1) pumping the liquid to high pressure, heating it in a heat exchanger, and extracting work via an expander; (2) using the refrigeration capacity of the liquid in another process, such as an air separation unit; and (3) separating rare gases from the atmosphere by using the low-temperature liquid [19]. These techniques may increase the appeal of storing hydrogen as a liquid in certain applications; however, the energy recovery is limited to 20-60% of the ideal work of liquefaction, which amounts to about 7-20% of the total work in a modern liquefaction plant with 35% Second Law efficiency. Losses in excess of the theoretical minimum work of liquefaction cannot be recovered by any technique. It becomes apparent that the efficiency of the liquefaction cycle directly translates into energy savings in the overall process. The lost liquefaction work detracts from the utility of hydrogen as an energy carrier. Clearly, liquefaction loss must be minimized if hydrogen is to play a meaningful role as an energy storage medium.

1.2. Hydrogen

To improve upon conventional liquefaction systems, an understanding of hydrogen's unique properties is essential. The differences between hydrogen's two forms, orthohydrogen and parahydrogen, will be evaluated, as will the transition from ortho to para and the need for effective catalysis of this transition. The effect of parahydrogen concentration on the properties of hydrogen will be discussed, and the significance of the transition with respect to the overall work of liquefaction will be shown.

1.2.1. Orthohydrogen and parahydrogen

Hydrogen is composed of a mixture of orthohydrogen and parahydrogen whose equilibrium composition is a function of temperature. The difference between orthohydrogen and parahydrogen

molecules is the relative orientation of the nuclear spins of the atoms that comprise the hydrogen molecule. The nuclear spins of an orthohydrogen molecule are parallel, while those of a parahydrogen molecule are antiparallel. Ortho and parahydrogen have important property differences.

The equilibrium ortho-para composition of hydrogen is a function of temperature only and can be seen in Figure 2 [20]. The orthohydrogen molecule has three possible quantum substates, while the parahydrogen molecule has only one substate. At high temperatures, all substates become equally populated and the ratio of orthohydrogen to parahydrogen becomes three to one. At room temperature (300 K) the mixture's equilibrium composition of 75% orthohydrogen and 25% parahydrogen reflects this three to one ratio. Hydrogen with this ortho-para ratio is referred to as *normal hydrogen*. Conversely, at 20 K the equilibrium mixture is nearly 100% parahydrogen. At an arbitrary temperature the equilibrium mixture is termed *equilibrium hydrogen*.
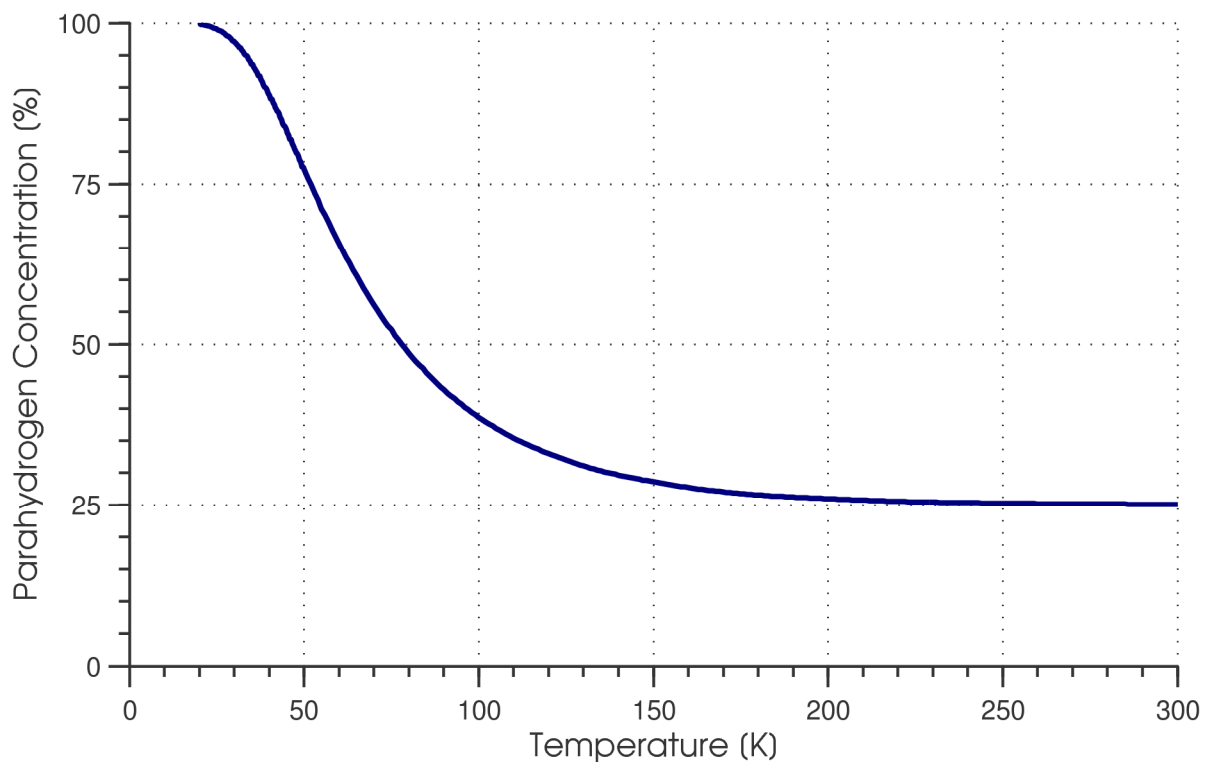
Figure 2: Equilibrium parahydrogen concentration vs. temperature [20].

Nonequilibrium hydrogen undergoes a slow conversion process in the absence of catalyst [21]. Natural ortho-para conversion occurs when the magnetic dipoles of orthohydrogen molecules in the fluid become close enough to interact [22]. For liquid hydrogen, the rate of orthohydrogen concentration decrease is proportional to the square of the concentration [21]:

$$\frac{dx_o}{dt} = -kx_o^2 \tag{1}$$

where x_o is the mass fraction of orthohydrogen at time t and k is the rate constant for the reaction. The value of the rate constant for saturated liquid hydrogen, as measured by Scott et al. [21], is 0.0114 h^{-1}. Additionally, this rate changes with density and temperature [22].

In a very slow liquefaction process, hydrogen would be expected to remain at the equilibrium parahydrogen concentration as its temperature is reduced. However, in practice, the characteristic time of the ortho-para conversion is very long compared to the residence time in a liquefaction cycle. If left unaltered, a hydrogen liquefaction system produces liquid hydrogen before the ortho-para conversion has time to occur. The resulting liquid product has a lower-than-equilibrium parahydrogen content.

Since parahydrogen is a lower energy state than orthohydrogen, the conversion from ortho to para releases thermal energy. In the previously discussed case where hydrogen is liquefied without any regard to the ortho-para conversion, the liquid product has a para concentration that is below the equilibrium concentration. As time passes, the orthohydrogen in the liquid converts to parahydrogen. Since the conversion is exothermic, some of the liquid product must evaporate to accommodate this heat release. If left unchecked in a completely adiabatic, vented, constant pressure container, the complete self-induced conversion from liquid normal hydrogen to liquid parahydrogen results in evaporation of about 50% of the mixture after 100 hours and 65% after 1000 hours. Integration of equation 1 with a starting orthohydrogen mass fraction of 75% corresponding to normal hydrogen reveals the nature of this boiloff. The liquid mass fraction remaining, which is the liquid mass at time t m(t) divided by the initial mass m_i, and the parahydrogen mass fraction of the remaining liquid x_p are plotted versus time in Figure 3. This

behavior presents a problem in a commercial system, where the evaporation of the liquid product is a loss mechanism. Additional refrigeration at the liquid temperature must be supplied to avoid loss of the liquid product; no amount of vessel insulation can prevent this evaporative loss.

Fortunately, the ortho-para conversion can be catalyzed, so that liquefaction plants can remove the conversion energy at higher temperatures. Boiloff and the need for auxiliary refrigeration at liquid temperature are reduced by using catalysts on hydrogen vapor as it cools, thereby producing liquid with high parahydrogen content.
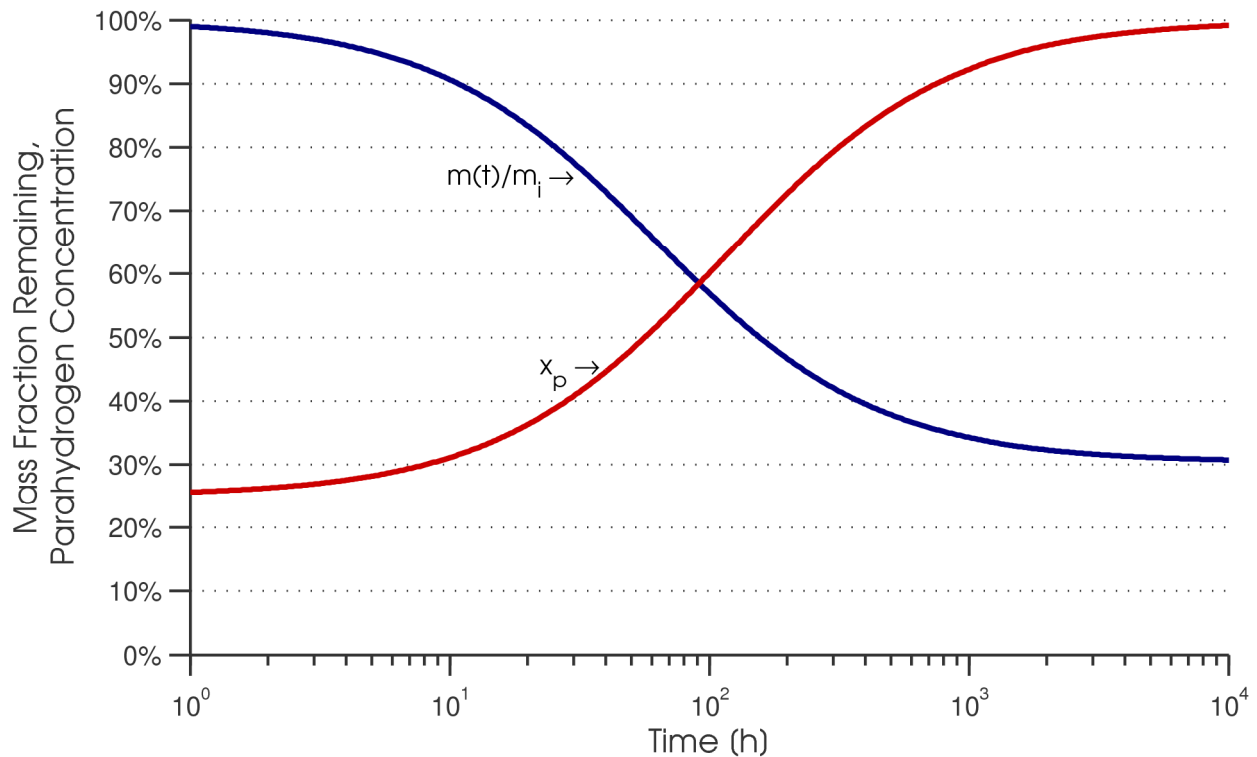
Figure 3: Mass fraction remaining and parahydrogen content for a completely adiabatic, vented, constant pressure container of liquid hydrogen, as a function of time.

1.2.2. Ortho-para catalysts

Indeed, liquefying normal hydrogen and removing all of the conversion heat at the lowest temperature in the cycle is detrimental to a system's efficiency. In general, the heat of conversion should be removed the highest-possible temperature in the system. This is done by using catalysts that speed up the ortho-para conversion process. Ideally, hydrogen should be kept at equilibrium concentration throughout the cooling process, so that ortho-para conversion is always done at the highest-possible temperature. However, the difficulty of incorporating catalysts into the hydrogen-cooling heat exchangers has led most liquefaction plants to approximate the continuous limit with staged catalyst beds. Four-stage ortho-para conversion is common in industrial-scale plants [23] [24], while other plants have overcome the difficulties associated with continuous ortho-para conversion. Lipman et al. designed and tested a heat exchanger with integrated catalyst material that successfully approached the continuous conversion limit, and alluded to the use of a similar setup in a 26 ton/day Linde hydrogen liquefaction plant in Ontario, California [25]. Sullivan and Zhou also experimented with incorporating a catalyst material into a heat exchanger [26].

A substantial amount of research has been done on ortho-para catalyst materials. The ortho-para transition can be caused by two methods: dissociation and recombination of a hydrogen molecule, and interaction between the magnetic fields of hydrogen nuclei and an external magnetic field [27]. Since dissociative methods lose effectiveness or require energy input at cryogenic temperatures, the magnetic mechanism must be used to catalyze the ortho-para transition in a hydrogen liquefier. Schmauch and Singleton determined that an effective catalyst material "must have a high physical absorptive capacity for hydrogen, a high concentration of 'active' or magnetic specie, and a high paramagnetic susceptibility" [27].

Some ortho-para catalyst materials include chromium oxide on alumina [28], hydrous ferric oxide [29][30][31][32][33], Apachi nickel silica gel [27][34], and chromium oxide supported by silica gel [35].

Much research was focused on hydrous ferric oxide, a porous, granular material that is commercially available [36] and for which there is a wealth of experimental data. In particular, Hutchinson [33] studied the kinetics of the catalyzed ortho-para conversion with hydrous ferric oxide and tabulated data detailing the conversion process. This data can be used to estimate the required size of a catalyst bed in a hypothetical liquefaction plant of known capacity.

1.2.3. Property differences between ortho and para

Orthohydrogen and parahydrogen have important and significant property differences. Hust and Stewart summarized the property differences below 300 K [37]. Specific heat and related properties such as enthalpy, entropy and thermal conductivity exhibit the largest differences with changes in the ortho-para composition, while P-v-T data and viscosity are nearly independent of composition. Due to the molecular differences in orthohydrogen and parahydrogen, their rotational modes are excited differently and can be observed in their markedly different specific heats between 70 K and 300 K. The differences in the ideal gas specific heat between orthohydrogen and parahydrogen can be seen in Figure 4.

Haar et al. [38] and Woolley et al. [20] calculated the ideal gas enthalpy, entropy and specific heat of normal, ortho and parahydrogen. For ideal gas mixtures of orthohydrogen and parahydrogen, the properties of the mixture can be determined using mixing equations [37]:

$$h_{mix} = x_p h_p + x_o h_o \tag{2}$$

$$s_{mix} = x_p s_p + x_o s_o - R(x_p \, ln \, x_p + x_o \, ln \, x_o) \tag{3}$$

where h is specific enthalpy, s is specific entropy, x is the mass fraction of ortho (o) or para (p), and R is the gas constant for hydrogen. The heat of mixing is assumed to be negligible. The third term on the right hand side of equation 3 represents the entropy of mixing. Since properties of orthohydrogen are very rarely reported, it is more convenient to express these equations so that the mixture properties can be calculated from normal and parahydrogen properties. Using equations 2 and 3, the specific enthalpy
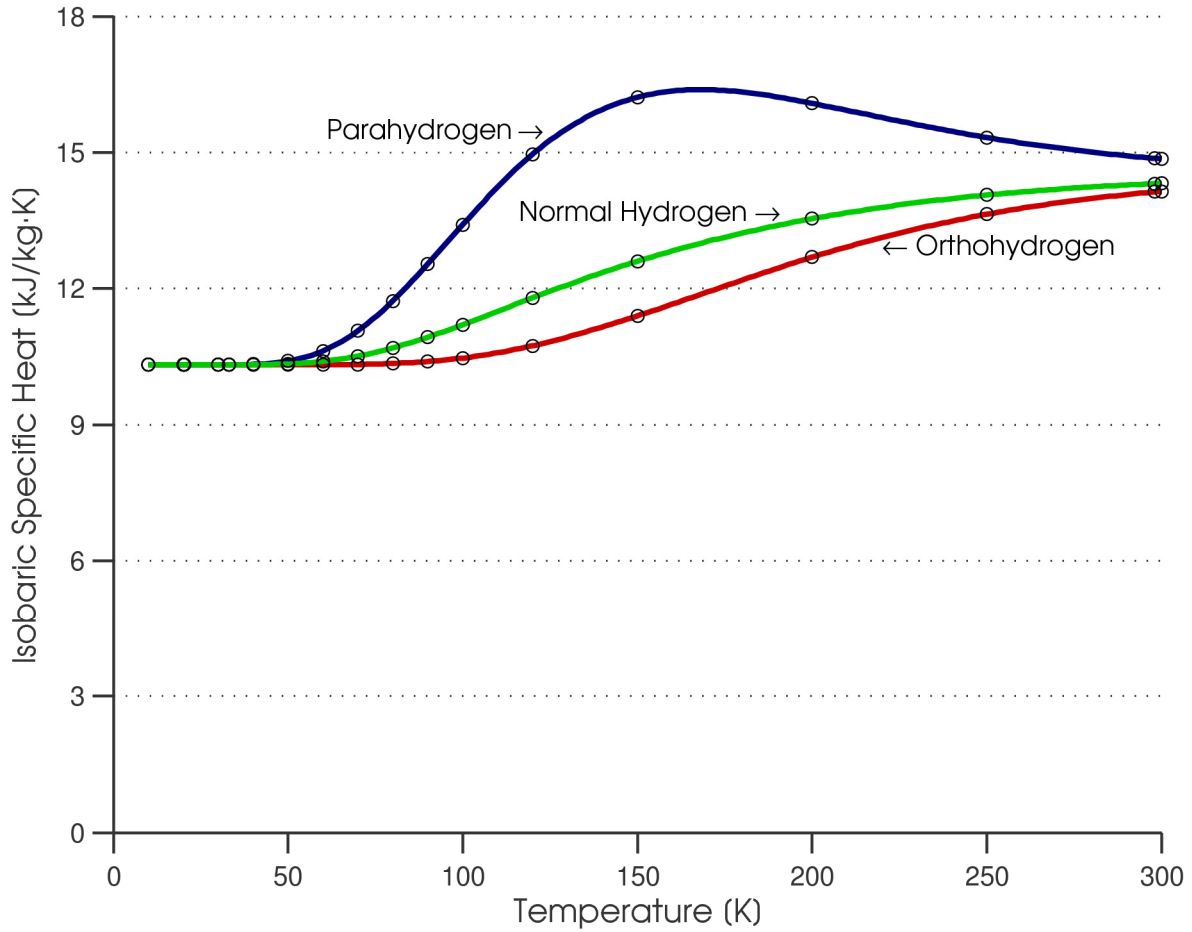
Figure 4: Ideal gas isobaric specific heat for parahydrogen, normal hydrogen and orthohydrogen. The circles indicate the original, tabulated data from [20].

and entropy of normal hydrogen (h_n and s_n) can be written as

$$h_n = \frac{1}{4}h_p + \frac{3}{4}h_o \quad \text{and} \tag{4}$$

$$s_n = \frac{1}{4}s_p + \frac{3}{4}s_o - R\left(\frac{1}{4}ln\frac{1}{4} + \frac{3}{4}ln\frac{3}{4}\right). \tag{5}$$

Solving equations 4 and 5 for the orthohydrogen enthalpy and entropy and substituting into equations 2 and 3 yields

$$h_{mix} = \left(x_p - \frac{1}{3}x_o\right)h_p + \frac{4}{3}x_o h_n \quad \text{and} \tag{6}$$

$$s_{mix} = \left(x_p - \frac{1}{3}x_o\right)s_p + \frac{4}{3}x_o\left[s_n + R\left(\frac{1}{4}\,ln\frac{1}{4} + \frac{3}{4}\,ln\frac{3}{4}\right)\right] - R\left(x_p\,ln\,x_p + x_o\,ln\,x_o\right). \tag{7}$$

Equation 7 simplifies to

$$s_{mix} = \left(x_p - \frac{1}{3}x_o\right)s_p + \frac{4}{3}x_o\left[s_n - 0.562335\cdot R\right] - R\left(x_p\,ln\,x_p + x_o\,ln\,x_o\right), \tag{8}$$

which is consistent with the equation reported by Hust and Stewart [37]. Equations 6 and 8 can be used to determine the enthalpy and entropy of a hydrogen mixture of arbitrary parahydrogen concentration from known normal hydrogen and parahydrogen properties. However, care must be taken to ensure that the normal hydrogen and parahydrogen properties have a consistent reference state, because the mixing equations contain absolute values of enthalpy and entropy that originate from, presumably, different equations of state.

Since the P-v-T properties of normal hydrogen and parahydrogen are virtually identical, the equations above are also useful for higher pressures. Hust and Stewart pointed out that "experimental specific heats confirm the postulate that the specific heat differences due to ortho-para concentration are essentially independent of pressure" [37].

Various equations of state exist for normal and parahydrogen. Leachman conducted a survey of the available experimental data on normal and parahydrogen and formulated "Helmholtz explicit" equations of state to represent the most accurate of these data [39]. These equations, which represent experimental results to within the uncertainty of the data, are currently the most comprehensive and accurate equations of state for hydrogen. Leachman directly compared his parahydrogen equation of state (EOS) to Younglove's parahydrogen EOS, which is commonly used in engineering. Leachman found that his EOS represented experimental data more accurately and also exhibited fundamentally correct thermodynamic behavior. For example, in Leachman's EOS the isochoric specific heat of the saturated liquid states increases with temperature, an indication (as Leachman asserts) of thermodynamically correct behavior. This is in direct contrast to the non-monotonic behavior of the corresponding quantities

in the Younglove EOS. The Leachman EOS for both normal and parahydrogen are used in NIST's thermodynamic property software REFPROP 8.0 [40], and were chosen for the required property lookups in this work.

In this work, to ensure a consistent reference state for the property values obtained from the two different equations of state (normal hydrogen and parahydrogen), the following procedure was used. First, properties were obtained from the EOS at a temperature of 300 K and a pressure of 0.01 bar for both normal hydrogen and parahydrogen. Next, values of enthalpy were obtained from the reduced ideal gas values at 300 K tabulated by Haar et al. [38]. The difference between these enthalpies was noted and compared to the difference in the EOS-calculated enthalpies at 300 K and 0.01 bar. The enthalpy difference between normal and parahydrogen obtained from the EOS was much different than the enthalpy difference calculated from tabulated data. This was because the reference state in the EOS software imposes an arbitrary offset on the absolute values of enthalpy. Most applications only require a difference, so the offset is transparent to the user; however, since enthalpies of two different substances are being compared directly in this work, the reference states must be consistent. Therefore, an offset was added to the normal hydrogen enthalpy that was output from the EOS. After application of the offset, the difference in enthalpy between normal and para was consistent with the expected ideal gas difference. A similar offset was applied to the values of normal hydrogen entropy called from the EOS. By applying these enthalpy and entropy offsets, the normal hydrogen properties called from the EOS become consistently referenced with respect to the parahydrogen properties, allowing proper use of equations 6 and 8 to model the properties of a hydrogen mixture with arbitrary parahydrogen concentration.

1.2.4. Ideal work of liquefaction

Transforming a quantity of hydrogen from a gas at ambient temperature and pressure to a saturated liquid requires work input. This work input is used to extract entropy from the low-temperature hydrogen and reject it at ambient temperature. The amount of work required by a reversible cycle to bring

hydrogen from the starting conditions – in this paper, 300 K, 1 bar and 25% parahydrogen – to the final, saturated liquid state at 1 bar and equilibrium parahydrogen concentration is referred to as the *ideal work of liquefaction*.

To calculate the ideal work of liquefaction, a stream of hydrogen cooled by a reversible cyclic device is considered, as shown in Figure 5. The quantity of heat removed Q_L per unit mass m can be determined by applying the First Law of Thermodynamics to the hydrogen stream:

$$-\frac{Q_L}{m} = h_f - h_i \tag{9}$$

Next, the heat rejected to the thermal reservoir representing the ambient conditions is determined. The reversible cyclic device has no entropy generation, so that the entropy S_L removed from the hydrogen stream must be equal to the entropy S_H rejected to the thermal reservoir. S_L is determined by applying the Second Law to the hydrogen stream. The isothermal heat rejection Q_H to the ambient temperature T_{amb} is determined from the entropy S_H.

$$-\frac{S_L}{m} = -\frac{S_H}{m} = \left(s_f - s_i\right) \tag{10}$$

$$\frac{Q_H}{m} = T_{amb}\frac{S_H}{m} = -T_{amb}\left(s_f - s_i\right) \tag{11}$$

The First Law applied to the cyclic device yields the ideal work per unit mass W_{ideal}/m.

$$\frac{W_{ideal}}{m} = \frac{Q_H - Q_L}{m} = \left(h_f - h_i\right) - T_{amb}\left(s_f - s_i\right) \tag{12}$$

The two scenarios shown in Table 2 demonstrate the difference in the ideal work due to ortho-para conversion. For the state of the hydrogen mixture at the initial and final point to be fully defined, three unique thermodynamic parameters must be specified. In addition to temperature and pressure, parahydrogen concentration was specified to accurately define the ideal work. The initial state was
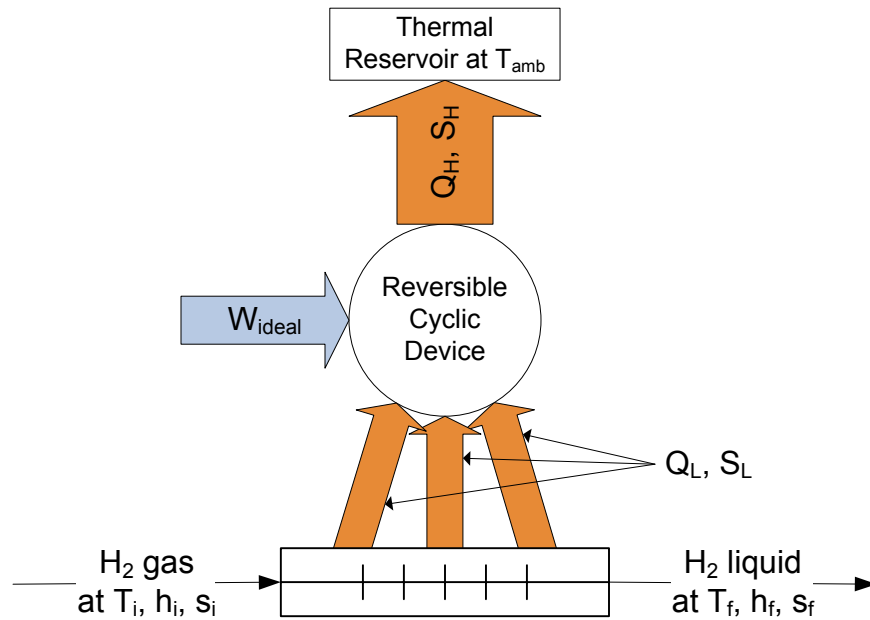
Figure 5: A stream of hydrogen cooled by a reversible cyclic device.

Table 2: Ideal Work of Liquefaction

	T [K]	P [bar]	x_p [-]	W_{ideal} [kJ/kg]
Initial state	300	1	0.251	-
Final state, saturated liquid, full ortho-para conversion	20	1	0.998	14,327
Final state, saturated liquid, no ortho-para conversion	20	1	0.251	12,147

assumed to have the equilibrium para concentration at 300 K. Two final saturated liquid states at 1 bar are

shown: no ortho-para conversion and full conversion to equilibrium.

In Table 2 it can be seen that more work is required when the final state consists of equilibrium

hydrogen. This result is not surprising given that the conversion from ortho to para is exothermic and

results in significant energy release from the product stream. The work associated with the removal of the

ortho-para heat of conversion represents a substantial portion of the work required to bring hydrogen to a

low temperature. Figure 6 shows the minimum work of cooling and conversion for a stream of gaseous

equilibrium hydrogen, and also separately shows only the work of ortho-para conversion. It can be seen
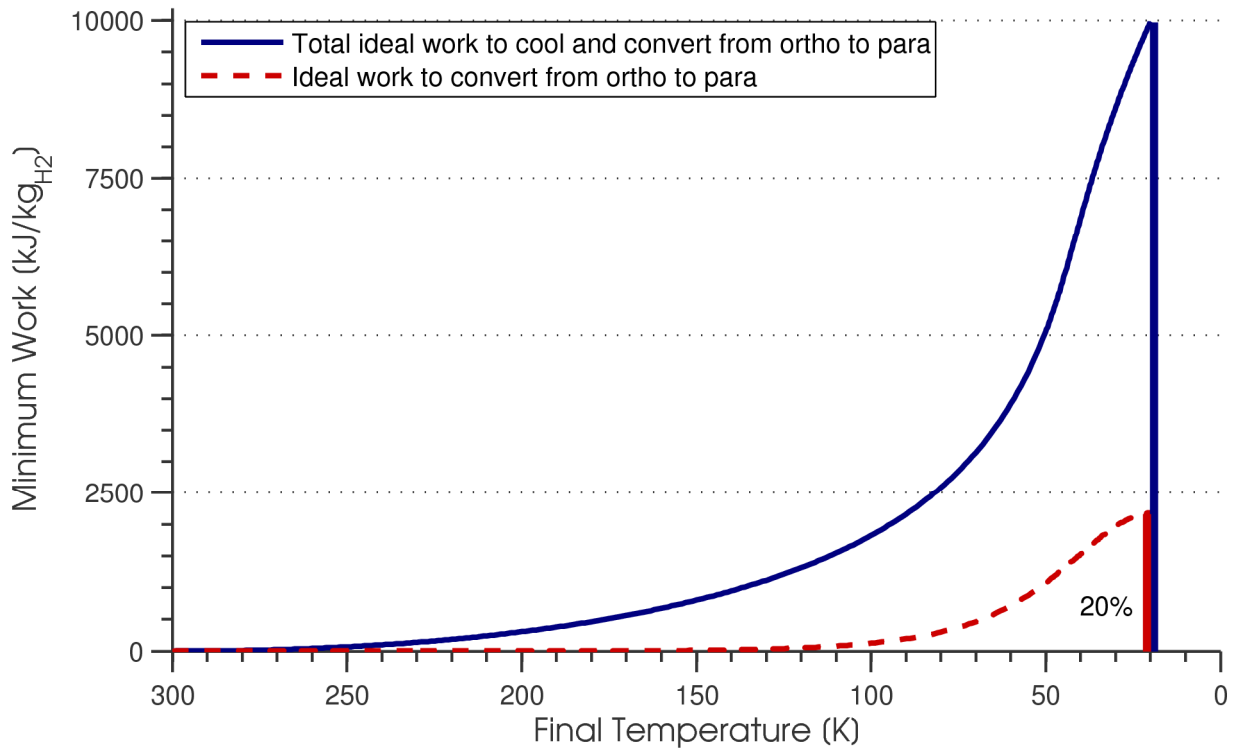
Figure 6: Ideal work vs. temperature for gaseous equilibrium hydrogen. Also shown is the ideal work of ortho-para conversion, which was determined by subtracting the ideal work to cool gaseous normal hydrogen from the ideal work to cool gaseous equilibrium hydrogen.

that the ortho-para conversion constitutes about 20% of the total work required to cool the hydrogen gas to the saturation temperature. It is also evident that the ideal work associated with ortho-para conversion does not contribute appreciably to the total ideal work until the final temperature is below about 100 K.

1.3. Hydrogen liquefaction plants

This section will begin by introducing some fundamental liquefaction cycles. Additionally, a history of large-scale hydrogen liquefaction and case studies of several commercial plants will be presented. Finally, the particular challenges of hydrogen liquefaction will be reviewed.

1.3.1. Basic hydrogen liquefaction cycles

Although large industrial liquefaction cycles are typically complex, many are based on the Claude cycle [23][24]. In this cycle, hydrogen is both the product and the working fluid. One or more expanders remove work from the working fluid, reducing its temperature. Finally, a Joule-Thomson valve brings the fluid into the two-phase regime, and saturated liquid is removed from the cycle. Makeup gas at the warm end ensures a constant mass in the system. The expander work in the Claude cycle reduces the compressor work and efficiently reduces the temperature of the working fluid. A simple Claude cycle can be seen in Figure 7.

Often, the Claude cycle is modified to have two compressors and is termed a "dual pressure" Claude cycle. The first compresses from low to intermediate pressure, and the second compresses from intermediate to high pressure. The expander operates between the intermediate and low pressures, and its exhaust provides additional cooling to the high-pressure stream. It is also possible to expand between the high and intermediate pressure. The high-pressure stream expands across the J-T valve to the low-pressure storage tank. Low-pressure vapor recirculates and cools the intermediate- and high-pressure streams. Variations of the dual pressure Claude cycle are widely used in hydrogen liquefaction plants [23], often with a separate product stream that is cooled by the working fluid portion of the cycle. Most plants use liquid nitrogen precooling, multiple stages of ortho-para catalysis, and more than one expander. Figure 8 shows a simple, dual pressure Claude cycle.
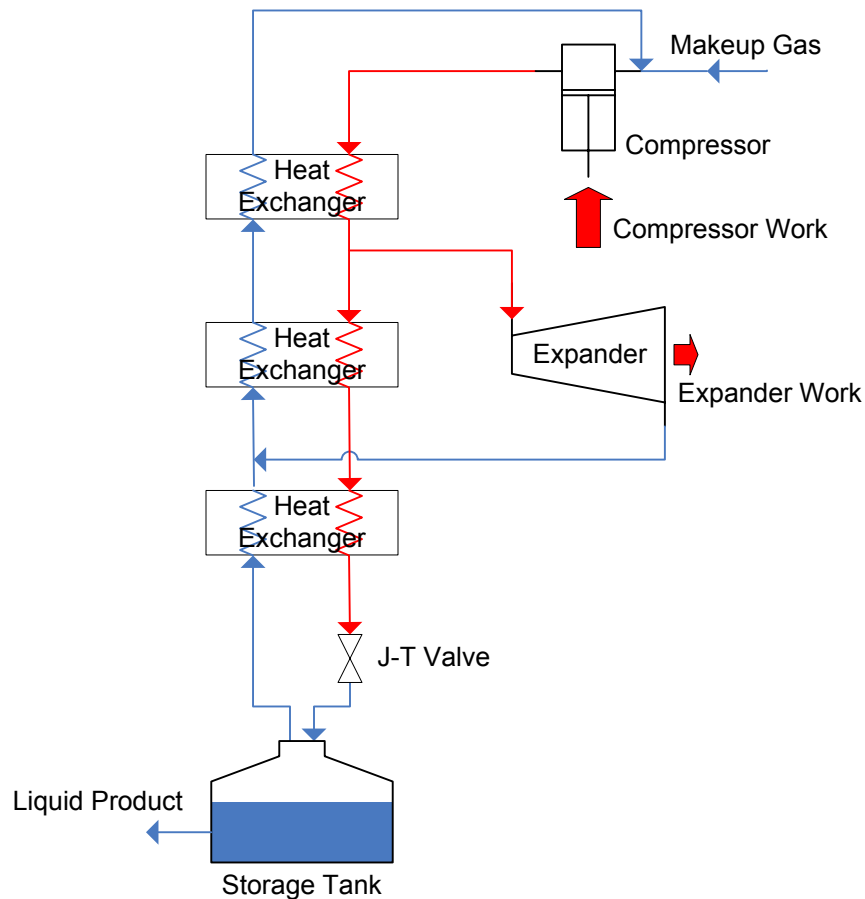
Figure 7: A simple Claude cycle [41].

1.3.2. Previous and current plants

Industrial hydrogen liquefaction began in the 1950s when the US atomic weapons program and the NASA Apollo missions created demand for large quantities of liquid hydrogen [42][43]. The National Bureau of Standards experimented with large laboratory-scale hydrogen liquefaction starting in 1952 and construction of commercial plants in Ohio, Florida and California occurred in the late 1950s.

Peschka [23] summarized several industrial hydrogen liquefaction plants; this summary can be seen in Table 3 with plants mentioned by Gross et al. [24] and Flynn [44] added. It can be seen that the industry has many years of experience in running plants with tonnage capacities. Additionally, Flynn
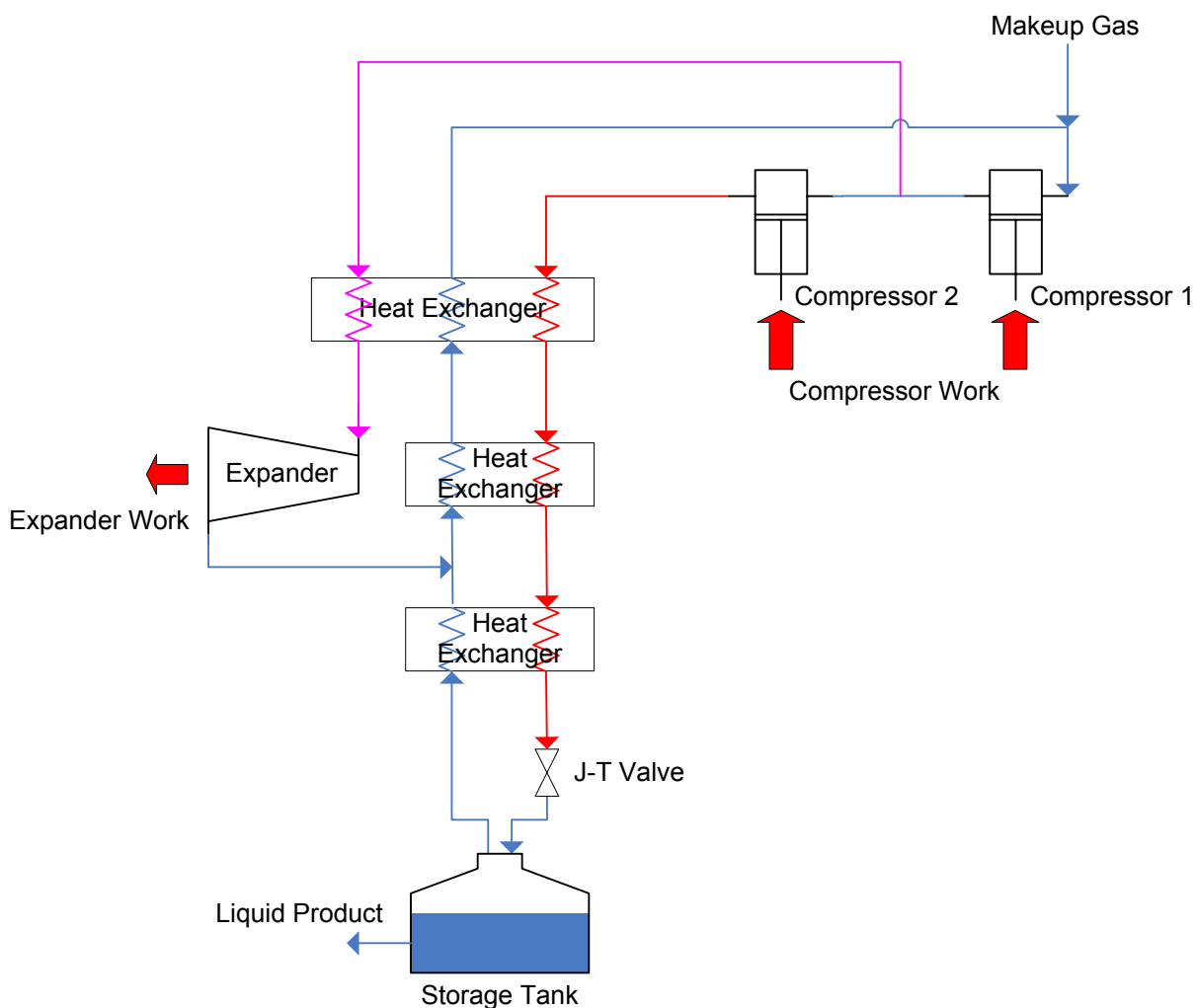
Figure 8: A dual pressure Claude cycle [41].

estimated the total US liquid hydrogen capacity to be 172 t/day in 1990, which is an order of magnitude short of the previously estimated 4100 t/day requirement to satisfy 1% of the US motor gasoline consumption. Therefore, many additional industrial-scale liquefaction plants will have to be constructed if hydrogen is to be used as an energy carrier.

In 1961, Vander Arend described one of the aforementioned first generation industrial-scale hydrogen liquefiers: an Air Products 27 ton/day hydrogen production and liquefaction facility [28]. The 17% efficiency of the liquefier does not compare favorably to some of the plants surveyed by Strobridge

Table 3: Hydrogen Liquefaction Plants

Place	Producer, Operator	Capacity	In Operation
Mississippi - Test Facility [23]	Air Products	36 t/day	1960
Long Beach, California [23]	Air Products	30 t/day	1958
Ontario, California [23]	Union Carbide, Linde Division	30 t/day	1962
Sacramento, California [23] [44]	Union Carbide, Linde Division	60 t/day	1966[a]
Los Angeles, California [44]	Linde	20 t/day	no date given
New Orleans, Louisiana [44]	Air Products	60 t/day	1976
Niagara Falls, New York [44]	Linde	30 t/day	no date given
Lille, France [23]	L'Air Liquide	10 t/day	1985
Rozenburg, Netherlands [23] [24]	Air Products	5.0 t/day	1986
Ingolstadt, Germany [24]	Linde	4.4 t/day	1992

[a] no longer in operation

[15]; however, reliability was of paramount importance, which precluded the selection of a thermodynamically superior design. For instance, only one expansion engine is used in the system to avoid potential failures of additional engines, and this expansion engine's work is not recovered. The cycle consists of a dual pressure hydrogen working fluid with nitrogen precooling and expansion between the intermediate and low hydrogen pressures. A separate product stream of hydrogen is purified and cooled by an auxiliary Freon refrigeration system and finally by the hydrogen working cycle. Ortho-para catalysis using chromic oxide on alumina occurs at "various temperatures," with no further details given.

Gross et al. described a Linde hydrogen liquefaction plant in Ingolstadt, Germany in 1994 [24]. The plant is based on a Claude cycle and has liquid nitrogen precooling. Two reciprocating compressors provide dual pressure operation, and three turboexpanders in series operate between the high (22 bar) and intermediate (3 bar) pressures. Work is extracted from the expanders, but it is unclear whether or not this work is used to offset the compressor work input. The main J-T valve operates between the high and low (1.3 bar) pressures. Ortho-para catalysis is accomplished in four stages with hydrous ferric oxide catalyst, and acts only on the separate hydrogen product stream. The product stream is thoroughly purified in a pressure swing adsorption plant before entering the liquefier and final purification is achieved at liquid

nitrogen temperature in an additional, low-temperature adsorber. In the publication, a table lists the "thermodynamic efficiency" of the liquefier as 33%. Assuming that the provided compressor powers and flow rates are accurate, a calculation of the Second Law efficiency reveals that this number is accurate only if the energy cost of the liquid nitrogen cooling is neglected. Taking this into account and assuming a nitrogen liquefaction Second Law efficiency of 40%, a 20% overall Second Law efficiency can be calculated for the Ingolstadt plant.

Strobridge conducted a survey of 144 cryogenic refrigerators and liquefiers in 1974 [15]. The second law efficiency, which is sometimes referred to as *percent Carnot*, defined as

$$\eta = \frac{W_{ideal}}{W_{actual}} \,, \tag{13}$$

was plotted versus the refrigeration capacity for 1.8-9 K, 10-30 K, and 30-90 K machines in Strobridge's survey, and can be seen in Figure 9. Several large capacity, 10-30 K machines in the survey reported efficiencies between 30 and 40%. In addition to efficiency, Strobridge studied the approximate cost of refrigerators and liquefiers operating in the 1.8-90 K range and established a relationship stating that, as a first approximation, capital cost is proportional to the input power raised to the 0.7 power.

1.3.3. Challenges of hydrogen liquefaction

McIntosh identified hydrogen turboexpanders as one of the most challenging aspects of liquefaction [43]. The low molecular weight and high speed of sound necessitate that very high peripheral speeds be maintained. Material properties restrict the speed and limit each stage to a low pressure ratio. Additional, practical considerations of using turbomachinery with hydrogen include the difficulty of forming reliable seals and the propensity of hydrogen to cause material embrittlement.

Aside from the turbomachinery issues, using hydrogen as the working fluid in a cycle has other problems. In a system with a J-T valve expanding into the saturated regime, only a small portion of the incoming stream is extracted as liquid. Often, the yield is a small portion of the cycle flow rate [41], but
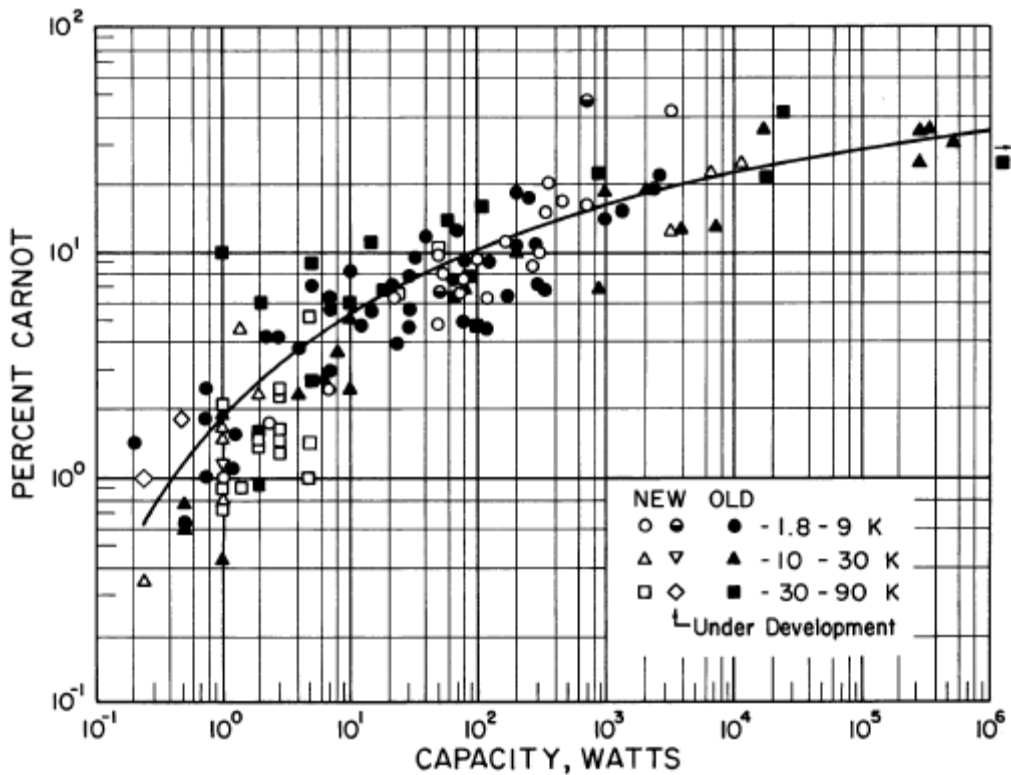
Figure 9: Second Law efficiency versus capacity for cryogenic refrigerators and liquefiers surveyed in 1974 [15].

can be as high as 60% in a dual pressure Claude cycle with ideal components and heat exchangers [23]. The compressor, heat exchangers, and expanders must be sized to handle hydrogen flow rates substantially larger than the plant's capacity. Extra components, connection points, and hydrogen-filled plumbing introduce more possible leak sites that can be dangerous due to the wide flammability range of hydrogen in air.

The J-T valve is a source of inefficiency. In a J-T valve, the fluid flows from high pressure to low pressure and, provided the fluid has a positive Joule-Thomson coefficient, results in a temperature drop. Fluid flow through a J-T valve generates entropy, which represents a loss in the system and is detrimental to the overall plant efficiency. However, a system with no J-T valve still requires a method of reducing the product stream pressure to the storage pressure. The difficulties of designing an expander to be

operable in the two-phase regime, along with associated reliability concerns, make the J-T valve appealing despite its inherent entropy generation.

The hydrogen makeup gas must be thoroughly purified to avoid the introduction of oxygen and other contaminants into the system. Contaminants other than helium freeze in the system, which can clog a J-T valve or damage an expander. Buildup of frozen oxygen in the product tank can result in an explosion hazard. Purification requirements for hydrogen liquefiers can be as stringent as 1 ppm. McIntosh identifies "explosion proof requirements on equipment and facility design" as an important consideration in liquefier design [43].

The substantial variation in heat load imposed on the cycle by the hydrogen stream presents a challenge in the balancing of the heat exchangers. Recalling Figure 4, the specific heat varies substantially with temperature and parahydrogen concentration. To minimize heat exchange temperature differences, the cycle temperatures and flow rates must be carefully selected. If staged catalyst beds are employed in the cycle, their operating temperatures must also be chosen judiciously.

Baker and Shaner simulated a 250 ton/day, dual pressure Claude cycle with nitrogen precooling and continuous conversion catalysis [45]. Parameters such as feed pressure, recycle return pressure, component efficiencies, heat exchanger temperature differences, and turbine refrigeration levels were varied. The base scenario, whose parameters were selected to provide a realistic simulation, had a Second Law efficiency of 36%. The system losses were itemized and can be seen in Table 4.

Table 4 highlights another challenge: improvements in component efficiency. Baker and Shaner point out that, due to their long development histories, improvements in modern components such as compressors and expanders can be "marginal and difficult to achieve" [45]. However, as plants become larger and more numerous, it may become more economically feasible to develop compressors or expanders specifically suited to a liquefaction cycle's flow rates and pressure levels. Additionally, heat exchanger losses can be reduced by increases in area. Often, capital costs constrain this area, but the

Table 4: Component Contributions to Cycle Work [45]

	Loss [kJ/kg]	% of Total Loss
Recycle Compressor	7,343	29.35
Feed Compressor	2,153	8.61
Expanders	3,242	12.96
Heat Exchangers	3,166	12.65
Catalysts	1,021	4.08
Throttling	1,127	4.50
Mixing	408	1.63
Heat Leak	286	1.14
N_2 Refrigerator	6,260	25.02
Miscellaneous	15	0.06
Total	25,021	100.00
Ideal Work	14,070	
Actual Work	39,091 (36% Carnot)	

efficiency improvement associated with lower heat exchange losses would reduce operating costs.

Clearly, hydrogen liquefaction presents many challenges to a cycle designer. Practical challenges arise from hydrogen's flammability, resistance to being contained by seals, and tendency to cause embrittlement in some common engineering materials. Thorough purification of the feed stream must also be performed to avoid freezing of gaseous impurities and potential explosion hazards due to accumulated oxygen. Hydrogen's low molecular weight and resultant high speed of sound cause turbine expanders to be less effective. Additionally, hydrogen's properties present thermodynamic challenges. For example, the ortho-para transition, which must be catalyzed to avoid excessive boiloff losses during storage, contributes a significant amount of the heat removed from the product stream and has a noticeable effect on the cycle work input. Depending on how the catalysts are staged, large heat loads can occur at low temperatures in the system. Finally, the strongly temperature-dependent specific heat and significant property differences between ortho and parahydrogen can cause entropy-generating heat exchanger imbalances in the cycle and demand careful selection of system operating temperatures and flow rates.

CHAPTER 2. CYCLE SIMULATIONS

Based on the assessment of some current liquefaction cycles, several areas of improvement were pursued. Using these ideas and computer simulations of some system configurations, a cycle that addresses the targeted improvements is proposed. The proposed configuration, its features, and its advantages over the typical cycle will be discussed. Additionally, this section will also review the details, assumptions, and inner workings of the simulations used to arrive at and validate the proposed cycle.

2.1. Design goals and component feasibility

Many attributes are desirable in a new cycle design, including overall efficiency, scalability, and simplicity. Obviously, the efficiency of a liquefier determines the energy use and most of the operating cost. Scalability makes a cycle desirable for more diverse applications and allows for less expensive feasibility testing of a large system via the construction of a smaller system. As mentioned by Vander Arend [28], uptime is critical in a commercial liquefaction plant, so simplicity of design was considered throughout the process.

Two plant sizes were considered: a *pilot plant*, which is a 500 kg_{H2}/day liquefaction plant, and a *large plant,* which is a 50,000 kg_{H2}/day plant. Since testing of the large plant (a 50 t/day liquefier) would require an enormous capital investment, it is desirable to have the pilot plant very similar in configuration to the large plant so that some validation tests could be applicable to both designs. The desirability of keeping the cycle scalable was considered in the selection of the system components.

Using a high-pressure product stream was considered due to the availability of high pressure from hydrogen sources. In particular, many water electrolyzers operate at high pressure. If a high-pressure electrolyzer were coupled to the liquefier, some compression work could be avoided in the liquefier. The plant would be able to take advantage of the relatively efficient compression process associated with an

electrolyzer rather than having to use a reciprocating machine. In addition, high-pressure hydrogen as the inlet state requires less theoretical ideal work input. Figure 10 shows the reduction in the ideal work associated with a pressurized inlet state. Caution should be used in interpreting Figure 10, however: the reduction in the overall cycle work will not be nearly as dramatic as the reduction in the ideal work. If the cycle is thought of as a refrigerator removing heat from a distributed load, the total amount of heat that must be removed from the hydrogen is virtually identical with the pressurized inlet, since the enthalpy is a very weak function of pressure at room temperature. Thus, for the working portion of the cycle little change occurs, although the heat load imposed by the product stream will be distributed in a different manner because the specific heat changes appreciably with pressure. Effectively, starting with pressurized hydrogen eliminates the work associated with compression of the product stream, which can be small in the context of the entire system. Therefore, with a pressurized inlet, the ideal work may change
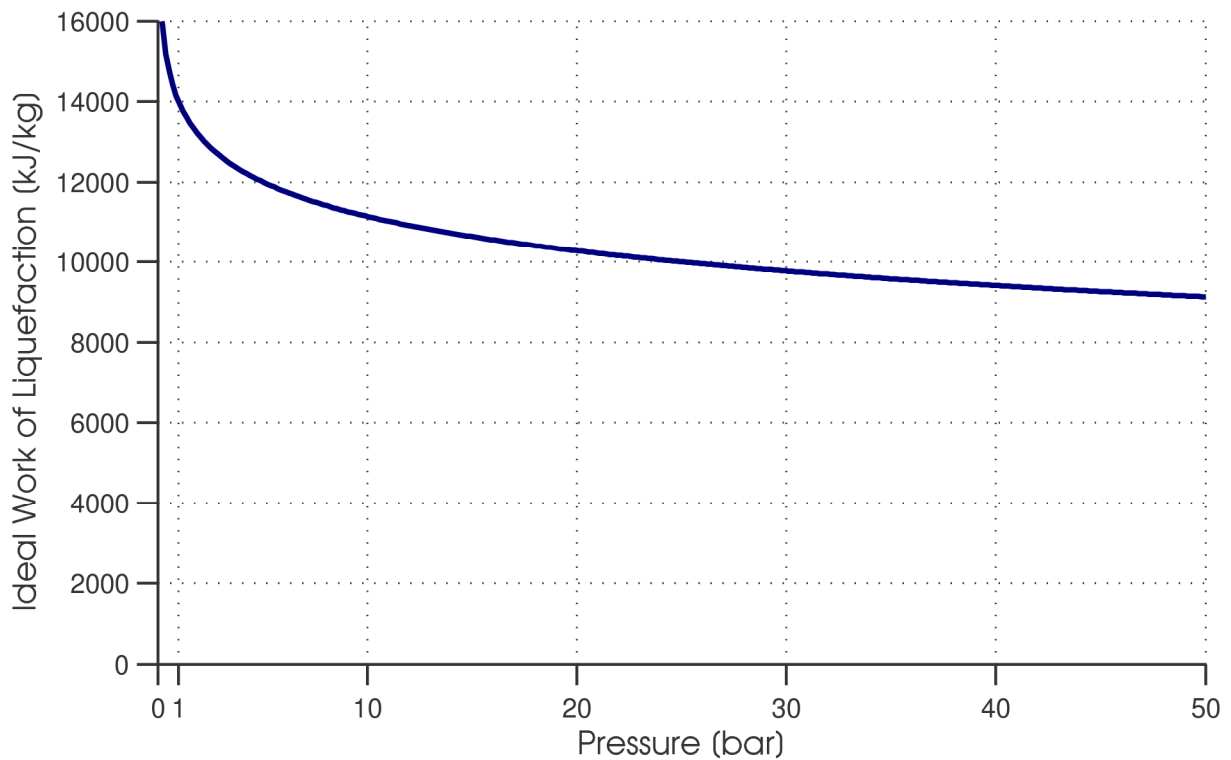
Figure 10: Ideal work of liquefaction vs. inlet hydrogen pressure, for a final state of 20 K, 1 bar
and 95% parahydrogen

significantly but the overall cycle work may only change slightly. Since the Second Law efficiency is defined as the ratio of the ideal work to the actual work, the Second Law efficiency changes significantly with a change in the inlet state used to determine the ideal work. When examining reported plant efficiencies, it is important to note the reference states with which the ideal work is determined.

In addition to eliminating the product stream compression, a high-pressure inlet state can reduce the severe or infinite peaks in specific heat that occur near or below the critical temperature. The heat capacity of hydrogen is shown in Figure 11 for pressures at and above the critical pressure of 13 bar. It is clear that as the pressure approaches the critical pressure the heat capacity diverges at a temperature of 33 K. At pressures below the critical pressure the heat capacity of all isobars diverge when the fluid undergoes the gas to liquid transition. In many liquefaction cycles the wildly varying heat capacity makes the heat load of the product stream very difficult to match and can lead to unnecessary losses, which suggests that cooling the hydrogen supercritically can lead to improved efficiency.

Simplicity was another important criterion in the cycle design process. Using helium as the working fluid makes some of the hydrogen liquefaction challenges more surmountable. First, helium turboexpanders, which are commonly used in helium liquefaction cycles, operate more effectively than hydrogen turboexpanders. The speed of sound in helium is lower than in hydrogen because of helium's greater molecular weight. Thus, larger pressure ratios can be achieved in a turbine stage for the same material-limited tip speed. Second, material degradation of components does not occur due to exposure to helium as it can with hydrogen. In addition, helium remains gaseous in the required operating temperatures of the cycle. The combination of a supercritical hydrogen product stream and an all-gaseous helium working fluid eliminates difficulties associated with multiphase expansion. Finally, helium is inert, providing inherent safety in the event of a leak to the environment or to the hydrogen stream.
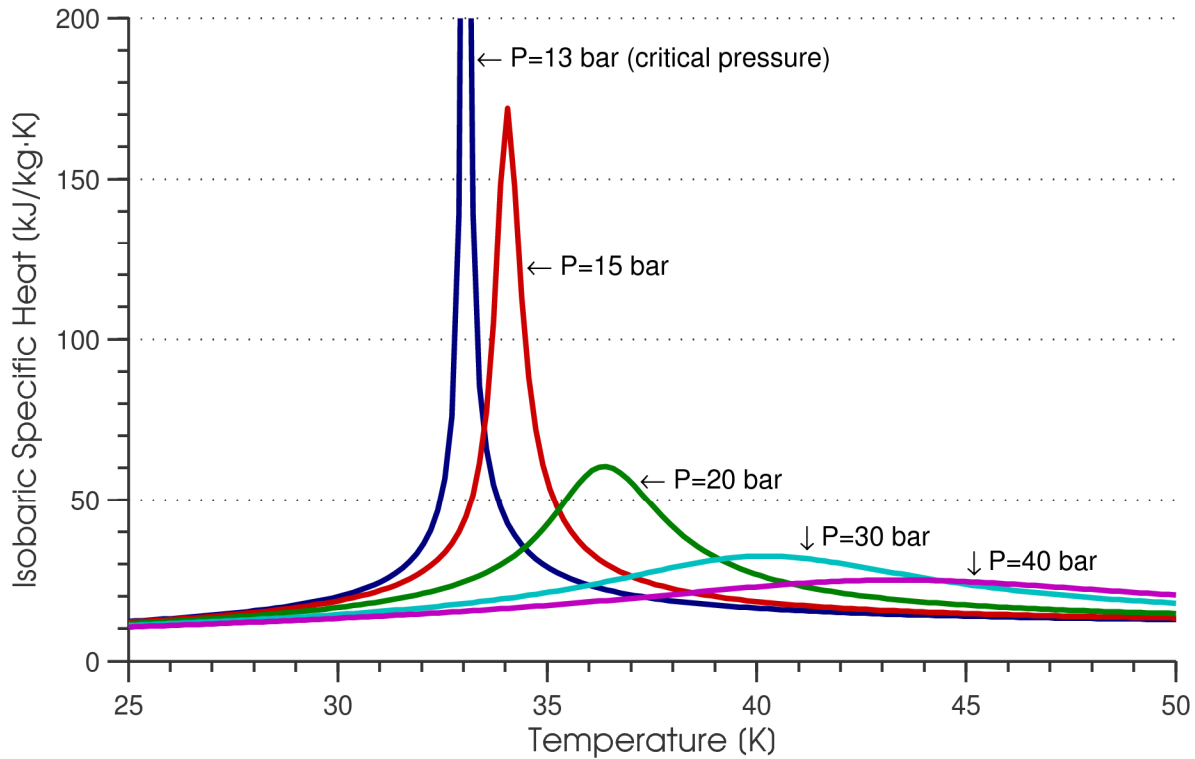
Figure 11: Specific heat of equilibrium hydrogen vs. temperature at various pressures.

2.2. Proposed cycle

In the simple Claude cycle that typified a conventional hydrogen liquefaction plant, several problems were identified: the inherently inefficient J-T valve, the large hydrogen flow rates in system, and the use of hydrogen turboexpanders.

A system that addresses these problems can be seen in Figure 12. In this configuration, hydrogen passes through a series of heat exchangers until it reaches a temperature slightly above the storage temperature of 20 K, where all of the hydrogen is a liquid rather than a two-phase mixture. The final reduction in temperature to the storage temperature is accomplished with a single-phase wet expander, which will be discussed in more detail in Section 3.2. The heat removed from the hydrogen goes into a refrigeration loop – a helium cycle. The properties of helium are more conducive to the use of

turbomachinery, and helium expanders are commonly used in the cryogenics industry. As mentioned previously, helium is not flammable, so the number of potential hydrogen leak points and the danger of explosion are reduced in comparison with a system using hydrogen as the working fluid.

The design cools a hydrogen stream that is maintained at a supercritical pressure. In this way, the divergent behavior of the hydrogen heat capacity in the two phase region is avoided and is replaced by the relatively benign thermal behavior of the supercritical stream. This allows the temperatures and the capacity flow rates in the helium streams to be better matched to the temperatures and capacity flow rates of the hydrogen stream in the low-temperature heat exchangers, reducing the losses in the cycle.

The elimination of the J-T valve is another advantage of maintaining supercritical hydrogen pressure. Rather than undergoing a distinct phase change like subcritical hydrogen, the supercritical gaseous hydrogen stream gradually increases in density until it reaches liquid density. At the bottom of the system, the hydrogen stream is a high-pressure liquid. A single-phase wet expander extracts a small amount of work from the liquid to reduce its pressure to atmospheric.

Three stages of ortho-para conversion can be seen in Figure 12. Ideally, the ortho-para catalyst would somehow be incorporated into the hydrogen passages in each heat exchanger. However, to keep ease of construction a high priority it was assumed that the first iteration of the system would employ conventional, staged catalysis. The low-pressure helium stream provides cooling to the catalyst bed to maintain the bed at near-isothermal conditions.

The spans of the two lowest-temperature expanders overlap. This configuration provides additional cooling in the critical temperature region where the specific heat of the hydrogen peaks. In addition, there is a substantial heat load due to the ortho-para conversion in the low-temperature catalyst bed. The overlapping expander design also helps to match the thermal load imposed by this catalyst bed.
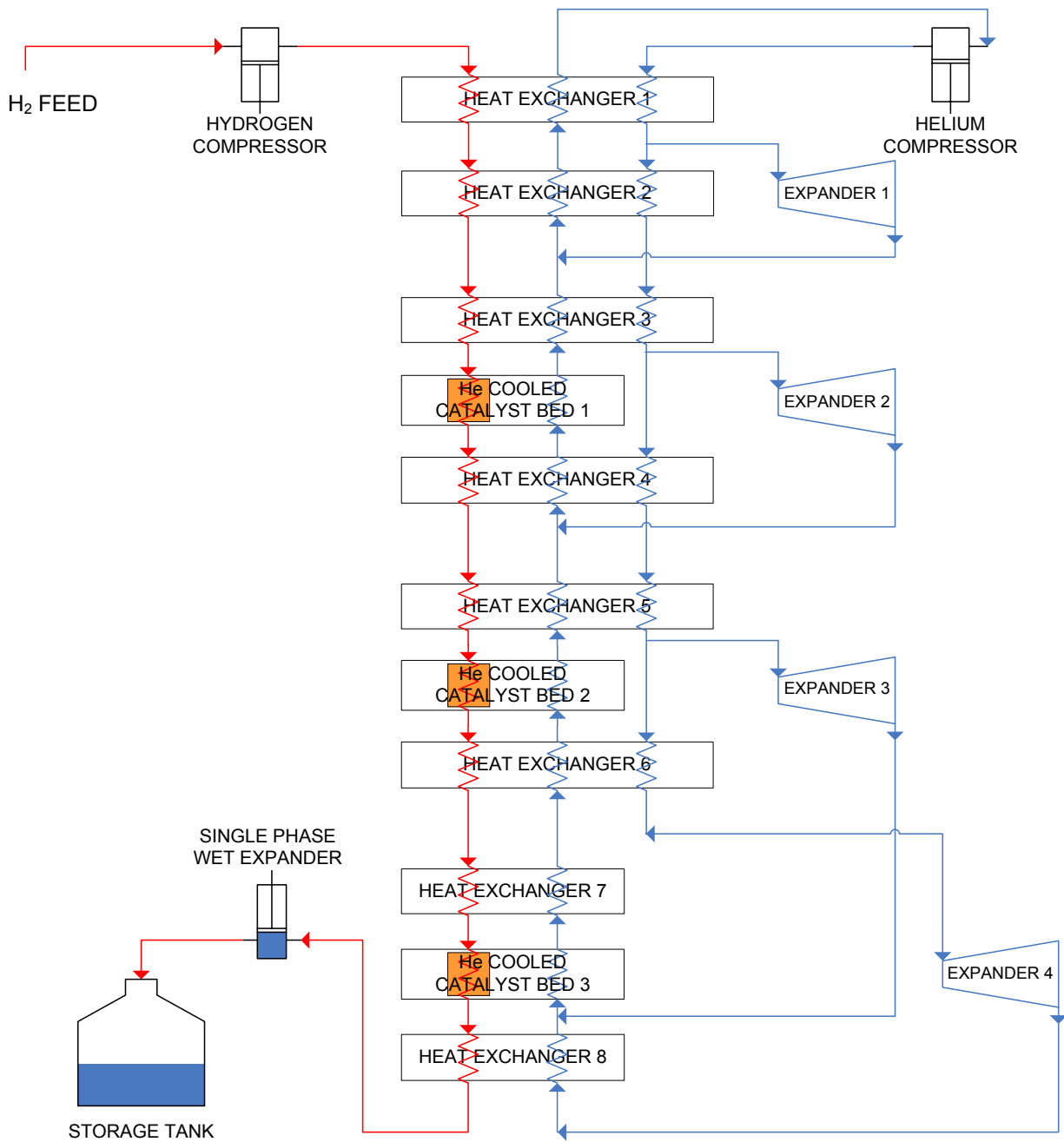
Figure 12: Schematic of the proposed system.

2.3. Numerical simulations

Both the proposed cycle and several preliminary, simpler cycles were simulated numerically. Initially, a spreadsheet-based model was created that allowed nearly simultaneous solution and graphical output of the solved system operating points. Simple two-, three- and four-stage cycles were solved, but as the systems grew more complex, the deficiencies of the spreadsheet-based solver became apparent and a program-based model was created using MATLAB [46]. The system proposed in the preceding section was fully simulated and the effects of altering basic system parameters were studied.

2.3.1. Spreadsheet-based

A cycle analysis tool was created in a spreadsheet using Microsoft Excel [47]. The motivation behind using spreadsheet-based simulations was the nearly simultaneous graphical outputs that were available when solving a system. In the spreadsheet, a system's governing energy balance equations were solved while being subjected to constraints imposed by cycle conditions and the Second Law. The variation of parameters to find a maximum in the system efficiency was accomplished using Excel's Solver add-in program.

Systems explored in the simulations consisted of a hydrogen product stream cooled by a Collins-type helium cycle. Figure 13 shows a diagram of one of the systems that were simulated, and Figure 14 shows the graphical interface associated with this system in the spreadsheet-based solver. The helium is compressed and the high-pressure stream enters the first stage, which consists of heat exchanger (HX) 1, HX 2, and expander 1. The cool, low-pressure helium stream cools the hydrogen and the high-pressure helium stream. The capacity rates of the high-pressure helium and low-pressure helium streams approximately balance each other in heat exchanger 1. Addition of the hydrogen stream causes the downward flow in the heat exchanger to have a larger net capacity flow rate, which results in the tendency of temperatures of the streams to pinch at the top. A fraction of the high-pressure helium is diverted into expander 1 so that heat exchanger 2 has a larger net capacity flow rate in the upward

direction and pinches at the bottom. In a balanced-flow heat exchanger, a low stream-to-stream temperature difference can be maintained, which results in lower entropy generation. Since it is impossible to balance the flows with the addition of the hydrogen stream, the balanced-flow scenario is approximated by allowing the stream temperatures to diverge and converge by altering the relative flow rates of the two helium streams. High-pressure helium diverted into an expander rejoins the low-pressure stream after work is extracted and its temperature is reduced. The unavoidable heat exchanger imbalance losses can be minimized by choosing appropriate flow rates in each expander. Addition of more expanders also helps to reduce this loss.
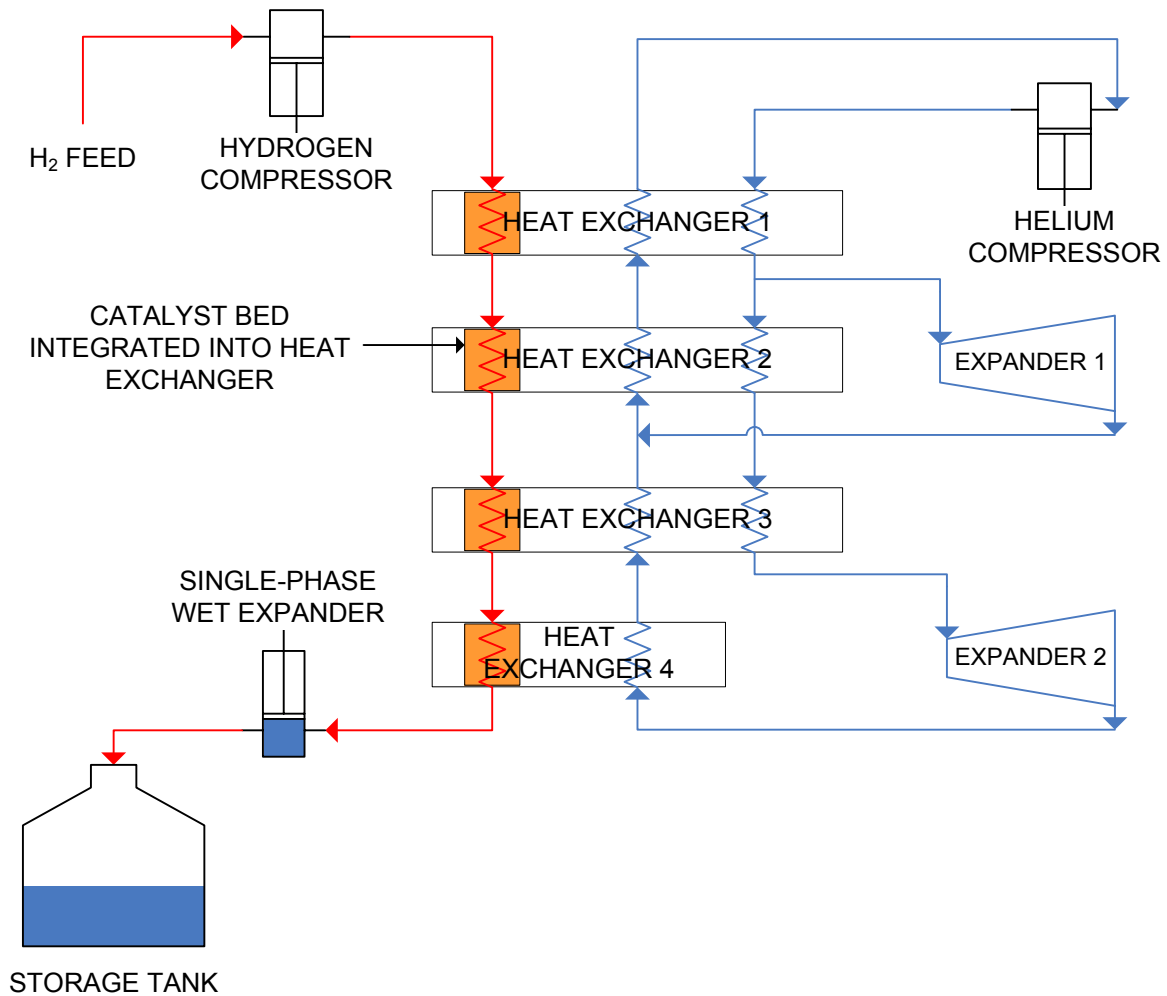
Figure 13: A two-stage, helium-cooled hydrogen liquefaction cycle that is typical of the systems simulated.

mdot H2 1.0 ↓		↑		→		→					
						compressor					
				←							
						T1	300.0	T2	285.7		
Tc 300.0	T2 285.7	top	300.0 T1			P1	1.5	P2	0.3		
	mdot4 35.7	**HX1**	35.7 mdot1								
Td 177.5	T4 129.7	bottom	153.3 T3								
↓	↑		↓ → 16.4 mdot3	**expander 1**							
				T3 153.3							
				P3 1.5							
Td 177.5	T4 129.7	top	153.3 T3		T6 95.2						
	mdot4 35.7	**HX2**	19.2 mdot5		P6 0.3						
Te 100.0	T6 95.2	bottom	100.0 T5								
↓	↑		← ← 16 mdot6								
Te 100.0	T6 95.2	top	100.0 T5								
	mdot8 19.2	**HX3**	19.2 mdot5								
Tf 73.9	T8 48.7	bottom	57.8 T7								
↓	↑		↓ → 19.2 mdot7	**expander 2**							
				T7 57.8							
				P7 0.0							
Tf 73.9	T8 48.7	top			T10 19.0						
	mdot8 19.2	**HX4**			P10 0.0						
Tg 20.0	T10 19.0	bottom									
↓	↑		← ← 19 mdot10								

Figure 14: Graphical output of the spreadsheet-based solver for the two-expander system. The depicted operating point values update when the system is solved.

To completely solve the system, some assumptions were necessary. A set of temperatures was assumed for the hydrogen stream. The hydrogen stream temperatures, after the system was solved, were changed until a maximum efficiency was approached. It was assumed for simplicity that the temperature of the high-pressure helium stream would be the same as the temperature of the hydrogen stream at each stage point.

Following the work of Minta and Smith [48] for a given liquefier design, the total heat exchanger area is most effectively distributed when the value of $\Delta T/T$, defined as

$$\frac{T_{hydrogen} - T_{helium,LP}}{T_{helium,LP}} = \frac{\Delta T}{T} ,$$

(14)

is given a constant value at all stage points. The $\Delta T/T$ constraint was not strictly enforced at each stage point, but a constraint was imposed to prevent the stream-to-stream temperature difference from becoming less than this value. When the system efficiency was maximized, the actual $\Delta T/T$ values tended to push this constraint to its limit at each stage point as expected. This constraint limits the total heat exchange area in the simulation – without it, the stream-to-stream temperature differences would be driven to zero, making the efficiency greater but implying infinite heat exchange area.

In the catalyst beds it was assumed that the low-pressure helium cooling stream maintained the temperature of the hydrogen stream at a constant value. The change in enthalpy of the hydrogen in a catalyst bed occurred solely because of the change in the parahydrogen concentration. The heat given off by the ortho-para conversion was taken up by the low-pressure helium stream. This isothermal catalyst bed behavior has been approximated in experiments. For example, Hutchinson maintained small catalyst beds at nearly constant temperature to determine ortho-para conversion rates for hydrous ferric oxide catalyst material [33]. In the simulations in this work, it was also assumed that the catalyst beds were large enough to allow the hydrogen to reach the equilibrium parahydrogen concentration.

Initial simulations were performed to determine the value of additional stages. In these simulations, the adiabatic efficiencies of each expander and the isothermal efficiencies of each compressor were assumed to be 80% and 65%, respectively. The $\Delta T/T$ value at each stage was restricted to 5%. The temperature of the thermal reservoir into which the compressors reject heat was assumed to be the ambient temperature of 300 K. The Second Law efficiency was defined as

$$\eta_{system} = \frac{W_{net,system}}{W_{liquefaction,ideal}} = \left| \frac{W_{comp,He} + W_{comp,H2} - \displaystyle\sum_{i=1}^{N_{stages}} W_{exp(i)}}{\left[\left(h_{final} - h_{initial} \right) - T_{amb} \left(s_{final} - s_{initial} \right) \right]_{hydrogen}} \right| ,$$

(15)

Table 5: Efficiencies for Two-, Three- and Four-Stage Cycles

Number of Stages	Second Law Efficiency
2	0.163
3	0.33
4	0.356

where the final state is hydrogen at 20 K, 1 bar and 95% parahydrogen and the initial state is at 300 K, 1 bar and 25% parahydrogen. The 95% parahydrogen concentration of the final state is a typical target value for liquefaction plants [24]. Table 5 shows the overall efficiencies of two-, three- and four-stage cycles. As can be seen in Table 5, increasing the number of stages from two to three results in a large efficiency increase of 0.167, while increasing from three to four yields a less pronounced gain of only 0.026. Numerical problems surfaced with cycles having greater than four stages, and these systems were not solved. From the trend shown in Table 5, it is expected that adding another stage in a cycle would not be worth the considerable associated increase in capital cost.

While the spreadsheet-based simulations are capable of solving the system, much care had to be taken in doing so. With improper choices for the initial values of the expander mass flows, the system encountered difficulty in finding the solution. Solving the system often became laborious because the solver's sensitivity to the initial guess values required manual adjustment of parameters until the system was capable of convergence. Despite the convenience of the quickly updating graphical interface, the deficiencies of the spreadsheet-based solver showed that a more robust solving program was needed.

2.3.2. Program-based

In order to take advantage of powerful built-in optimization algorithms, freedom to compartmentalize portions of code into subfunctions, and ease of interfacing with REFPROP for fluid properties, MATLAB programs (m-files) were created to simulate the system. The heart of the program-based simulations consists of two files: the *cycle solver* (cycle.m) and the *cycle optimizer* (optimize.m). For an input of the system flow rates, the cycle solver can return either (1) a value related to the cycle

efficiency or (2) an array of numbers representing inequality constraints imposed by the Second Law and the ΔT/T limits. Invalid combinations of flow rates can be passed to the cycle solver, and an efficiency will be returned; however, the inequality constraint array will reflect the constraint violations and indicate that the returned efficiency has no meaning.

The cycle optimizer calls an optimization routine and performs the maximization of the system efficiency. The cycle optimizer requests the efficiency and constraint array from the cycle solver for a combination of mass flow rates. These flow rates are varied until the constraints are satisfied and the efficiency has converged to a maximum. When this occurs, the system operating points are either displayed or stored in the program workspace.

The cycle solver calls several auxiliary m-files for basic functions. The *REFPROP-MATLAB interface* is a function provided with REFPROP that allows fluid properties to be called from within MATLAB m-files. Data from Woolley et al. [20] were used to create the *parahydrogen lookup* (para.m), a program that interpolates the ortho-para equilibrium data to return the equilibrium parahydrogen concentration for a temperature input. Due to the frequency of hydrogen mixture property lookups, the *hydrogen property calculator* (H2props.m) was designed to return the specific enthalpy and entropy of a hydrogen mixture for an input of the mixture's temperature, pressure and parahydrogen fraction. This function looks up the normal and parahydrogen properties, adds the required reference state offsets to the normal hydrogen properties, and applies the normal/para mixing equations detailed in section 1.2.3 to determine the mixture properties. Finally, the *expander output calculator* (expander.m) determines the required inlet temperature for an expander of known adiabatic efficiency, inlet and outlet pressure, and outlet temperature. This program provided a convenient means to incorporate the expander equations into the cycle solver.

To proceed with the solution of a system, assumptions about the cycle components were required. The expanders were assumed to have a fixed adiabatic efficiency. After several personal communications

with the R&D Dynamics Corporation, the expected efficiency for each expander in both the pilot and large plant was estimated and incorporated into the model. R&D Dynamics suggested that the highest-temperature expander be split into two expanders in series. One benefit to this configuration is that the effective adiabatic efficiency of the two-expander ensemble is greater than the reported efficiency of either by itself. The efficiencies reported by R&D Dynamics were for helium expanders operating at a discharge pressure of 2.5 bar and a pressure ratio of 6. These pressures were not changed in the simulations, because deviation from these pressures would cast doubt on the legitimacy of the expander efficiency estimates. A summary of the expander efficiencies incorporated into the simulation can be seen in Table 6.

In addition to the expanders, efficiency estimates were needed for the compressors. Based on discussions with Gas Equipment Engineering Corporation (GEECO) and R&D Dynamics, and on typical reciprocating compressor efficiencies reported in literature [19][41][45], isothermal efficiencies were assumed for the pilot and large plant helium compressors. Literature on hydrogen compressors was unavailable, so conservative isothermal efficiencies of 60% were assumed. The compressor efficiencies for the pilot and large plants are summarized in Table 6.

The systems specified in Table 6 will be referred to as the *base configurations* of the pilot and large plants. These systems were solved using the numerical solving routine described above. The base configuration efficiencies for the pilot and large plant are listed in the bottom row of Table 6. The temperatures that were calculated by the simulation of the pilot plant are shown in Figure 15; the large plant results are summarized in Figure A - 1 of the appendix.

Simulations of the system were run using the m-files described above. After the establishment of the base configuration operating point and efficiency, the efficiency of each component was varied to determine its impact on that of the cycle. Relative to the base configuration, the change in cycle efficiency

Table 6: Summary of Base Configuration Parameters

	Pilot Plant	Large Plant
Expander 1 Adiabatic Efficiency	0.60	0.85[a]
Expander 2 Adiabatic Efficiency	0.70	0.83
Expander 3 Adiabatic Efficiency	0.75	0.86
Expander 4 Adiabatic Efficiency	0.65	0.86
He Compressor Isothermal Efficiency	0.65	0.80
H_2 Compressor Isothermal Efficiency	0.60	0.60
Wet Expander Adiabatic Efficiency	0.90	0.90
$\Delta T/T$	0.05	0.05
Hydrogen Pressure [bar]	21	21
Atmospheric Temperature [K]	300	300
Atmospheric Pressure [bar]	1	1
H_2 Product Temperature [K]	20	20
H_2 Product Pressure [bar]	1	1
H_2 Product Para Content [-]	0.95	0.95
System Second Law Efficiency [-]	0.184	0.391

[a]effective efficiency of two-stage expander combination. Individual expander
efficiencies were η_{1A}=0.82 and η_{1B}=0.83

is plotted versus the change in component efficiency for the pilot plant in Figure 16. The component
efficiencies were varied independently, so combined effects are not reflected; however, the slope of the
line corresponding to a component gives a good idea of the magnitude of the system's response. The
system efficiency was most sensitive to changes in the efficiency of the helium compressor and that of
expander 3. An analogous plot for the large plant can be seen in Figure A - 2 of the appendix.
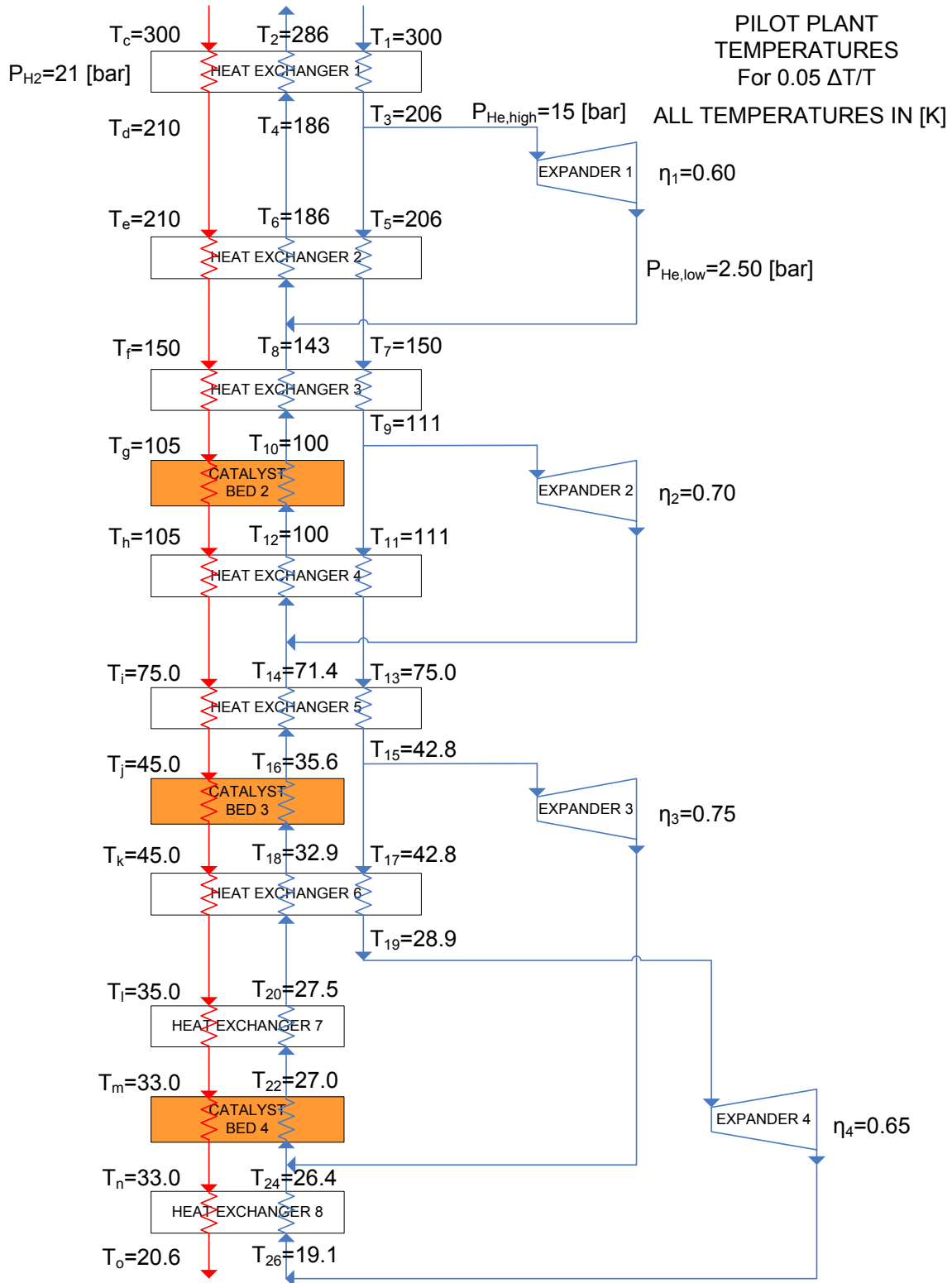
Figure 15: Results of pilot plant cycle simulation.
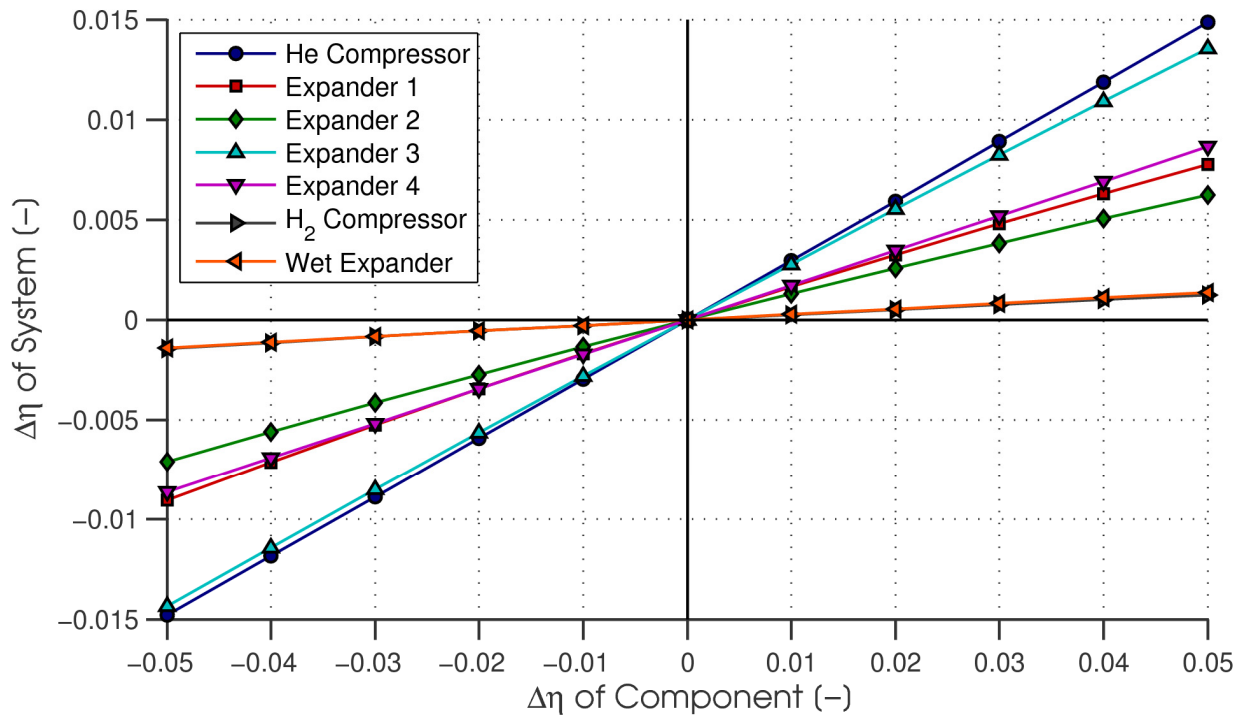
Figure 16: Change in pilot plant system efficiency vs. change in component efficiency, with respect to the base configuration. All of the points coincide at the center which represents the base configuration. The components corresponding to the steeper lines affect the system efficiency most significantly. The parameters were varied from the base configuration one at a time.

As Figure 16 suggests, the most significant component efficiencies are those of the helium compressor and expander 3. Some of the inefficiency of the helium compressor can be compensated for by increasing the size of the heat exchangers. Figure 17 shows the improvement of the overall cycle efficiency associated with improvements in the helium compressor efficiency and the $\Delta T/T$ parameter. A reasonable conclusion from Figure 16 and Figure 17 is that finding an efficient helium compressor should be a very high priority in the system development process.

The pressure of the hydrogen stream does have some impact on the cycle efficiency. As previously discussed, higher hydrogen pressures tend to smooth out the temperature defect between the hydrogen and helium streams at low temperatures. On the other hand, this comes at a cost of the additional work required to compress the hydrogen stream to a higher pressure. The net effect, shown in

Figure 18, is that for pressures above about 19 bar, the efficiency of the cycle does not change much with hydrogen pressure. The base configuration lies in a region where the cycle efficiency is relatively insensitive to hydrogen pressure. This allows some flexibility in the operating conditions of the cycle's hydrogen compressor to ensure that these conditions coincide with the efficiency "sweet spot" of available hydrogen compressors.
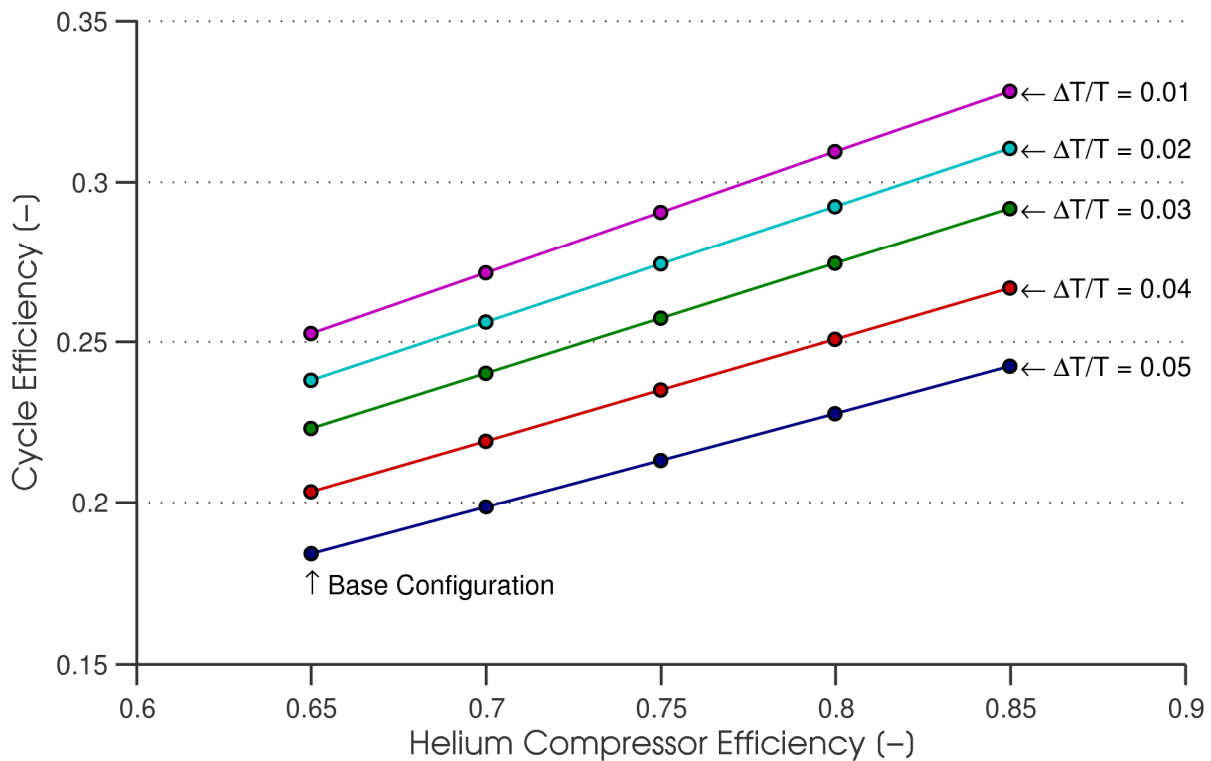
Figure 17: Effect of helium compressor efficiency on cycle efficiency for the pilot plant.
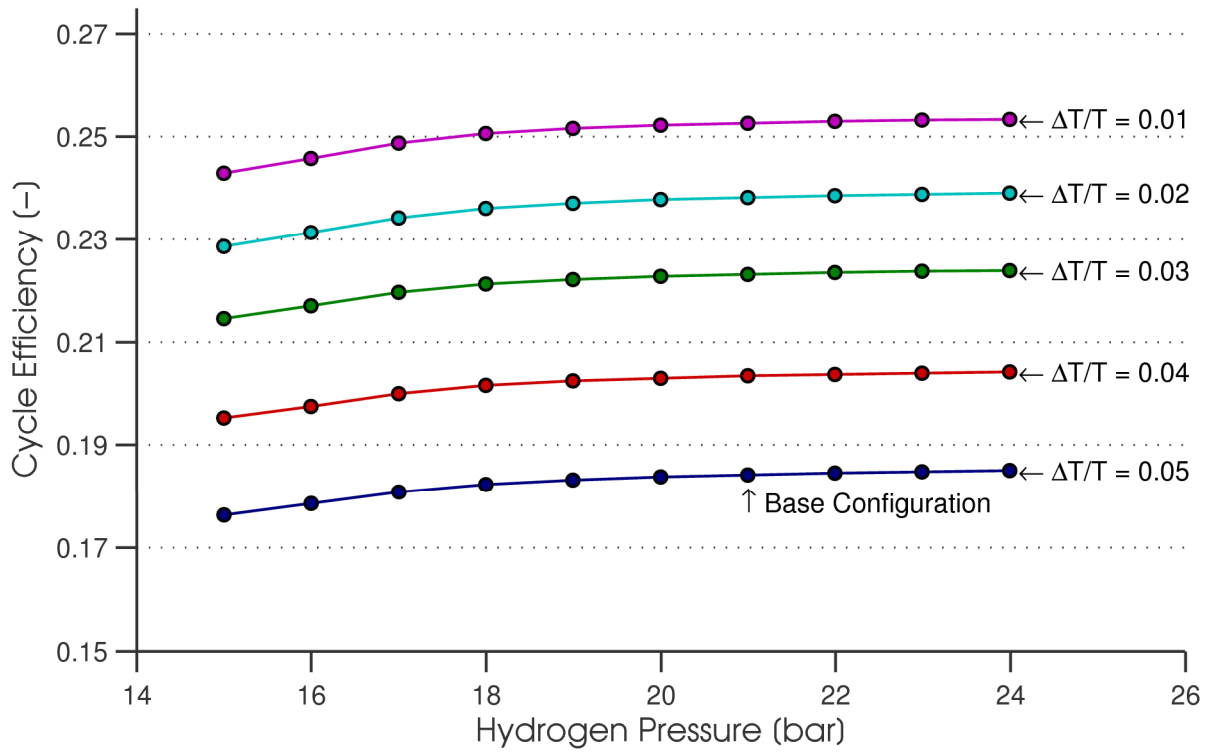
Figure 18: Effect of hydrogen pressure on cycle efficiency for the pilot plant.

CHAPTER 3. COMPONENT SIMULATIONS

The cycle simulations allowed the investigation of various system parameters and their effect on the overall efficiency. However, inherent assumptions were present involving the cycle components. More detailed calculations were performed to determine if component sizes were reasonable. In specific, the catalyst beds were scrutinized to verify that they would be capable of effecting the desired conversion without being excessively large. Additionally, the consequences of deviations in the performance of certain components were explored. The single-phase wet expander can be viewed as a risk to the uptime of the cycle since the J-T valve it replaces is simple and considered to be more reliable. To justify the use of the single-phase wet expander, its operation and the associated cycle performance advantage were studied. Finally, to ensure no internal Second Law violations, the operation of the heat exchangers was simulated by constructing governing differential equations and solving them numerically. These simulations were also used to determine the overall heat exchange area and to quantify the effect of this area on system performance.

3.1. Catalyst beds

To estimate the size of the catalyst beds needed for the pilot plant, a simple model was formulated based on the data that Hutchinson gathered in experiments on hydrous ferric oxide [33]. This model assumed that diffusion of the hydrogen from the stream to the catalyst limited the overall process, and occurred much slower than the actual ortho to para conversion. In practice, this is not necessarily the case [27], but as will be shown below, the model works well to a first approximation. With the available data, the diffusion model correlated the data with reasonable accuracy.

Using a simple one-dimensional mass transfer model, the flow through a porous, packed bed [49] of catalyst material can be analyzed with good accuracy. The governing equation for the 1-D mass transfer in the bed is

$$\frac{x_{exit} - x_{equilibrium}}{x_{inlet} - x_{equilibrium}} = e^{-gPL/\dot{m}}, \tag{16}$$

where x is the mass fraction of parahydrogen, g is the overall mass transfer conductance, P is the transfer perimeter, L is the length of the packed bed, and $\dot{m}$ is the mass flow rate of hydrogen through the packed bed. The term on the left hand side of equation 16 is sometimes referred to as the *approach*. The transfer perimeter P is

$$P = \frac{6}{D_P}(1 - \varepsilon_v)A_c, \tag{17}$$

where D_P is the particle diameter, ε_v is the void fraction, and A_c is the bed cross sectional area [49]. The particle diameter was assumed to be 0.5 mm, corresponding to 30-50 mesh catalyst particles, which is a common size for hydrous ferric oxide [31]. The void fraction was assumed to be 0.3, which is a typical value for packed beds of spherical particles. Equations 16 and 17 can be combined and simplified:

$$-ln\left(\frac{x_{exit} - x_{equilibrium}}{x_{inlet} - x_{equilibrium}}\right) = g\frac{6(1 - \varepsilon_v)A_c L}{D_P\dot{m}}. \tag{18}$$

Using Hutchinson's experimental data, the left hand side of equation 18 can be directly calculated. The terms on the right hand side can be calculated from Hutchinson's data by making reasonable estimates of the geometry of his test apparatus based on pictures and available dimensions. Using the data and the mass transfer governing equation, a fit was obtained for g. It should be noted that some of Hutchinson's data were omitted in obtaining the fit. Hutchinson et al. [50] discussed these data and expressed doubt about the accuracy of points taken at very low space velocity (which correspond to high PL/$\dot{m}$). The uncertainty in the low-space-velocity experimental trials arose because, for these trials, the majority of the hydrogen flow passed through an ortho-para analyzer in which the flow rate was

measured with a less accurate flow meter than that used in the higher velocity trials. In obtaining the fit for g, the points in Hutchinson's data for which more than 20% of the total hydrogen flow was diverted through the less accurate flow meter were not included. Figure 19 shows the fit obtained for g from Hutchinson's data.

The required size of the beds in the pilot plant was estimated by using the value obtained in the curve fit for g. By choosing the desired approach and mass flow – in this case, the mass flow is determined from the cycle simulations – the bed length and transfer perimeter can be determined, effectively specifying the volume $A_c \cdot L$ of the catalyst bed. The approach was chosen to be 2.5% - that is,

$$-ln\left(\frac{x_{exit} - x_{equilibrium}}{x_{inlet} - x_{equilibrium}}\right) = \left(1.34 \cdot 10^{-3}\right)\frac{PL}{\dot{m}}$$
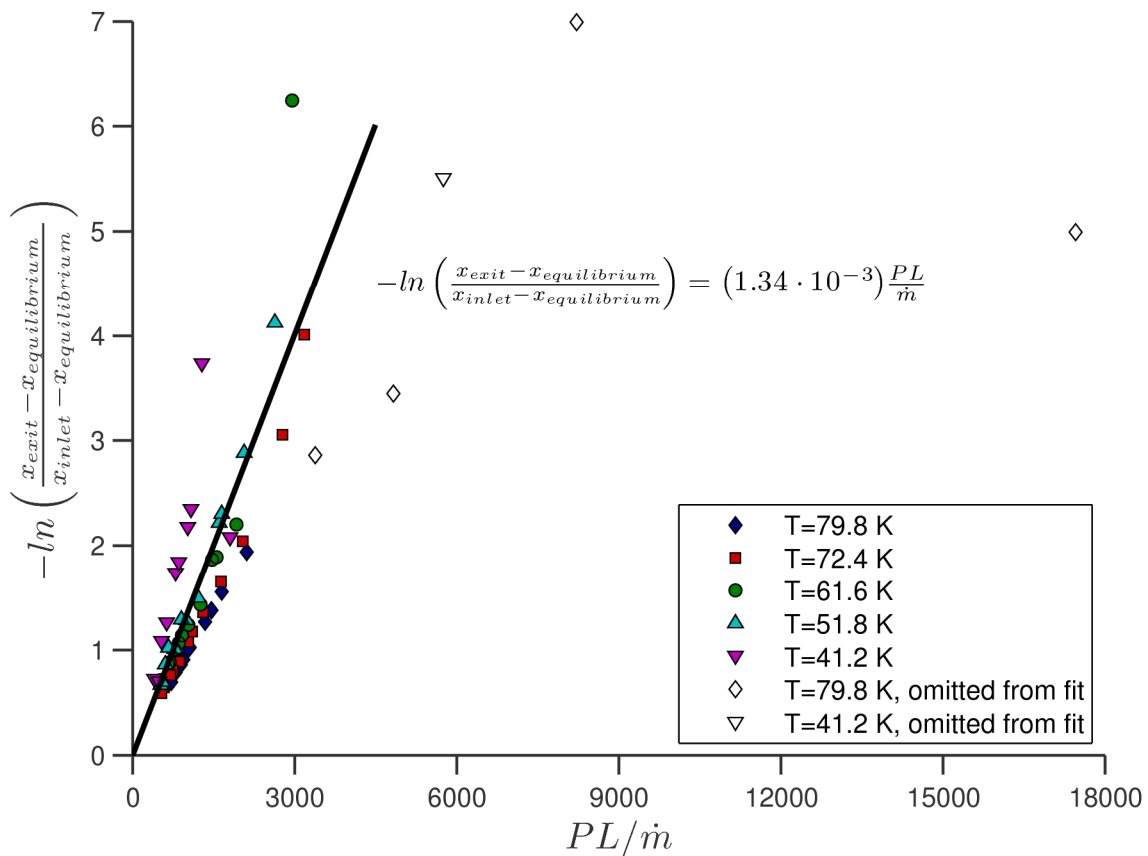
Figure 19: Estimation of the mass transfer conductance from experimental data.

for a fluid element going through the bed, ortho para conversion proceeds 97.5% of the way towards equilibrium before reaching the bed exit. It was assumed that the bed geometry would be wide enough to avoid excessive pressure drop but narrow enough to avoid flow maldistribution in the packed bed. For the pilot plant mass flows, about 1.9 liters of bed volume was required to effect the desired 2.5% approach. The CEL-NBS liquefier described by Weitzel et al., which liquefied hydrogen at about 82% of the pilot plant mass flow, had a hydrous ferric oxide catalyst bed with a volume of about 1.5 liters [30]. This reported size agrees well with the estimated pilot plant size obtained from Hutchinson's data.

A cylindrical bed geometry with a length to diameter ratio of 6 was chosen to determine the Reynolds number and the pressure drop across the packed bed. The characteristic length

$$L_{char} = D_P \left(\frac{\varepsilon_v}{1 - \varepsilon_v} \right) \tag{19}$$

and characteristic velocity

$$v_{char} = \left(\frac{\dot{m}}{\rho \varepsilon_v A_c} \right) \tag{20}$$

were used in the calculation of the Reynolds number:

$$Re = \frac{\rho v_{char} L_{char}}{\mu} . \tag{21}$$

The drop in pressure p was calculated using the Ergun equation [49],

$$\frac{dp}{dx} = \frac{150 \mu v_{char}}{L_{char}^2} + \frac{1.75 \rho v_{char}^2}{L_{char}}, \tag{22}$$

which is valid for $1 < Re < 10^4$. The maximum Reynolds number in the pilot plant catalyst beds was about 280, so the Ergun equation was deemed a satisfactory correlation. For the chosen bed geometry, the largest pressure drop was 0.1 bar, and occurred in the high-temperature catalyst bed. The pressure drops across the medium- and low-temperature beds were 0.04 bar and 0.01 bar, respectively. These pressure drops are not excessive given that the hydrogen stream is compressed to 21 bar. Therefore, the hydrous

ferric oxide catalyst beds in the pilot plant are not expected to present any alarming sizing or pressure drop issues.

Finally, three different configurations of catalysts were tested in the cycle simulation. First, the cycle was simulated with three thermally isolated catalyst beds that received cooling from the helium stream only via an intermediate heat exchanger as shown in Figure 20. Next, helium cooling was added to each catalyst bed to make the hydrogen stream more nearly isothermal, as can be seen in Figure 21. Finally, continuous conversion catalysis was tested in the cycle to see the effect of integrating the catalyst material into the heat exchangers, as shown in Figure 22. The pilot plant improved from 19.8 to 22.1% efficiency in the upgrade from adiabatic to isothermal catalysts. Another increase from 22.1 to 23.3% was gained in the transition from the isothermal beds to continuous conversion. Table 7 summarizes the three scenarios tested. Clearly, removing the heat of conversion must be done with care due to the large impact the catalysis arrangement has on cycle efficiency. In the construction of a liquefaction plant, effort should be put into making the catalyzed ortho-para transition approach continuous conversion as closely as possible.
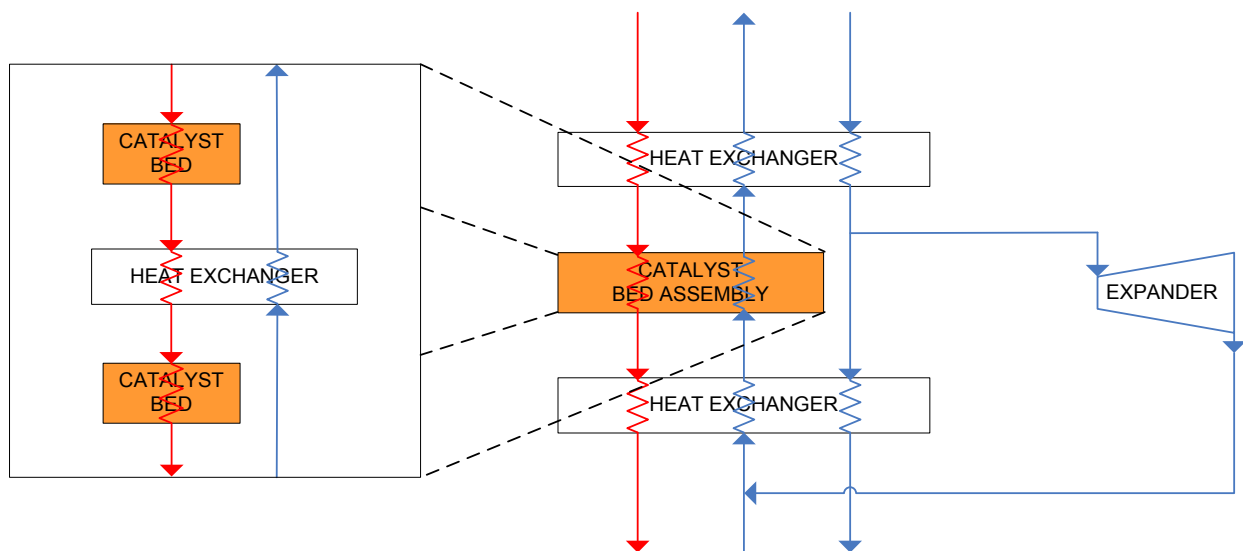
Figure 20: Adiabatic catalyst beds with an intermediate heat exchanger.
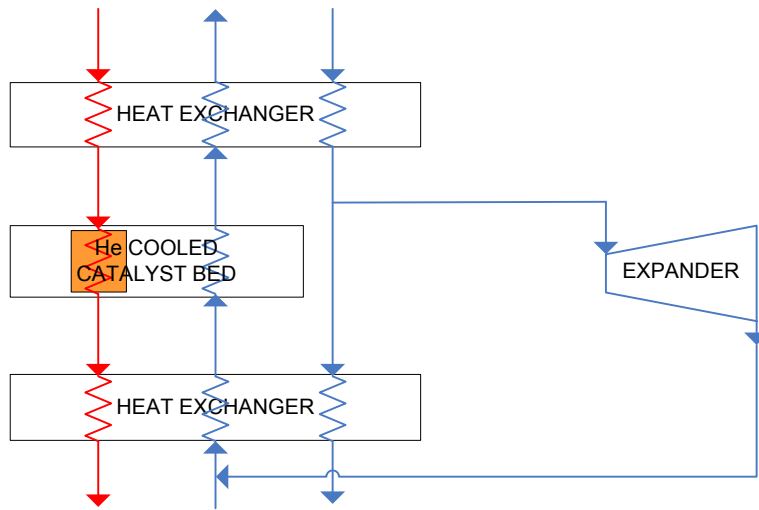
Figure 21: A helium-cooled catalyst bed.
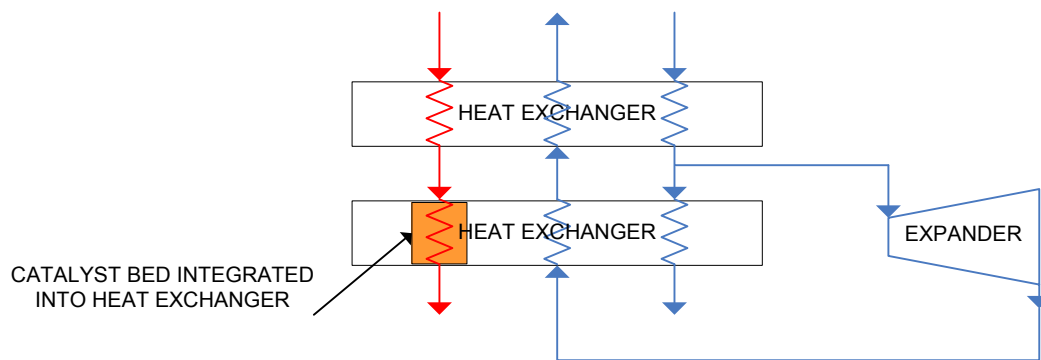
Figure 22: A continuous conversion catalyst bed, in which the ortho para transition occurs over a continuous temperature distribution and takes place as the hydrogen is cooled in the HX.

Table 7: Summary of Three Catalyst Bed Arrangements

		Pilot, 3 adiabatic catalysts	Pilot, 3 isothermal catalysts	Pilot, continuous conversion
	$\Delta T/T$	0.03	0.03	0.03
	η_{exp1}	0.6	0.6	0.6
	η_{exp2}	0.7	0.7	0.7
	η_{exp3}	0.75	0.75	0.75
System parameters	η_{exp4}	0.65	0.65	0.65
	$\eta_{comp,He}$	0.65	0.65	0.65
	$\eta_{comp,H2}$	0.6	0.6	0.6
	$\eta_{wet\_expander}$	0.9	0.9	0.9
	p_{H2} [bar]	21	21	21
	$p_{He,high}$ [bar]	15	15	15
	$p_{He,low}$ [bar]	2.5	2.5	2.5
	T_{atm} [K]	300	300	300
	p_{atm} [bar]	1	1	1
Environmental and final properties	$x_{para,in}$ [-]	0.25	0.25	0.25
	T_f [K]	20	20	20
	p_f [bar]	1	1	1
	$x_{para,f}$ [-]	0.95	0.95	0.95
	η_{cycle}	0.1976	0.2214	0.2333
Simulation result	W_{ideal} [kJ/kg]	14,010	14,010	14,010
	W_{net} [kJ/kg]	70,901	63,279	60,051

3.2. Single-phase wet expander

The single-phase wet expander is used to reduce the pressure of the liquid hydrogen from the supercritical system pressure to the storage pressure of 1 bar. In the pilot plant, the expander would likely be a reciprocating piston and a hydraulic actuator to add and remove work from the piston. It is also conceivable that the expander could be a liquid turbine similar to those used in some nitrogen cycles [51].

A diagram of a basic reciprocating liquid expander can be seen in Figure 23. Valves on the bottom allow the displacement volume to be exposed to the supercritical pressure (intake) and the storage pressure (exhaust). Sensors near the top of the piston indicate when the limits of travel have been reached. The piston is sealed on the warm end with an o-ring, and a small annular gap is

maintained along the length of the piston. Thermal isolation is accomplished with a vacuum space surrounding the cylinder. The piston's length and material provide a large heat conduction resistance to minimize the effects of axial conduction. The small annular gap does not fill with liquid because liquid entering the gap evaporates as the temperature rises, increasing the gap pressure and forcing the liquid back into the displacement volume.
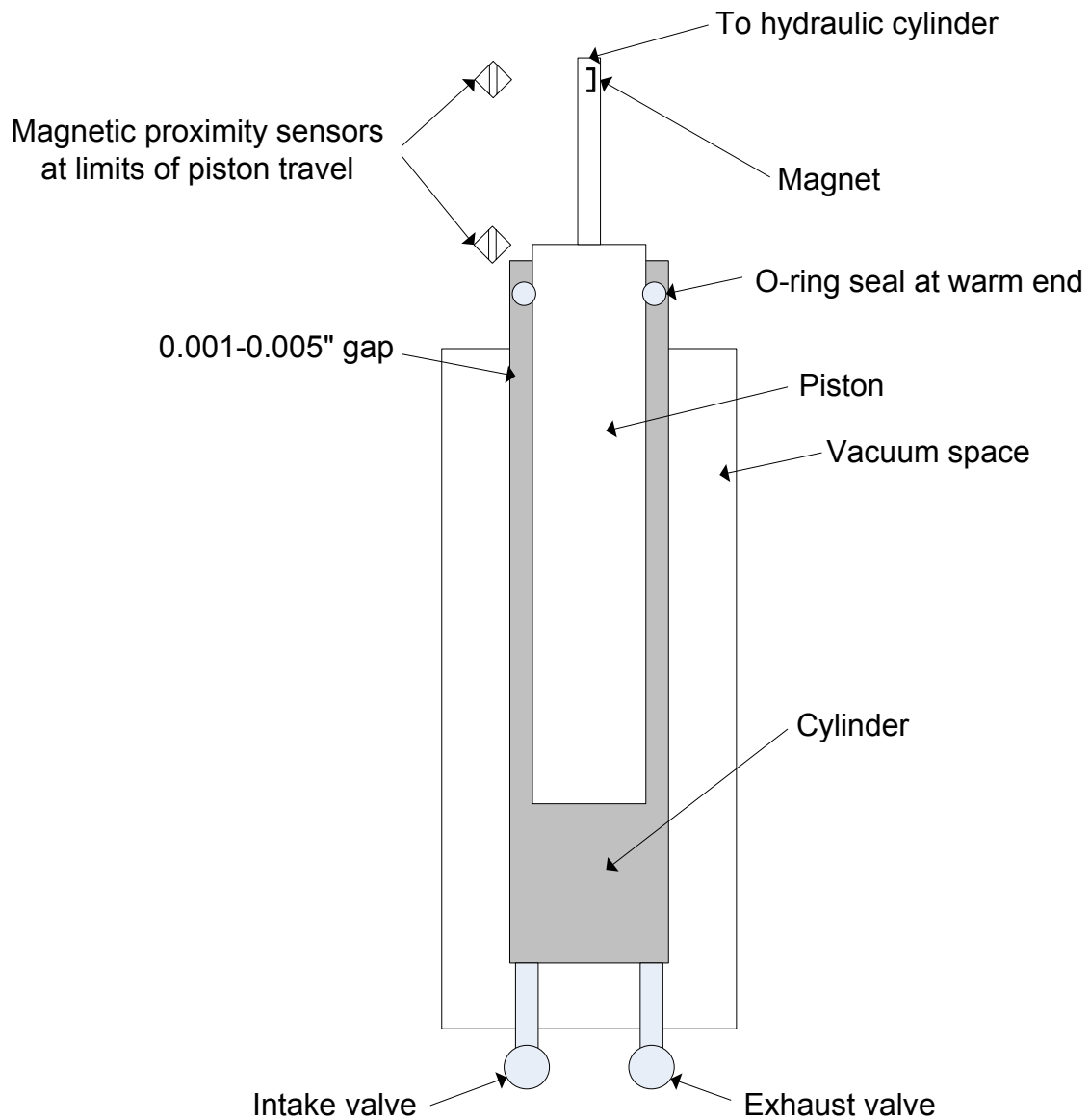
Figure 23: Schematic diagram of the single-phase wet expander.

The expander operates in a four-step process. At the minimum displacement volume, the intake valve opens. High-pressure liquid enters the cylinder as the hydraulic actuator increases the volume and removes work. At the maximum displacement volume, the intake valve closes and the exhaust valve opens, which quickly depressurizes the liquid. Next, the hydraulic actuator forces the low-pressure liquid out until the minimum displacement volume is reached. Finally, the exhaust valve closes and the intake valve opens, and another cycle begins. A simple drawing of a hypothetical pressure volume diagram can be seen in Figure 24. One potential loss mechanism in the wet expander occurs due to the slightly compressible nature of the liquid. When the exhaust valve opens a throttling loss occurs as the high-pressure liquid depressurizes across the valve. Alternatively, after the intake valve closes, the piston can be expanded further to depressurize the liquid, thereby extracting a small amount of work instead of suffering the throttling loss. By looking up the adiabatic compressibility of liquid hydrogen at the expected wet expander conditions [40], this lost work was calculated to be about two orders of magnitude smaller than the net work per stroke. A wet expander very similar in operation to the expander described above has been in operation in the helium liquefier in the MIT Cryogenic Engineering Lab (CEL) for over 30 years.

The approximate size of the expander can be estimated based on the expected mass flow rate

$$\dot{m} = \rho_{H2} f V_{piston} \ , \tag{23}$$

where ρ_{H2} is the average density of liquid hydrogen for the operating pressures, f is the operating frequency, or stroke rate, of the expander, and V_{piston} is the displacement volume of the expander. For a mass flow rate of 500 kg_{H2}/day at a stroke rate of 30 strokes/min (roughly equal to the MIT CEL wet expander stroke rate), a piston volume of 5.5 cubic inches is required. On a 1.5 inch bore piston this corresponds to a stroke of about 3 inches, which is very similar to the MIT CEL wet expander stroke.
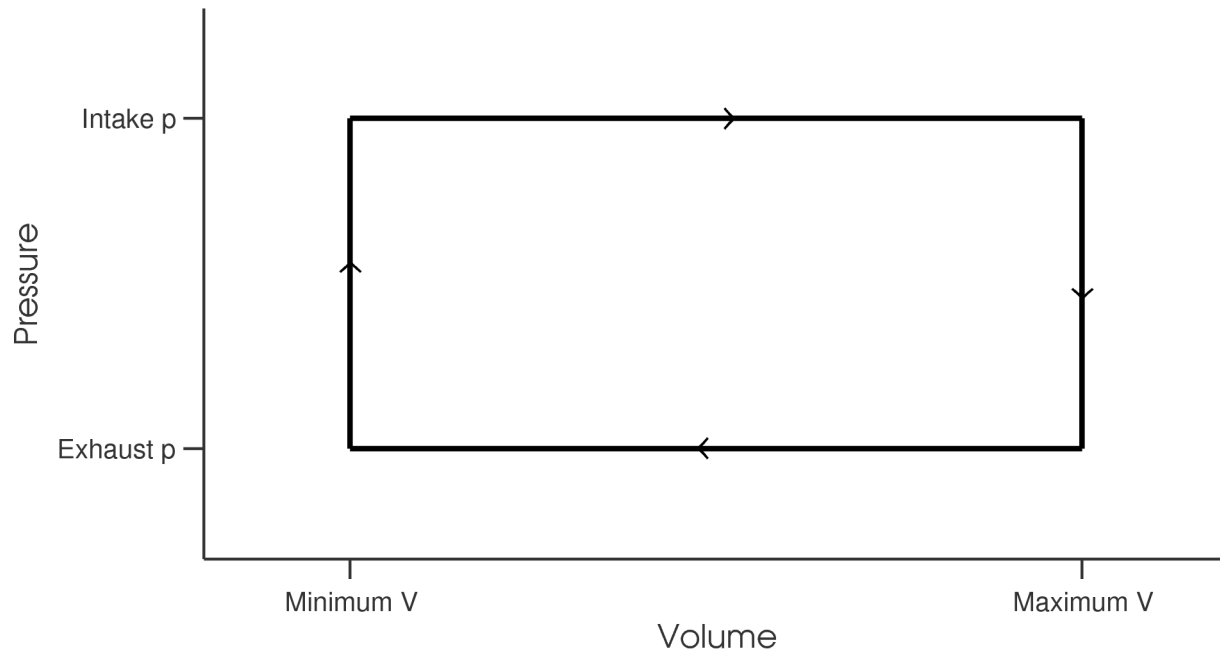
Figure 24: A simple pressure vs. volume diagram for the single-phase wet expander.

The efficiency η of the wet expander is defined as

$$\eta_{wet\_expander} = \frac{h_{in} - h_{out}}{\left(h_{in} - h_{out}\right)_{ideal}} \; , \tag{24}$$

where h_{in} and h_{out} are the specific enthalpy at the intake and exhaust. The ideal state is defined by the exhaust pressure and the intake specific entropy, such that the ideal state would occur at the outlet if the device operated with no entropy generation. For a particular outlet state (in the case of the liquefier, for a particular storage temperature and pressure), a more efficient wet expander allows the intake to be at a higher temperature. The efficiency of the wet expander is bounded by the isentropic case (η=1) and the isenthalpic case (η=0). The isenthalpic case results in no net work output from the expander and is equivalent to a J-T valve. The MIT CEL wet expander operates at over 90% efficiency.

The program-based cycle simulation was run with various wet expander efficiencies. Figure 25 shows the wet expander inlet temperature and pilot plant efficiency for various wet expander efficiencies. The intake temperature for wet expander efficiencies below about 70% is *below* the outlet temperature of

20 K. This means that the system must provide cooling to the hydrogen to offset the losses in the expander. The worst case – the zero efficiency expander, which is equivalent in performance to a J-T valve – requires an intake temperature of 17.7 K. This is substantially lower than the exhaust temperature of 20 K. If a J-T valve is replaced with a 90% efficient wet expander in the pilot plant it results in an efficiency improvement of 2.8 efficiency points, going from 19.4 to 22.2%. With an efficient wet expander, unnecessary subcooling of the hydrogen stream that decreases the system efficiency can be avoided. Although more complex than a J-T valve, a wet expander substantially improves the cycle efficiency.
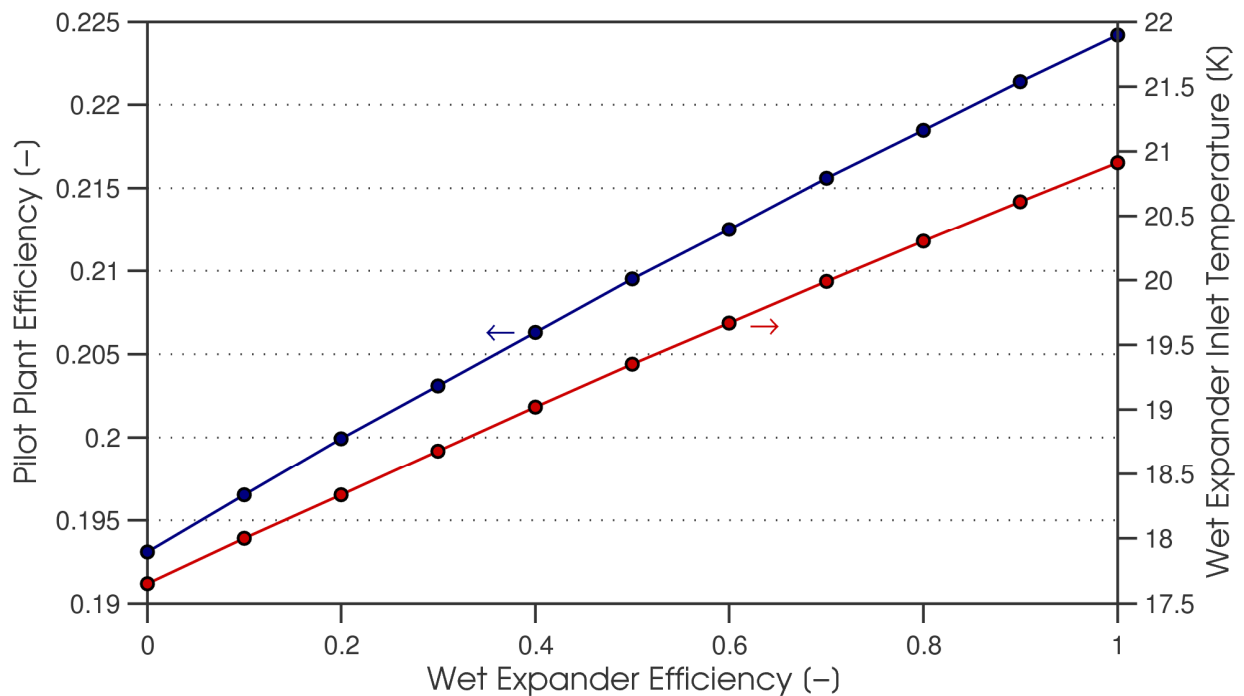
Figure 25: Pilot plant efficiency and wet expander inlet temperature vs. wet expander efficiency. A J-T valve corresponds to a zero efficiency wet expander.

3.3. Heat exchangers

To ensure the accuracy of the simulation results, it was necessary to look deeper into the physics that govern the interactions between the streams in each heat exchanger. Although the First Law will always be satisfied in each heat exchanger in the system simulation, it is possible, in looking at only the inlets and outlets, to have situations in which the First and Second Laws will appear to be satisfied but are, in fact, violated within a heat exchanger. This can be checked by explicitly determining the temperature profiles in each heat exchanger. In addition to providing a reality check to the system simulation results, a detailed heat exchanger simulation determines the size of the heat exchanger (UA) needed to achieve the performance predicted by the cycle. This is important because the cycle simulations only provide information about the temperature approaches of the heat exchangers through the $\Delta T/T$ parameter, and the actual area must be known for accurate estimates of the heat exchanger costs in a plant. Finally, by finding the area of the heat exchangers, more conclusions can be drawn from the cycle simulations. For example, the relationship between heat exchanger area and plant efficiency can be determined for various operating conditions. This information can prove valuable in cost benefit analysis.

3.3.1. Single heat exchanger

While the temperature profiles in a two-pass heat exchanger can be explicitly determined knowing the temperatures at one end, the mass flows, the heat transfer properties and the total heat exchange area [52], similar expressions for a three-pass heat exchanger are more complex. Using a differential equation solver program in MATLAB, the temperature profile in each of the cycle's heat exchangers was determined. Since some of the heat exchangers have three streams, assumptions had to be made about the heat exchanger to solve the differential equations. It was assumed that thermal communication does not occur between the hydrogen stream and the high-pressure helium stream. In addition, it was assumed that the heat transfer coefficient (U) was constant in each heat exchanger and was not a function of temperature. Axial conduction and pressure drop were neglected. Finally, it was

assumed that a certain, constant fraction X of each heat exchanger's total UA was devoted to cooling the hydrogen stream. For a given heat exchanger, then, the UA devoted to the hydrogen stream was UA·X.

A differential element of a three-pass heat exchanger can be seen in Figure 26. The streams are labeled A, B, and C to keep the expression general – in the cycle, A corresponds to the hydrogen stream, B to the low-pressure helium, and C to the high-pressure helium. The First Law for the heat exchanger element,

$$0 = \dot{m}_A c_{p,A}\left(T_A - \left(T_A + dT_A\right)\right) + \dot{m}_B c_{p,B}\left(\left(T_B + dT_B\right) - T_B\right) + \dot{m}_C c_{p,C}\left(T_C - \left(T_C + dT_C\right)\right), \tag{25}$$

where $\dot{m}$ is the mass flow, T is the temperature, and c_p is the isobaric specific heat capacity, can be simplified to

$$\dot{m}_B c_{p,B} dT_B = \dot{m}_A c_{p,A} dT_A + \dot{m}_C c_{p,C} dT_C . \tag{26}$$

Also, the First Law can be applied to stream A to obtain an expression for δQ_A:

$$\delta Q_A = \dot{m}_A c_{p,A}\left(T_A - \left(T_A + dT_A\right)\right), \tag{27}$$

which simplifies to

$$\delta Q_A = -\dot{m}_A c_{p,A} dT_A . \tag{28}$$

Applying a similar technique to stream C, it can be shown that

$$\delta Q_C = -\dot{m}_C c_{p,C} dT_C . \tag{29}$$

The convective heat transfer from streams A and C provide alternate expressions for δQ_A and δQ_C by introducing the heat transfer coefficient U, the area A, and the fraction of the heat exchange area devoted to heat transfer between A and B, X. The expressions

$$\delta Q_A = \left(T_A - T_B\right) X d\left(UA\right) \tag{30}$$

and

$$\delta Q_C = \left(T_C - T_B\right)\left(1 - X\right) d\left(UA\right) \tag{31}$$

can be equated to the expressions from the First Law, equations 28 and 29, to eliminate the variables δQ_A and δQ_C. The resulting two equations, along with equation 26, can be solved to obtain a set of three coupled ordinary differential equations (ODEs):

$$\frac{dT_A}{d(UA)} = -\frac{(T_A - T_B)X}{\dot{m}_A c_{p,A}},$$ (32)

$$\frac{dT_C}{d(UA)} = -\frac{(T_C - T_B)(1 - X)}{\dot{m}_C c_{p,C}}, \text{ and}$$ (33)

$$\frac{dT_B}{d(UA)} = \frac{\dot{m}_A c_{p,A}}{\dot{m}_B c_{p,B}} \frac{dT_A}{d(UA)} + \frac{\dot{m}_C c_{p,C}}{\dot{m}_B c_{p,B}} \frac{dT_C}{d(UA)}.$$ (34)

A program was created that solves equations 32-34 using ode45, a MATLAB ODE solver. The temperatures at the top of the heat exchanger, the mass flow rates, the heat exchanger UA, and X are
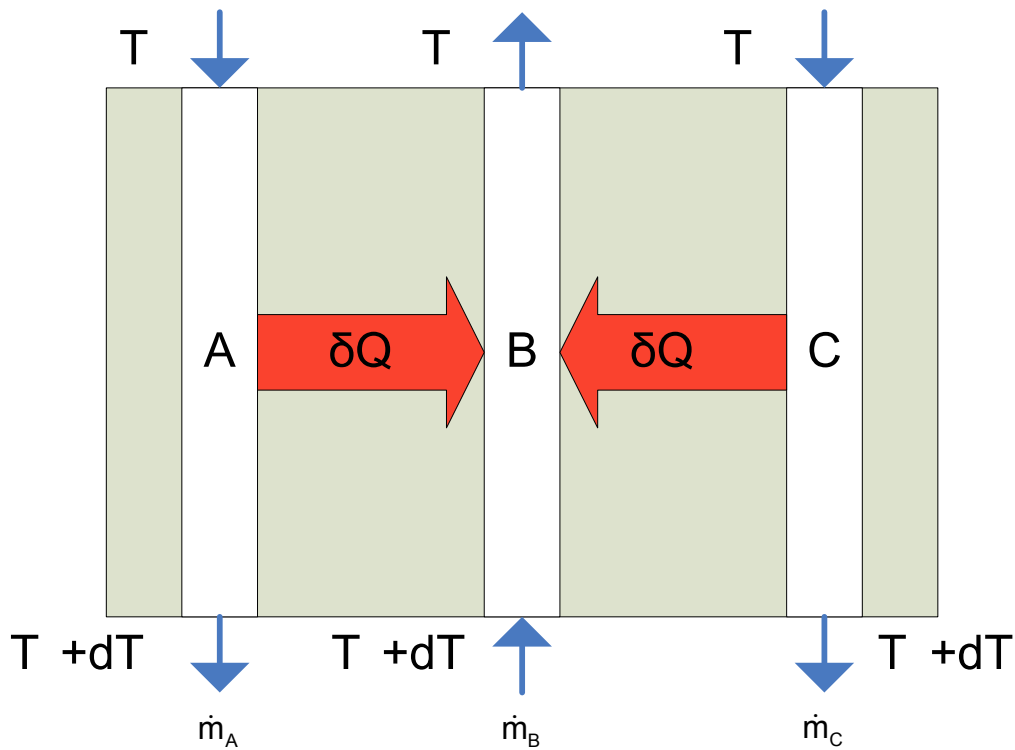
Figure 26: A differential three-pass heat exchanger element.

entered as inputs to the function. The equations are integrated numerically to the final UA and the program returns the temperatures at the bottom of the heat exchanger.

The heat exchanger simulation was designed to account for variations in the fluid properties of each stream because these properties can be strongly temperature dependent. These properties are calculated for each fluid at each iteration of the differential equation solver. Fluid properties are called from REFPROP from within the MATLAB code. An example of one of the calculated temperature profiles can be seen in Figure 27. The circles indicate an iteration point and the arrows indicate the direction of flow for a particular fluid.
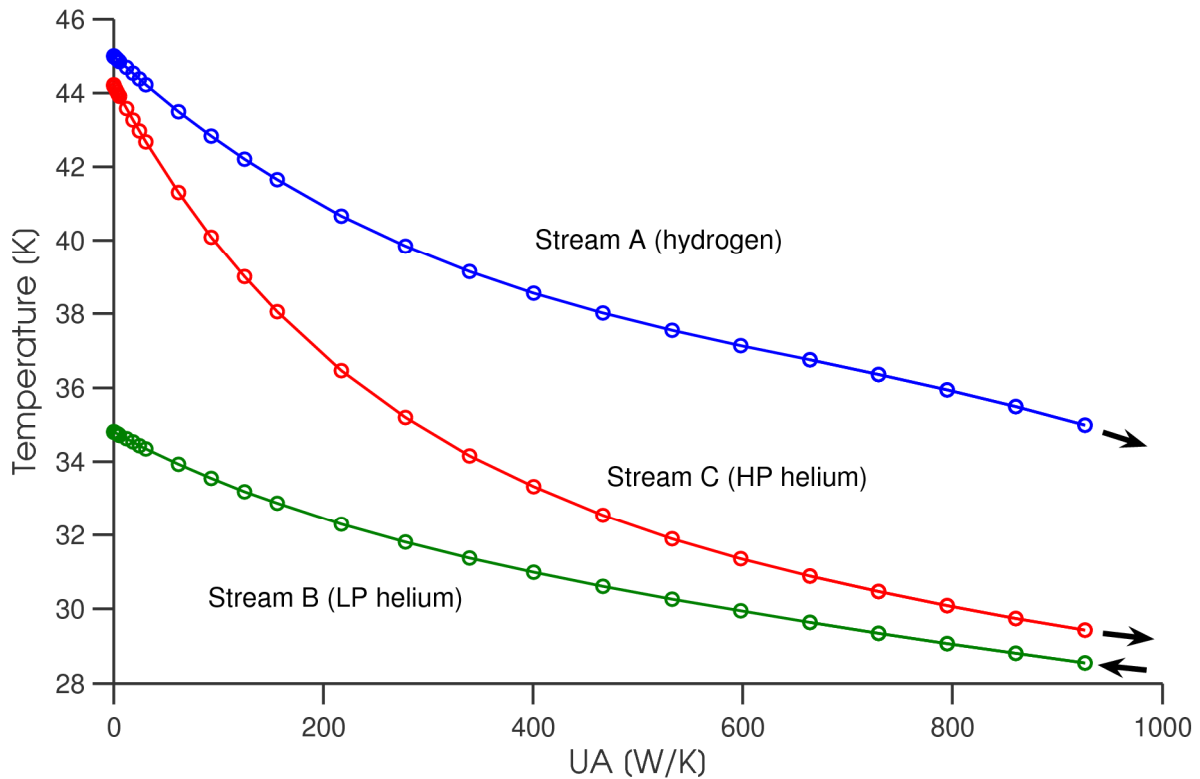
Figure 27: Example of results of three-way HX simulation. Circles indicate iteration points used by the ODE solver.

3.3.2. Heat exchange area

The single HX simulation provided a way to determine the temperatures at one end of a three-pass HX with known UA and X; however, this functionality is of limited use because the cycle simulator returns temperatures at both ends of each HX, while UA and X are unknown. At first, the desired functionality was achieved "manually" by repeatedly solving the single HX simulation with different inputs until the desired output temperatures were realized. The difficulty associated with this technique made it apparent that a method of automatically determining UA and X for a HX with known temperatures was needed.

A MATLAB function – the *UA finder* – was created to determine UA and X for the heat exchangers described by the cycle simulation. The inputs to the function are the endpoint temperatures, the mass flows, the pressures, and the para content of the hydrogen stream. First, the function uses the temperatures, flow rates and average fluid properties to make rough estimates of UA and X using a basic log mean temperature difference (LMTD) method. The single HX function described above is then called using the input top temperatures and the newly estimated values of UA and X. The resulting estimated bottom temperatures are subtracted from the input bottom temperatures to obtain an error term for each stream. These error terms are squared and summed: the program iterates to minimize this total error. In valid HXs, the minimized total squared error is very small, but the error can be substantial if a HX has internal Second Law violations. Large errors rarely occurred in the simulations – most of the time the error in each temperature output was less than 0.1 K. Alteration of the hydrogen stream temperatures in the cycle simulation allowed any potentially flawed heat exchanger profiles to be corrected.

The total system UA was determined by incorporating the UA finder into the cycle simulation program. After the temperatures in the cycle were determined, the UA finder determined the required UA of each HX in the system. A schematic of the base configuration can be seen in Figure 12, and a summary

of the assumptions and parameters for the pilot and large plants can be seen in Table 6. Figure 28 and Figure 29 show the UA distribution for the base configuration of the pilot plant and of the large plant.

More interestingly, Figure 30 shows the effect of UA on cycle efficiency for the large plant for various compressor isothermal efficiencies. For a given helium compressor efficiency, the system efficiency initially increases rapidly with increasing UA, but returns quickly diminish with further increases. The base configuration operating point is indicated in Figure 30. Since the base configuration lies on the steep part of the curve, it can be concluded that adding UA would be a good way to improve the system efficiency. Figure 30 also demonstrates the importance of building a cycle with adequate heat exchange area; a small decrease in UA can cause the cycle efficiency to plummet if the design point is on the steep part of the curve.
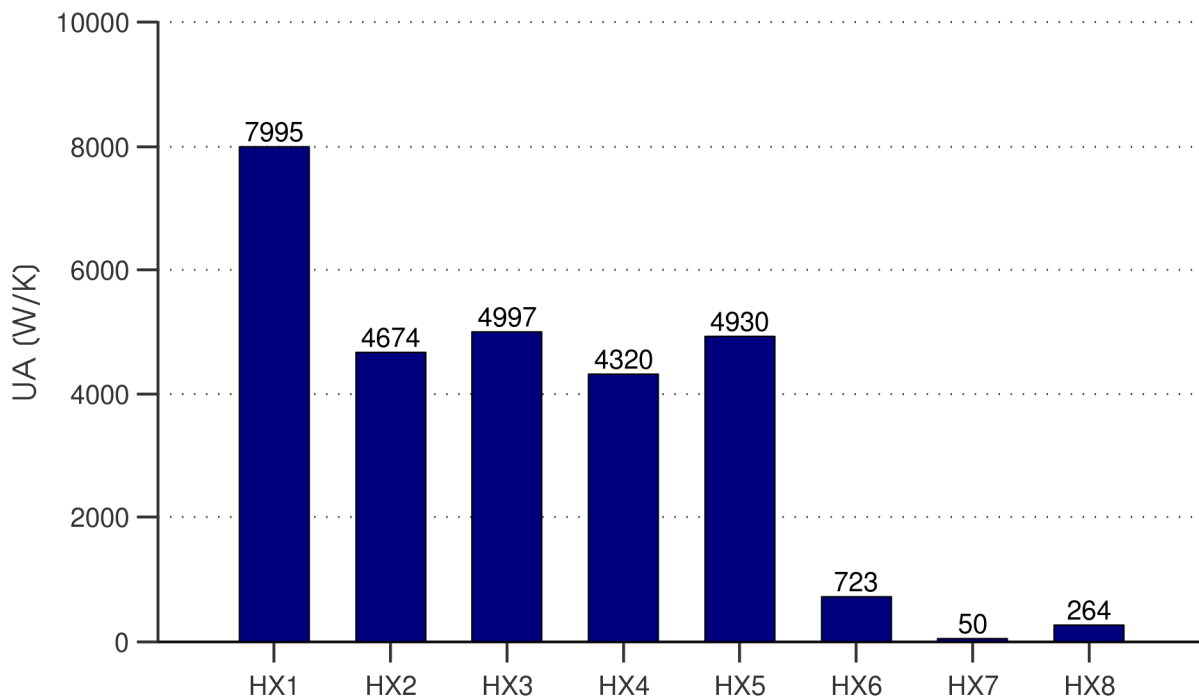
Figure 28: UA for each heat exchanger in the pilot plant.
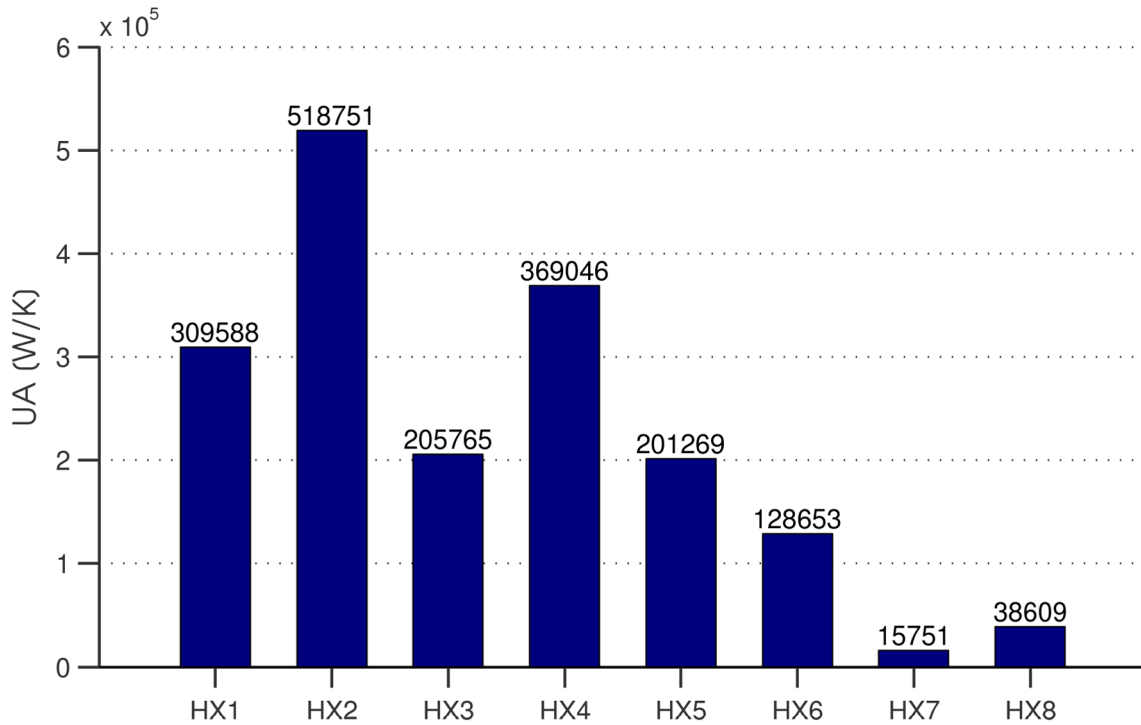
Figure 29: UA for each heat exchanger in the large plant.
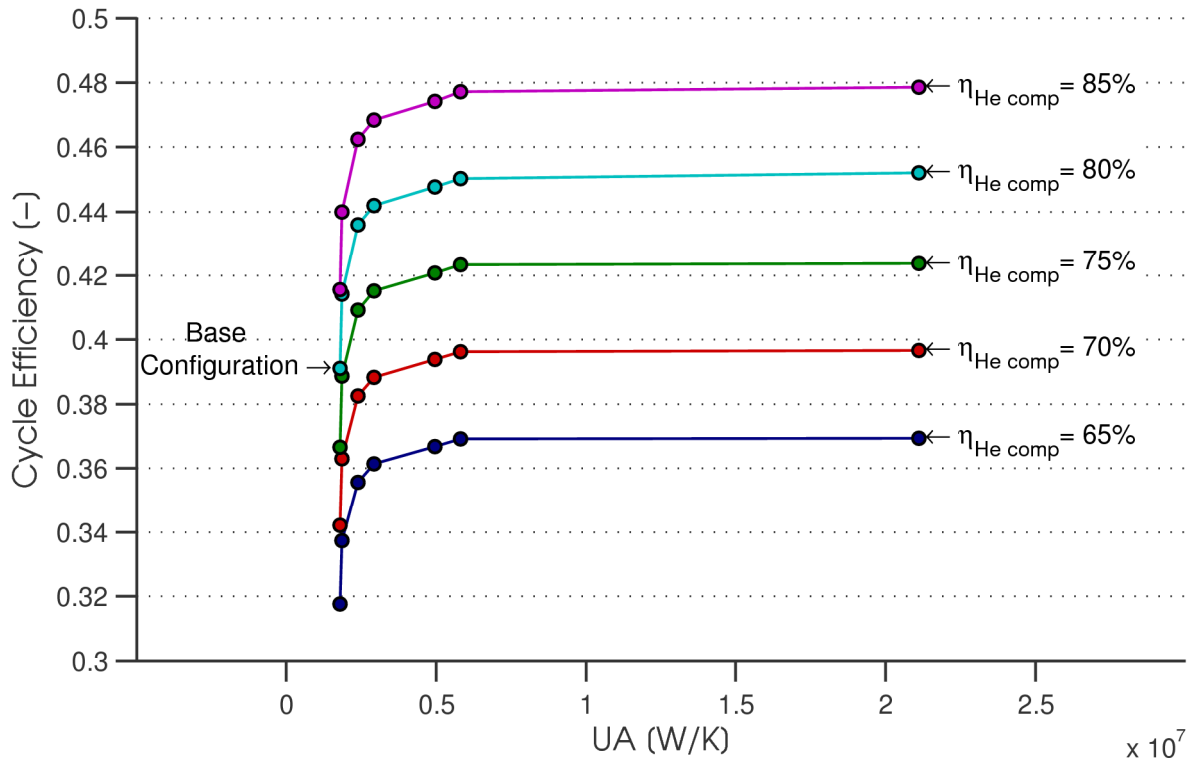
Figure 30: Effect of UA on cycle efficiency for the large plant.

CHAPTER 4. SUMMARY

The proposed cycle offers several advantages over a conventional Claude-cycle-based hydrogen liquefaction system. These benefits include

- a simple, full-yield hydrogen stream;

- minimal hydrogen sealing and no hydrogen turbomachinery;

- a supercritical hydrogen stream with well-balanced heat exchangers and no distinct phase change;

- efficient pressure reduction using a single-phase wet expander;

- a working fluid that is safe and chemically inert, and for which efficient cryogenic expanders are readily procurable;

- overlapping low-temperature expanders that accommodate the large heat load imposed by the hydrogen stream near the critical point;

- a design that can be upgraded with the addition of integrated ortho-para catalyst in the hydrogen stream of the heat exchangers;

- a scalable architecture that facilitates the construction of a smaller pilot plant before the full industrial-scale plant.

Simulations of the proposed cycle yielded encouraging results. A base configuration was created for the pilot plant and the large plant based on an assessment of reasonable component efficiencies. To determine effective ways to improve the performance, various parameters were changed and the simulations were rerun at these new operating points. The parameters considered were hydrogen pressure, total heat exchanger UA (a function of $\Delta T/T$), and individual component efficiencies. It was shown that the cycle efficiency was sensitive to the helium compressor efficiency and, for the pilot plant, the efficiency of expander 3. Depending on the operating point, changes in the heat exchanger UA had either a strong or weak effect on the cycle efficiency.

The efficiency of the large plant appears to meet or exceed that of a current industrial-scale hydrogen liquefaction plant. According to Voth and Parrish [19] and Strobridge [15], the most efficient liquefaction plants have Second Law efficiencies of 30-35%. For the base configuration of the proposed large plant, the Second Law efficiency was calculated to be 39%, and could possibly be made as high as 44% with increases in heat exchanger area. For the smaller pilot plant with less efficient components the efficiency ranged between about 18 and 25%. If the hydrogen liquefaction industry grows due to increased demand, the improvements offered by the large plant could result in great energy savings and appreciably reduced operating expenses, thereby improving the utility of liquid hydrogen as an energy carrier.

References

[1] I. L. Drell and F. E. Belles, "Survey of Hydrogen Combustion Properties," Lewis Flight Propulsion Laboratory, Cleveland, OH, NACA Report 1383, 1957.

[2] F. Barbir and T. Gómez, "Efficiency and Economics of Proton Exchange Membrane (PEM) Fuel Cells," *International Journal of Hydrogen Energy,* vol. 21, no. 10, pp. 891-901, 1996.

[3] F. Barbir, *PEM Fuel Cells: Theory and Practice.* Burlington, MA: Elsevier Academic Press, 2005.

[4] G. D. Brewer, "The Prospects for Liquid Hydrogen Fueled Aircraft," *International Journal of Hydrogen Energy,* vol. 7, no. 1, pp. 21-41, 1982.

[5] J. Milliken, "Hydrogen Program: FY2009 Budget Request Briefing," *DOE Hydrogen Program: Budget,* 2008. [Online]. Available: http://www.hydrogen.energy.gov/pdfs/doe_h2_fy09_budget_rollout.pdf. [Accessed: April 29, 2008].

[6] California Hydrogen Highway Network, "Stations, Cars, and Transit Buses," [Online]. Available: http://www.hydrogenhighway.ca.gov/stations_cars/stations_cars.htm. [Accessed: May 8, 2008].

[7] BC Hydrogen Highway, "Hydrogen Highway | Welcome," [Online]. Available: http://www.hydrogenhighway.ca. [Accessed: May 8, 2008].

[8] W. Peschka, "Hydrogen: The Future Cryofuel in Internal Combustion Engines," *International Journal of Hydrogen Energy,* vol. 23, no. 1, pp. 27-43, 1998.

[9] G. Kiesgen, M. Klüting, C. Bock and H. Fischer, "The New 12-Cylinder Hydrogen Engine in the 7 Series: The H2 ICE Age has Begun," SAE Technical Paper Series, 2006-01-0431, 2006.

[10] A. K. Jaura, W. Ortmann, R. Stuntz, B. Natkin and T. Grabowski, "Ford's H^2RV: An Industry First HEV Propelled with a H_2 Fueled Engine – A Fuel Efficient and Clean Solution for Sustainable Mobility," SAE Technical Paper Series, 2004-01-0058, 2004.

[11] S. Aso, M. Kizaki and H. Mizuno, "Development Progress of the Toyota Fuel Cell Hybrid Vehicle," SAE Technical Paper Series, 2008-01-0420, 2008.

[12] A. Züttel, "Hydrogen Storage Methods," *Naturwissenschaften,* vol. 91, no. 4, pp. 157-172, 2004.

[13] M. Momirlan and T. N. Veziroglu, "Current Status of Hydrogen Energy," *Renewable and Sustainable Energy Reviews,* vol. 6, pp. 141-179, 2002.

[14] W. A. Amos, "Costs of Storing and Transporting Hydrogen," National Renewable Energy Laboratory, Golden, CO, NREL/TP-570-25106, 1998.

[15] T. R. Strobridge, "Cryogenic Refrigerators – an Updated Survey," Cryogenics Division, National Bureau of Standards, Boulder, CO, Technical Note 655, 1974.

[16] H. Quack, "Conceptual Design of a High Efficiency Large Capacity Hydrogen Liquefier," *Advances in Cryogenic Engineering*, vol. 47A, pp. 255-263, 2002.

[17] Energy Information Association. "Average Retail Price of Electricity to Ultimate Customers by End-Use Sector, by State," [Online]. Available: http://www.eia.doe.gov/cneaf/electricity/epm/table5_6_a.html. [Accessed: April 29, 2008].

[18] Energy Information Association. "Table 5.14c Heat Content of Petroleum Consumption: Transportation and Electric Power Sectors, Selected Years, 1949-2006," [Online]. Available: http://www.eia.doe.gov/emeu/aer/pdf/pages/sec5_37.pdf. [Accessed: April 29, 2008].

[19] R. O. Voth and W. R. Parrish, "Studies of Hydrogen Liquefier Efficiency and the Recovery of the Liquefaction Energy. Cryogenics Division, National Bureau of Standards, Boulder, CO, NBSIR 77-862, 1977.

[20] H. W. Woolley, R. B. Scott and F. G. Brickwedde, "Compilation of Thermal Properties of Hydrogen in its Various Isotopic and Ortho-Para Modifications," *Journal of Research of the National Bureau of Standards,* vol. 41, pp. 379-475, Research Paper RP1932, 1948.

[21] R. B. Scott, F. G. Brickwedde, H. C. Urey and M. H. Wahl, "The Vapor Pressures and Derived Thermal Properties of Hydrogen and Deuterium," *Journal of Chemical Physics*, vol. 2, pp. 454-464, 1934.

[22] Y. Y. Milenko, R. M. Sibileva and M. A. Strzhemechny, "Natural Ortho-Para Conversion Rate in Liquid and Gaseous Hydrogen," *Journal of Low Temperature Physics,* vol. 107, nos. 1-2, pp. 77-92, 1997.

[23] W. Peschka, *Liquid Hydrogen: Fuel of the Future.* Berlin: Springer-Verlag, 1992.

[24] R. Gross, W. Otto, A. Patzelt, and M. Wanner, "Liquid Hydrogen for Europe – the Linde Plant at Ingolstadt," *Reports on Science and Technology,* vol. 54, pp. 37-43, 1994.

[25] M. S. Lipman, H. Cheung and O. P. Roberts, "Continuous Conversion Hydrogen Liquefaction," *Chemical Engineering Progress,* vol. 59, no. 8, pp. 49-54, 1963.

[26] D. Zhou and N. S. Sullivan, "Efficient Ortho Hydrogen to Para Hydrogen Conversion," *Bulletin of the American Physical Society,* vol. 49, no. 1, 2004.

[27] G. E. Schmauch and A. H. Singleton, "Technical Aspects of Ortho-Parahydrogen Conversion," *Industrial Engineering Chemistry,* vol. 56, no. 5, pp. 20-31, 1964.

[28] P. C. Vander Arend, "Large-Scale Liquid Hydrogen Production," *Chemical Engineering Progress,* vol. 57, no. 10, pp. 62-67, 1961.

[29] C. R. Class, R. P. Spero, and G. E. McIntosh, "Efficient Utilization of Ortho-para Catalyst," *Advances in Cryogenic Engineering,* vol. 3, pp. 64-72, 1957.

[30] D. H. Weitzel, C. C. Van Valin, and J. W. Draper, "Design Data for Ortho-parahydrogen Converters," *Advances in Cryogenic Engineering,* vol. 3, pp. 73-84, 1957.

[31] W. A. Wilson and D. H. Weitzel, "Vapor Phase Ortho-para Conversion in the Large CEL-NBS Hydrogen Liquefier," *Advances in Cryogenic Engineering,* vol. 3, pp. 85-91, 1957.

[32] P. L. Barrick, L. F. Brown, H. L. Hutchinson, and R. L. Cruse, "Improved Ferric Oxide Gel Catalysts for Ortho-parahydrogen Conversion," *Advances in Cryogenic Engineering,* vol. 10, pp. 181-189, 1965.

[33] H. L. Hutchinson, "A Kinetics Study of the Para-ortho Shift of Hydrogen," M. S. Thesis, University of Colorado, Boulder, CO, 1964.

[34] I. F. Silvera, "The Solid Molecular Hydrogens in the Condensed Phase: Fundamentals and Static Properties," *Review of Modern Physics,* vol. 52, no. 2, part 1, pp. 393-452, 1980.

[35] N. S. Sullivan, D. Zhou and C. M. Edwards, "Precise and Efficient *in Situ* Ortho–Para-Hydrogen Converter," *Cryogenics,* vol. 30, pp. 734-735, 1990.

[36] Molecular Products, Inc. "IONEX® - Type O-P Catalyst: Hydrous Ferric Oxide," [Online]. Available: http://www.molecularproducts.co.uk/uploads/File/Inc/Datasheets/O-P%20Catalyst%20Doc%20166.pdf. [Accessed: May 9, 2008].

[37] J. G. Hust and R. B. Stewart, "A Compilation of the Property Differences of Ortho and Para Hydrogen or Mixtures of Ortho and Para Hydrogen," National Bureau of Standards, Boulder, CO, NBS Report 8812, 1965.

[38] L. Haar, A. S. Friedman and C. W. Beckett, "Ideal Gas Thermodynamic Functions and Isotope Exchange Functions for Diatomic Hydrides, Deuterides, and Tritides," National Bureau of Standards, Boulder, CO, NBS Monograph no. 20, 1961.

[39] J. Leachman, "Fundamental Equations of State for Parahydrogen, Normal Hydrogen, and Orthohydrogen," M. S. thesis, University of Idaho, 2007.

[40] E. W. Lemmon, M. L. Huber and M. O. McLinden, "REFPROP: Reference Thermodynamic and Transport Properties." NIST Standard Reference Database 23, Version 8.0, National Institute of Standards and Technology, Boulder, CO, 2007.

[41] R. F. Barron, *Cryogenic Systems,* 2nd ed., New York: Oxford, 1985.

[42] E. Almqvist, *History of Industrial Gases,* Boston: Kluwer Academic / Plenum Publishers, 2003.

[43] G. E. McIntosh, "Hydrogen Liquefiers Since 1950," *Advances in Cryogenic Engineering,* vol. 49, pp. 9-15, 2004.

[44] T. M. Flynn, *Cryogenic Engineering,* 2nd ed., New York: Marcel Dekker, 2005.

[45] C. R. Baker and R. L. Shaner, "A Study of the Efficiency of Hydrogen Liquefaction," *International Journal of Hydrogen Energy,* vol. 3, pp. 321-334, 1978.

[46] MATLAB version 7.2.0.232 (R2006a). Natick, Massachusetts: The MathWorks, Inc., 2006.

[47] Microsoft Office Excel 2003. Redmond, Washington: Microsoft Corporation, 2003.

[48] M. Minta and J. L. Smith, "Analytical and Experimental Studies of an Optimum Helium
        Liquefaction Cycle," Sc. D. Thesis, MIT, 1984.

[49] A. F. Mills, *Heat and Mass Transfer*, Boston: Irwin, 1995.

[50] H. L. Hutchinson, P. L. Barrick and L. F. Brown, "Experimental Study of Reaction Kinetics for
        Para-Orthohydrogen at 20º to 80º K," *Advances in Cryogenic Engineering,* vol. 10, pp. 190-196,
        1965.

[51] Cryostar, "Two Cryogenic Pumps Servicing a Liquid Expansion Turbine for a Unique Test,"
        [Online]. Available: http://www.cryostar.com/pdf/turbines/ltg1.pdf. [Accessed: May 15, 2008].

[52] E. G. Cravalho and J. L. Smith, *Engineering Thermodynamics*, Boston: Pitman, 1981.

Appendix A: Supplemental Plots
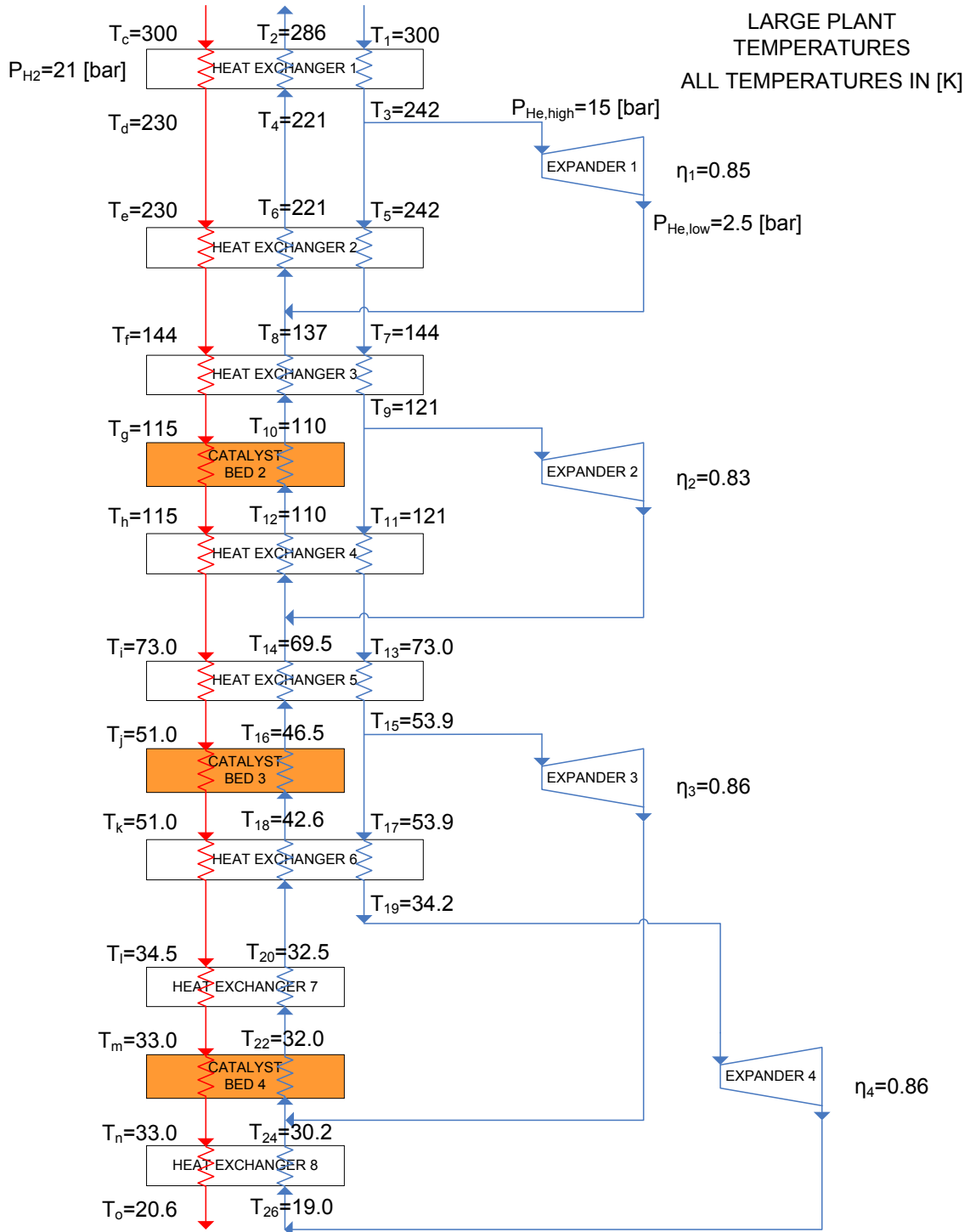
Figure A - 1: Results of large plant cycle simulation.
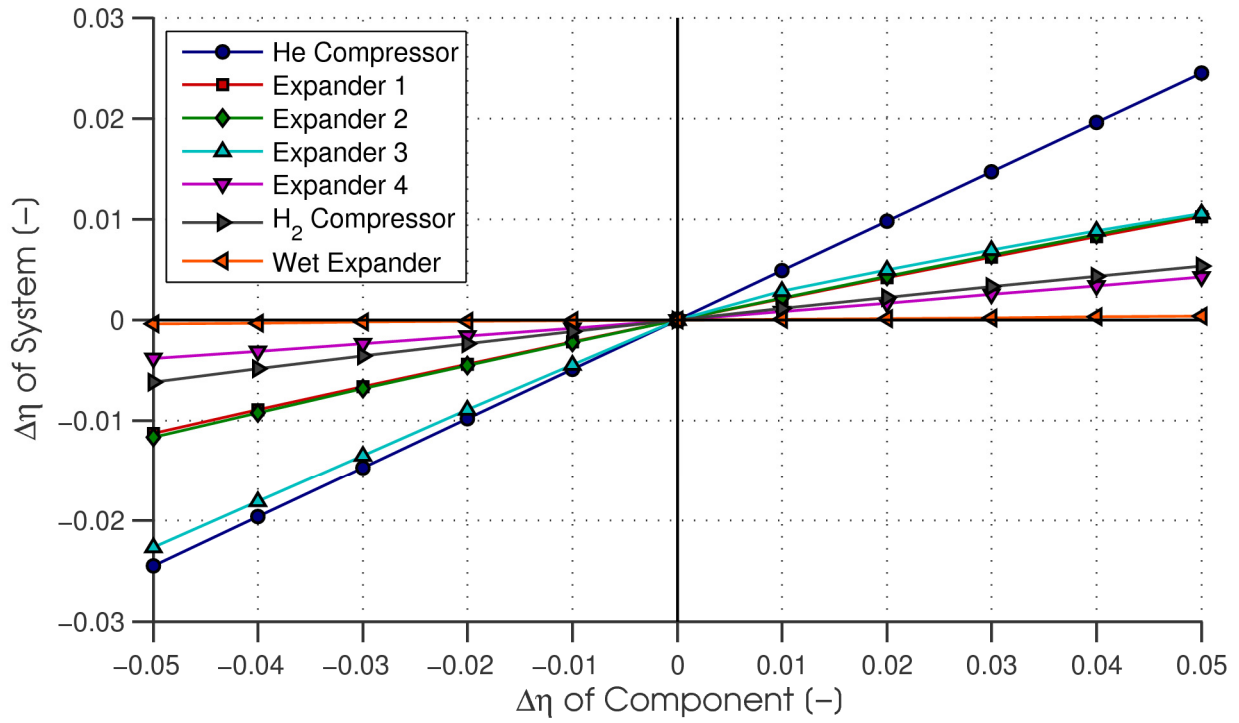
Figure A - 2: Change in large plant system efficiency vs. change in component efficiency, with respect to the base configuration.
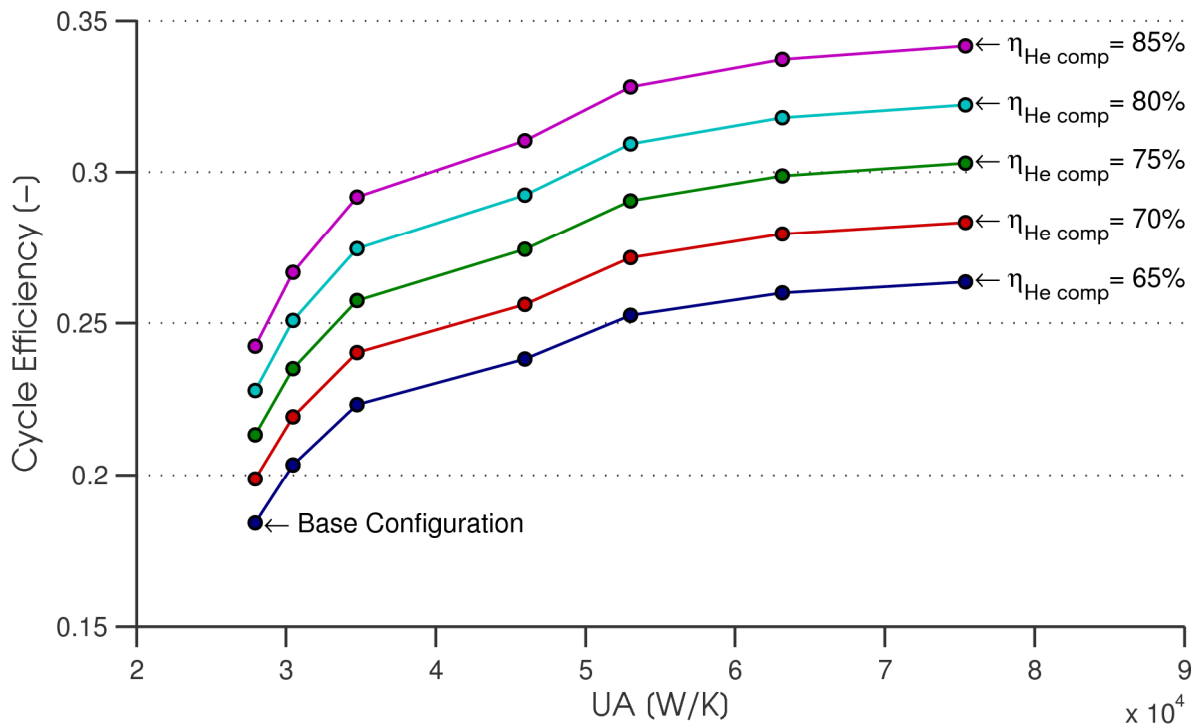
Figure A - 3: Effect of UA on cycle efficiency for the pilot plant.
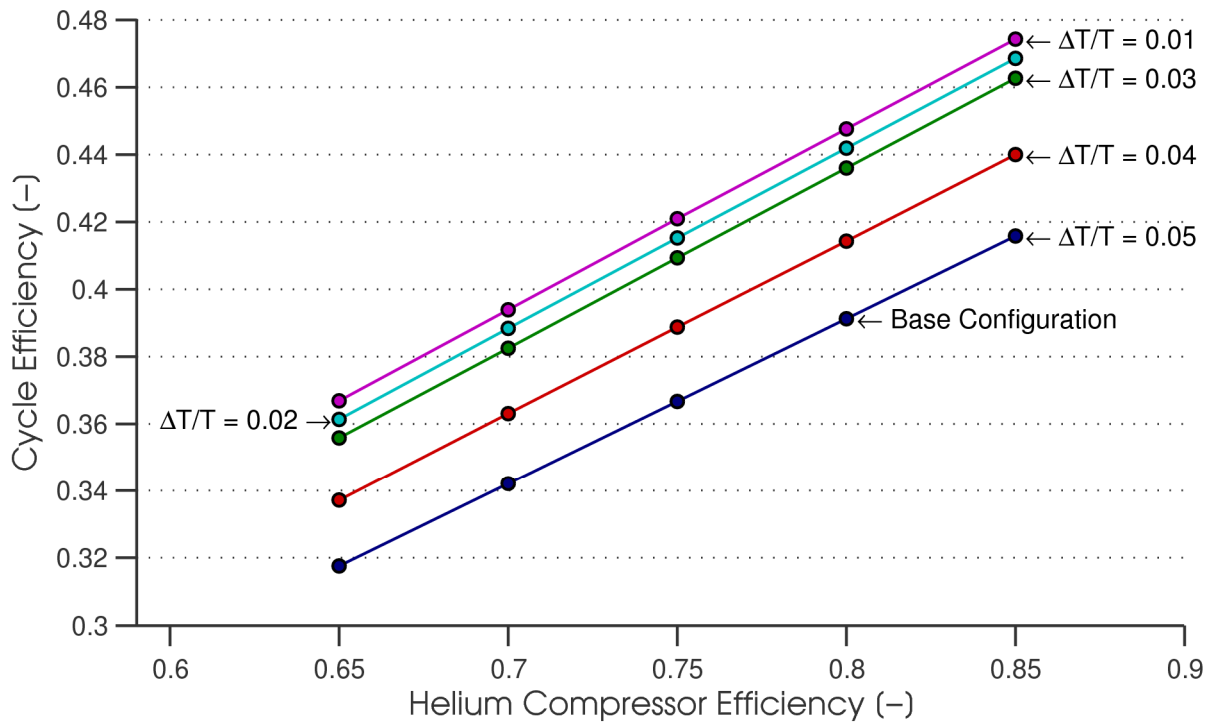
Figure A - 4: Effect of helium compressor efficiency on cycle efficiency for the large plant.
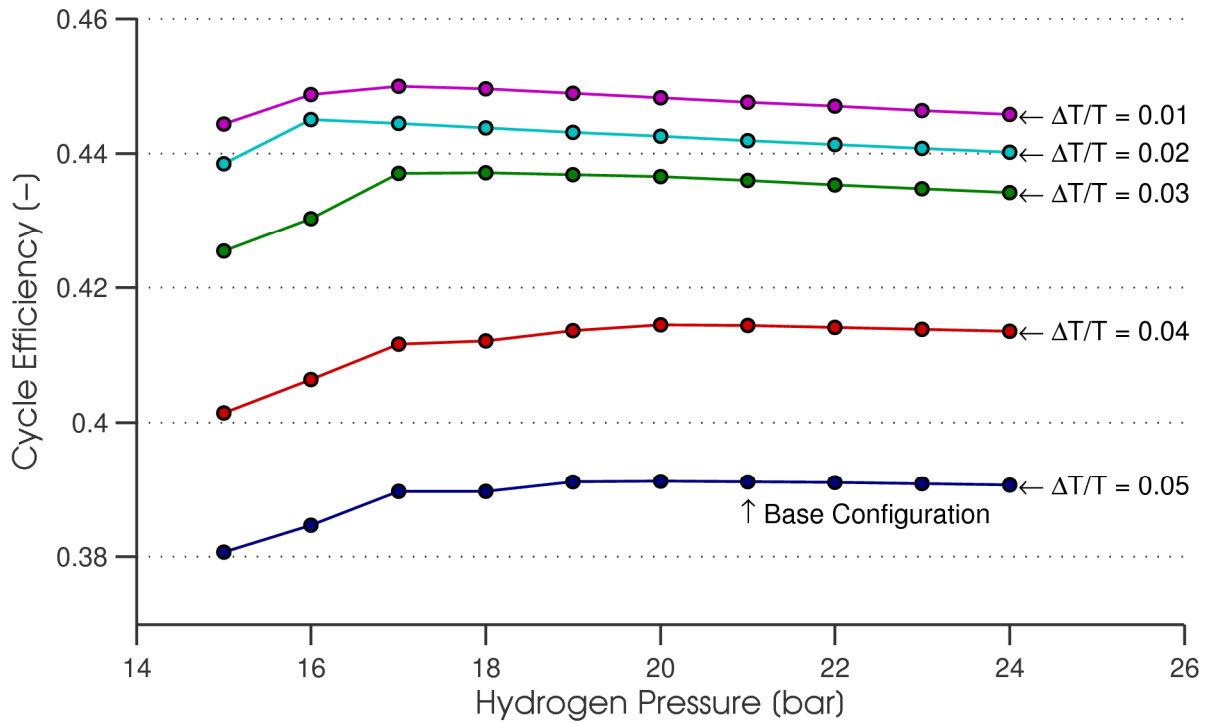
Figure A - 5: Effect of hydrogen pressure on cycle efficiency for the large plant.

Appendix B: MATLAB Code

B1. cycle.m

```matlab
%%%%%%%
%cycle.m
%function that is used in conjunction with optimize.m
%solves system for input of expander fractional mass flow rates and the
overall He mass flow:
%[x1 x2 x3 m_dot_He]
%also calculates a constraint vector for optimize.m

function [y, y2] = cycle(x,type) %x is a vector of the parameters: x1 x2 x3
and m_dot_He
%type 1 - solve system. type 2
%- output existing constr vector for optimization function

persistent constr
%tic

%these global variables allow changes to be made in the cycle parameters
%from within optimiz.m. T_nice and m_dot_nice are global so they are
%available to the user in the MATLAB workspace after optimize.m finishes
global H2_PRESS
global DT_OVER_T
global T_nice
global COMP_EFF
global m_dot_nice
%global energy

%----------SET PLANT TYPE HERE--------------%
variable_change=0;    %0 to set DT/T and P_H2 in cycle.m; 1 to set them in
optimize.m
plant=0;              %0 for pilot plant, 1 for large plant
%-------------------------------------------%




if nargout<1
    type=1;
    %x=[.265487,.264739,.810336,.157723];
    if nargin<1
        if plant==0

x=[0.22189055246724,0.314998846957739,0.794600744675434,0.212403191120857]
%optimum for DT/T=0.03 pilot
        else
```

```matlab
x=[0.218267317662674,0.237828404134626,0.77378776757145,13.353250321925913]
%optimum for DT/T=0.03 large
        end
    end
end


if type==1

    m_dot_He=x(4);

    %--------test to determine whether pilot or large plant--------%
    if plant==0             %pilot plant
        m_dot_H2_daily=500; %kg/day
        eta_ad=[.6 .7 .75 .65];
        %eta_ad=[.8 .8 .8 .8];
        %eta_comp=.8;
        eta_comp=0.65;
        eta_comp_H2=.6;
        T_H2=[300,210,210,150,105,105,75,45,45,35,33,33,20]; %K
        %T_H2=[300,210,210,150,105,105,70,45,45,35,33,33,20]; %K
    else                    %large plant
        m_dot_H2_daily=50000; %kg/day
        eta_ad=[.85 .83 .86 .86];
        eta_comp=0.8;
        eta_comp_H2=.6;
        T_H2=[300,235,235,144,115,115,72,48,48,34.5,33,33,20]; %K
        %T_H2=[300,235,235,144,115,115,69,48,48,34.5,33,33,20]; %K
    end
    %----------------------------------------------------------%


    %-test to determine whether cycle.m or optimize.m will change variables
    if variable_change==0    %values set here
        dToverT=0.05;        %deltaT/T value. base system for pilot plant is
0.05
        P_H2=2100;           %kPa
        H2_PRESS=P_H2;
        DT_OVER_T=dToverT;
        COMP_EFF=eta_comp; %set global variables, for user's peace of mind
    else                     %values set in optimize.m
        P_H2=H2_PRESS;
        dToverT=DT_OVER_T;
        eta_comp=COMP_EFF;


    end
    %-----------------------------------------------------------------%


    m_dot_H2=m_dot_H2_daily/24/3600; %kg/s
```

```matlab
T_atm=300; %K
P_atm=100; %kPa
P_He_high=1500; %kPa
P_He_low=250; %kPa
T_H2_final=20; %K

%find the para content of each H2 state
%equilibrium at c,e,h,k,n (or, in array indices, 1,3,6,9,12)
para_H2=zeros(1,13);
para_H2(1)=para(T_H2(1));
for i=6:3:12 %catalysis at 6,9,and 12
    para_H2(i)=para(T_H2(i));
end

%now, apply the same para content to stages after catalysis:
for i=1:13
    if para_H2(i)~=0
        current_para=para_H2(i);
    else
        para_H2(i)=current_para;
    end
end

%calculate enthalpy and entropy at each H2 state
h_H2=zeros(13);
s_H2=zeros(13);
%optional - energy vector showing energy flow from h2  in each hx/cat
energy=zeros(1,13);
for i=1:13
    [h_H2(i),s_H2(i)]=H2props(T_H2(i),P_H2,para_H2(i));
    if i>1
        energy(1,i-1)=m_dot_H2.*(h_H2(i-1)-h_H2(i));
    end
end

%-------------single-phase wet expander-------------%
eta_wet_expander=0.9; %setting this =0 is equivalent to a J-T valve
T_H2(14)=T_H2(13);
para_H2(14)=para_H2(13);
[h_H2(14),s_H2(14)]=H2props(T_H2(14),P_atm,para_H2(14));

%with the single-phase wet expander:
%from the wet_expander_performance program, the inlet temp can be
%correlated to the wet expander efficiency. a parabolic curve fit is
%obtained in the wet_expander_performance program:
T_H2(13)=(-0.2681)*eta_wet_expander^2 + (3.5264)*eta_wet_expander +
(17.6492);%for PH2=2100kPa
%T_H2(13)=(-0.1927)*eta_wet_expander^2 + (2.9242)*eta_wet_expander +
(18.0460);%1800kPa
[h_H2(13),s_H2(13)]=H2props(T_H2(13),P_H2,para_H2(13));
%----------------------------------------%
```

```matlab
%Helium properties - first zero everything out%
P_He=zeros(1,26);
T_He=P_He;
h_He=P_He;
s_He=P_He;
m_dot=P_He;

%Conservation of mass equations:
m_dot(1:3:4)=m_dot_He;
m_dot(3:5:8)=m_dot(1)*x(1);
m_dot(7)=m_dot(1)-m_dot(3);
m_dot(9:5:14)=m_dot(7)*x(2);
m_dot(13)=m_dot(7)-m_dot(9);
m_dot(15:9:24)=m_dot(13)*x(3);
m_dot(19:7:26)=m_dot(13)-m_dot(15);
m_dot(16)=m_dot(26)+m_dot(24);
m_dot(10)=m_dot(16)+m_dot(14);

%---------optional - nice formatting for m_dot-------%
m_dot_nice=zeros(12,3);
m_dot_nice(1:12,1)=m_dot_H2; %arrange everything into one m_dot matrix
m_dot_nice(1:3,2)=m_dot(4);
m_dot_nice(4:6,2)=m_dot(10);
m_dot_nice(7:11,2)=m_dot(16);
m_dot_nice(12,2)=m_dot(26);
m_dot_nice(1,3)=m_dot(1);
m_dot_nice(2:4,3)=m_dot(7);
m_dot_nice(5:7,3)=m_dot(13);
m_dot_nice(8:9,3)=m_dot(26);
%-------------------------------------------------%

%Pressures
%Odd-numbered points are at high pressure, and even-numbered points are
at
%low pressure:
P_He(1:2:25)=P_He_high;
P_He(2:2:26)=P_He_low;

%Start with the temperatures that are known.
%Temps known by assuming He is the same temp as H2 at stage points:
T_He(1)=T_H2(1);
T_He(7)=T_H2(4);
T_He(13)=T_H2(7);
%Temp known by DELTAT/T assumption at bottom stage:
T_He(26)=T_H2(13)*1/(1+dToverT);

%find these properties:
[h_He(1),s_He(1)]=refpropm('HS','T',T_He(1),'P',P_He(1),'helium');
[h_He(7),s_He(7)]=refpropm('HS','T',T_He(7),'P',P_He(7),'helium');
[h_He(13),s_He(13)]=refpropm('HS','T',T_He(13),'P',P_He(13),'helium');
[h_He(26),s_He(26)]=refpropm('HS','T',T_He(26),'P',P_He(26),'helium');
```

```matlab
    %First law equations:
    h_He(24)=m_dot_H2/m_dot(26)*(h_H2(12)-h_H2(13)) + h_He(26); %HX8
    h_He(22)=m_dot_H2/m_dot(16)*(h_H2(11)-h_H2(12)) + h_He(24); %cat4
    %s_He(24)=refpropm('S','H',h_He(24),'P',P_He(24),'helium');
    h_He(20)=m_dot_H2/m_dot(16)*(h_H2(10)-h_H2(11)) + h_He(22); %HX7

    T_He(19)=expander(eta_ad(4),P_He(26),P_He(19),T_He(26),1);%exp4
    h_He(19)=refpropm('H','T',T_He(19),'P',P_He(19),'helium');

    T_He(24)=refpropm('T','H',h_He(24),'P',P_He(24),'helium');
    T_He(15)=expander(eta_ad(3),P_He(24),P_He(15),T_He(24),1);%exp3
    h_He(15)=refpropm('H','T',T_He(15),'P',P_He(15),'helium');


    h_He(17)=h_He(15);
    h_He(18)=m_dot_H2/m_dot(16)*(h_H2(9)-h_H2(10)) +
m_dot(19)/m_dot(16)*(h_He(17)-h_He(19)) + h_He(20); %HX6
    h_He(16)=m_dot_H2/m_dot(16)*(h_H2(8)-h_H2(9)) + h_He(18); %cat3
    h_He(14)=m_dot_H2/m_dot(16)*(h_H2(7)-h_H2(8)) +
m_dot(13)/m_dot(16)*(h_He(13)-h_He(15)) + h_He(16);%HX5

    T_He(14)=refpropm('T','H',h_He(14),'P',P_He(14),'helium');
    T_He(9)=expander(eta_ad(2),P_He(14),P_He(9),T_He(14),1);%exp2
    h_He(9)=refpropm('H','T',T_He(9),'P',P_He(9),'helium');


    h_He(11)=h_He(9);
    h_He(12)=m_dot_H2/m_dot(10)*(h_H2(6)-h_H2(7)) +
m_dot(13)/m_dot(10)*(h_He(11)-h_He(13)) + h_He(14); %HX4
    h_He(10)=m_dot_H2/m_dot(10)*(h_H2(5)-h_H2(6)) + h_He(12); %cat2
    h_He(8)=m_dot_H2/m_dot(10)*(h_H2(4)-h_H2(5)) +
m_dot(7)/m_dot(10)*(h_He(7)-h_He(9))  +  h_He(10); %HX3

    T_He(8)=refpropm('T','H',h_He(8),'P',P_He(8),'helium');
    T_He(3)=expander(eta_ad(1),P_He(8),P_He(3),T_He(8),1);%exp1
    h_He(3)=refpropm('H','T',T_He(3),'P',P_He(3),'helium');


    h_He(5)=h_He(3);
    h_He(6)=m_dot_H2/m_dot(4)*(h_H2(3)-h_H2(4)) + m_dot(7)/m_dot(4)*(h_He(5)-
h_He(7)) + h_He(8); %HX2
    h_He(4)=m_dot_H2/m_dot(4)*(h_H2(2)-h_H2(3)) + h_He(6); %cat1
    h_He(2)=m_dot_H2/m_dot(4)*(h_H2(1)-h_H2(2)) + m_dot(1)/m_dot(4)*(h_He(1)-
h_He(3)) + h_He(4); %HX1

    %now, find the rest of the properties:
    for i=1:26
        switch i
            case {1,7,13,21,23,25,26}
                %do nothing...these properties are already known
            case {19,15,9,3}
                s_He(i)=refpropm('S','H',h_He(i),'P',P_He(i),'helium');
```

```matlab
            otherwise

[T_He(i),s_He(i)]=refpropm('TS','H',h_He(i),'P',P_He(i),'helium');
        end
    end


    W_comp=m_dot_He*((h_He(2)-h_He(1)) - T_atm*(s_He(2)-
s_He(1)))*(1/eta_comp); %Helium compressor work
    W_exp(1)=m_dot(3)*(h_He(3)-h_He(8)); %expander work
    W_exp(2)=m_dot(9)*(h_He(9)-h_He(14));
    W_exp(3)=m_dot(15)*(h_He(15)-h_He(24));
    W_exp(4)=m_dot(19)*(h_He(19)-h_He(26));

    %Hydrogen at atmospheric pressure/temperature:
    para_atm=para(T_atm);
    [h_H2_atm,s_H2_atm]=H2props(T_atm,P_atm,para_atm);

W_comp_H2=m_dot_H2*((h_H2_atm-h_H2(1)) - T_atm*(s_H2_atm-
s_H2(1)))*(1/eta_comp_H2);
%%%W_comp_H2=0 %only use this when setting the inlet/ref state to 21 bar
%(i.e. excluding the H2 compression work)


    %Now, find the total work and the ideal work, to calculate the cycle
    %efficiency:
    [h_H2_final,s_H2_final]=H2props(T_H2_final,P_atm,para_H2(13));
    %W_ideal_per_kg=( (h_H2_final-h_H2_atm) - T_atm*(s_H2_final-s_H2_atm) )
%J/kg
    W_ideal_per_kg=( (h_H2_final-h_H2(1)) - T_atm*(s_H2_final-s_H2(1))
)*(1/3600)*(1/1000); %kwh/kg

W_ideal=( (h_H2_final-h_H2_atm) - T_atm*(s_H2_final-s_H2_atm) )*m_dot_H2; %W
%%%W_ideal=( (h_H2_final-h_H2(1)) - T_atm*(s_H2_final-s_H2(1)) )*m_dot_H2 %W,
with pressurized inlet condition

    %constraints
    Sgen(1)=-( m_dot_H2*(s_H2(1) - s_H2(2)) + m_dot(4)*(s_He(4)-s_He(2)) +
m_dot(1)*(s_He(1)-s_He(3)) ); %HX1
    Sgen(2)=-( m_dot_H2*(s_H2(2) - s_H2(3)) + m_dot(4)*(s_He(6)-s_He(4)) );
%cat1
    Sgen(3)=-( m_dot_H2*(s_H2(3) - s_H2(4)) + m_dot(4)*(s_He(8)-s_He(6)) +
m_dot(7)*(s_He(5)-s_He(7)) ); %HX2
    Sgen(4)=-( m_dot(3)*(s_He(3)-s_He(8)) ); %exp1

    Sgen(5)=-( m_dot_H2*(s_H2(4) - s_H2(5)) + m_dot(10)*(s_He(10)-s_He(8)) +
m_dot(7)*(s_He(7)-s_He(9)) ); %HX3
    Sgen(6)=-( m_dot_H2*(s_H2(5) - s_H2(6)) + m_dot(10)*(s_He(12)-s_He(10))
); %cat2
    Sgen(7)=-( m_dot_H2*(s_H2(6) - s_H2(7)) + m_dot(10)*(s_He(14)-s_He(12)) +
m_dot(13)*(s_He(11)-s_He(13)) ); %HX4
    Sgen(8)=-( m_dot(9)*(s_He(9)-s_He(14)) ); %exp2
```

```matlab
    Sgen(9)=-( m_dot_H2*(s_H2(7) - s_H2(8)) + m_dot(16)*(s_He(16)-s_He(14)) +
m_dot(13)*(s_He(13)-s_He(15)) ); %HX5
    Sgen(10)=-( m_dot_H2*(s_H2(8) - s_H2(9)) + m_dot(16)*(s_He(18)-s_He(16))
); %cat3
    Sgen(11)=-( m_dot_H2*(s_H2(9) - s_H2(10)) + m_dot(16)*(s_He(20)-s_He(18))
+ m_dot(19)*(s_He(17)-s_He(19)) ); %HX6
    Sgen(12)=-( m_dot(15)*(s_He(15)-s_He(24)) ); %exp3


    Sgen(13)=-( m_dot_H2*(s_H2(10) - s_H2(11)) + m_dot(16)*(s_He(22)-
s_He(20)) ); %HX7
    Sgen(14)=-( m_dot_H2*(s_H2(11) - s_H2(12)) + m_dot(16)*(s_He(24)-
s_He(22)) ); %cat4
    Sgen(15)=-( m_dot_H2*(s_H2(12) - s_H2(13)) + m_dot(26)*(s_He(26)-
s_He(24)) ); %HX8
    Sgen(16)=-( m_dot(19)*(s_He(19)-s_He(26)) ); %exp4


    for i=1:13
        constr(i)=T_H2(i)-T_He(2*i);%make sure the LPHe stream is always
lower T than the H2 stream
    end
    for i=1:10
        constr(i+13)=T_He(2*i-1)-T_He(2*i); %make sure the HPHe stream is >
than the LPHe stream
    end
    constr(24)=T_He(1)-T_He(3);
    constr(25)=T_He(2)-T_He(4);
    constr(26)=T_He(4)-T_He(6);
    constr(27)=T_He(5)-T_He(7);
    constr(28)=T_He(6)-T_He(8);
    constr(29)=T_He(7)-T_He(9);
    constr(30)=T_He(8)-T_He(10);
    constr(31)=T_He(10)-T_He(12);
    constr(32)=T_He(11)-T_He(13);
    constr(33)=T_He(12)-T_He(14);
    constr(34)=T_He(13)-T_He(15);
    constr(35)=T_He(14)-T_He(16);
    constr(36)=T_He(16)-T_He(18);
    constr(37)=T_He(17)-T_He(19);
    constr(38)=T_He(18)-T_He(20);
    constr(39)=T_He(20)-T_He(22);
    constr(40)=T_He(22)-T_He(24);
    constr(41)=T_He(24)-T_He(26);


    %deltaT/T constraints
    constr(42)=(T_He(1)-T_He(2))/T_He(2)-dToverT;
    constr(43)=(T_He(7)-T_He(8))/T_He(8)-dToverT;
    constr(44)=(T_He(13)-T_He(14))/T_He(14)-dToverT;
    constr(45)=(T_He(19)-T_He(20))/T_He(20)-dToverT;


    constr(46:61)=Sgen;


    % a few additional dT/T constraints for the catalysts, added 1/18/08:
    constr(62)=(T_H2(5)-T_He(10))/T_He(10)-dToverT;
```

```matlab
        constr(63)=(T_H2(8)-T_He(16))/T_He(16)-dToverT;
        constr(64)=(T_H2(11)-T_He(22))/T_He(22)-dToverT;


        constr=-constr;%everything was made to be >0 above, but the optimizer
wants constraints<0

    if nargout<1 %if the user calls the fcn from matlab, display this stuff:
        T_nice=zeros(13,3);
        eta=abs(W_ideal/(W_comp+W_comp_H2+sum(W_exp)))
        T_nice(:,1)=T_H2(1:13)';
        T_nice(:,2)=[T_He(2) T_He(4) T_He(6) T_He(8) T_He(10) T_He(12)
T_He(14) T_He(16) T_He(18) T_He(20) T_He(22) T_He(24) T_He(26)]';
        T_nice(:,3)=[T_He(1) T_He(3) T_He(5) T_He(7) T_He(9)  T_He(11)
T_He(13) T_He(15) T_He(17) T_He(19) 0          0           0      ]'
        m_dot;
        m_dot_nice
    end


    %make nice T vector to visualize system
    T_nice(:,1)=T_H2(1:13)';
    T_nice(:,2)=[T_He(2) T_He(4) T_He(6) T_He(8) T_He(10) T_He(12) T_He(14)
T_He(16) T_He(18) T_He(20) T_He(22) T_He(24) T_He(26)]';
    T_nice(:,3)=[T_He(1) T_He(3) T_He(5) T_He(7) T_He(9)  T_He(11) T_He(13)
T_He(15) T_He(17) T_He(19) 0          0           0      ]';


    y=1-abs(W_ideal/(W_comp+W_comp_H2+sum(W_exp))); %efficiency: make
negative for optimization, because MATLAB must minimize


    %      %display properties
    %
    %      s_H2'
    %      Sgen'
    %       m_dot'
    % m_dot_H2
    % para_H2'

elseif type==2
    y=constr; %this was made persistent above, so it remains in memory from
the previous iteration.
    y2=[];
end


end
```

B2. optimize.m

```
%optimize.m
%works with cycle.m to solve the system and choose optimal expander flow
%rates. The vector [x1 x2 x3 m_dot_He] is varied until the cycle reaches
%the maximum efficiency.

global H2_PRESS %make global so that optimize.m can change it
global DT_OVER_T
global COMP_EFF
global T_nice %make global so it's available in the MATLAB workspace
global m_dot_nice
%global energy

%to allow this program to set DT_OVER_T, H2_PRESS, and COMP_EFF set this to 1
variable_change=0;    %0 to set DT/T and P_H2 in cycle.m; 1 to set them in
optimize.m
plant=0;              %0 for pilot, 1 for large


%select guess values, based on previous solutions of the system:
if plant==0
    %PILOT PLANT
    startingpoint=[0.2873    0.2689    0.8076    0.2614]
    lowerbound=[.1,.1,.6,.12]
    upperbound=[.6,.6,.95,.5]
else
    %LARGE PLANT
    startingpoint=[0.15    0.3    0.76    12.3]
    lowerbound=[.01,.01,.5,10]
    upperbound=[.7,.7,.95,50]
end

options = optimset('Display','iter','TolFun',1e-
10,'TolX',.000001,'TolCon',.000001,'MaxFunEvals',2000);

%alternately, disable display at each iteration:
%options = optimset('Display','final','TolFun',1e-
10,'TolCon',.0001,'MaxFunEvals',2000);

if variable_change==0 %H2_PRESS and DT_OVER_T will be set in cycle.m, not in
this program

[x,fval]=fmincon(@(x)cycle(x,1),startingpoint,[],[],[],[],lowerbound,upperbou
nd,@(x)cycle(x,2),options);
    T_nice;
    eta=1-fval
```

```matlab
else %this program will try various values of DT_OVER_T and H2_PRESS


    %clf
    hold on
    H2_PRESS=2100;
    if plant==0
        COMP_EFF=0.65;DT_OVER_T=0.05;
    else
        COMP_EFF=0.80;DT_OVER_T=0.05;
    end

%====================PARAMETER CHANGING RUNS BELOW====================
%====================================================================
%In the following section, for loops can be used to cycle through various
%values of DT_OVER_T, COMP_EFF, and H2_PRESS. The returned "fval" for each
%iteration can be stored so that upon completion of the program, efficiency
%data is available for every combination of parameters tested.
%====================================================================
%====================================================================



%%=======================================================
%%this section will try various compressor efficiency values
%%and store the results for each trial in vector "eta_c"
%%=======================================================
%           k=1;
%           for COMP_EFF=.65:.05:.8
%
[x(k,:),fval(k,1)]=fmincon(@(x)cycle(x,1),startingpoint,[],[],[],[],lowerboun
d,upperbound,@(x)cycle(x,2),options);
%               eta_c(k,1)=1-fval(k,1);
%               k=k+1;
%           end
%%=======================================================



%%=======================================================
%%this section will try various values of DT_OVER_T.
%%Then, it will calculate the UA and x for each heat exchanger in the
%%stored system, and store them in the vector "UA". The vector is of the
%%form UA(heat_exchanger_numner,UA(col1) or x(col2),dToverT_trial_number)
%%=======================================================
%           i=1;
%
%           options = optimset('Display','iter','TolFun',1e-
6,'TolCon',.00001,'MaxFunEvals',2000);
%           for DT_OVER_T=[.05,.04,.03,.02,.01,.005,.0025]
%
%
%
```

```matlab
%
[x(i,:),fval(i)]=fmincon(@(x)cycle(x,1),startingpoint,[],[],[],[],lowerbound,
upperbound,@(x)cycle(x,2),options);
%
%                    T_loop=[T_nice(1,:);T_nice(2,:);
T_nice(3,:);T_nice(4,:);    T_nice(4,:);T_nice(5,:);
T_nice(6,:);T_nice(7,:);    T_nice(7,:);T_nice(8,:);
T_nice(9,:);T_nice(10,:);    T_nice(10,:);T_nice(11,:);
T_nice(12,:);T_nice(13,:)];
%                    m_dot_loop=[m_dot_nice(1,:);    m_dot_nice(3,:);
m_dot_nice(4,:);    m_dot_nice(6,:);  m_dot_nice(7,:);  m_dot_nice(9,:);
m_dot_nice(10,:);  m_dot_nice(12,:)];
%                    para_loop(1:3)=para(T_nice(1,1));
%                    para_loop(4:5)=para(T_nice(6,1));
%                    para_loop(6:7)=para(T_nice(9,1));
%                    para_loop(8)=para(T_nice(12,1));
%                    for j=1:8   %j corresponds to the HX number
%                        switch j
%                            case {1,2,3,4,5,6}
%
UA(j,:,i)=whatisUA(T_loop(2*j,:),T_loop(2*j-1,:),[2100 250
1500],m_dot_loop(j,:),para_loop(j));
%                            case {7,8}
%
UA(j,1,i)=whatisUA(T_loop(2*j,1:2),T_loop(2*j-1,1:2),[2100
250],m_dot_loop(j,1:2),para_loop(j));
%                        end
%                    end
%            i=i+1;
%        end
%%========================================================




%%========================================================
%%this section will try various values of COMP_EFF and DT_OVER_T.
%%It calculates the efficiency at each point (i=COMP_EFF,j=DT_OVER_T)
%%and stores it in the vector "eta_cycle(i,j)"
%%========================================================
%            i=1;
%            eta_cycle=zeros(5,7);
%
%            for COMP_EFF=.65:.05:.85
%                j=1;
%                for DT_OVER_T=[.05,.04,.03,.02,.01,.005,.0025]
%
[x,fval]=fmincon(@(x)cycle(x,1),startingpoint,[],[],[],[],lowerbound,upperbou
nd,@(x)cycle(x,2),options);
%                    eta_cycle(i,j)=1-fval;
%                    j=j+1;
%                end
%                i=i+1;
%            end
%            eta_cycle
%%========================================================
```

```matlab
%%=========================================================
%%this section will try various values of H2_PRESS.
%%It calculates the efficiency at each H2_PRESS value
%%and stores it in the vector "eta_80turbs"
%%=========================================================
%       i=1;
%       for H2_PRESS=1500:100:10000
%
[x(i,:),fval(i)]=fmincon(@(x)cycle(x,1),startingpoint,[],[],[],[],lowerbound,
upperbound,@(x)cycle(x,2),options);
%           eta_80turbs(i)=1-fval(i);
%           i=i+1;
%       end
%%=========================================================

End
```

B3. para.m

```matlab
%para.m
%calculates the equilibrium para content for particular temperature
%input temp must be in [K]

function outputpara = para(inputtemp)

%o-p equilibrium / H2 properties
%interpolated data comes from para.csv. original data is from Woolley et al.
M=csvread('para.csv');
T=M(:,1)';
para_fract=(M(:,2)')/100;
outputpara=interp1(T,para_fract,inputtemp,'linear');
```

B4. H2props.m

```matlab
function [enthalpy,entropy] = H2props(T,P,para)

%REFERENCE STATE
T_ref=300; %K
P_ref=1; %kPa

%DESIRED VALUES AT REFERENCE STATE
%first, find the difference between normal and para:
R=8.314; %J/mol-K
MW_H2=2.0159; %g/mol
RH2=R/MW_H2*1000; %J/g-K

h_np_offset_ref=(3.41607 - 3.39382)*RH2*T_ref; %J/kg (data from Hust and
Stewart)
s_np_offset_ref=(15.72626 - 14.32057)*RH2; %J/kg-K

%The para values from REFPROP are the basis. These offsets will be applied
%to the para values to find out what the values for n-H2 should be. Then,
%the normal value will be looked up in REFPROP and compared to the
%calculated value. An offset for all REFPROP-obtained n-H2 values will be
%determined by subtracting the two.

[h_para_ref,s_para_ref]=refpropm('HS','T',T_ref,'P',P_ref,'parahyd');
%[J/kg,J/kg-K]

%these are what the values of h and s at the reference state SHOULD BE:
h_normal_ref=h_para_ref+h_np_offset_ref;
s_normal_ref=s_para_ref+s_np_offset_ref;

%these are what the values of h and s at the reference state ARE, as
%they're called from REFPROP:
[h_normal_ref_RAW,s_normal_ref_RAW]=refpropm('HS','T',T_ref,'P',P_ref,'hydrog
en'); %[J/kg,J/kg-K]

%now, the h and s offsets are found by subtracting the RAW values from the
%"should be" values:
h_offset=h_normal_ref - h_normal_ref_RAW;
s_offset=s_normal_ref - s_normal_ref_RAW;

%%%%%%%%now, find the hydrogen properties at the input T,P, and para
%%%%%%%%fraction:

ortho=1-para;
[h_n,s_n]=refpropm('HS','T',T,'P',P,'hydrogen');
h_n=h_n+h_offset;
s_n=s_n+s_offset;
[h_p,s_p]=refpropm('HS','T',T,'P',P,'parahyd');
```

```
enthalpy=h_p*(para-ortho/3) + 4/3*ortho*h_n;
entropy=s_p*(para-ortho/3) + 4/3*ortho*(s_n-RH2*0.562336) -
RH2*(ortho*log(ortho) + para*log(para));
```

B5. expander.m

```matlab
function T_final=expander(eta,P_LP,P_HP,T,direction)
%direction=0 ---> top down --->  T_in input, solves for T_out
%direction=1 ---> bottom up ---> T_out input, solves for T_in

if direction==0 %top down
    [h_in s_in]=refpropm('HS','T',T,'P',P_HP,'helium');
    h_out_ideal=refpropm('H','P',P_LP,'S',s_in,'helium');
    h_out=h_in-eta*(h_in-h_out_ideal);
    T_final=refpropm('T','P',P_LP,'H',h_out,'helium');

else %bottom up
    h_out=refpropm('H','T',T,'P',P_LP,'helium');
    T_guess=T/eta;
    fsolve_options=optimset('display','off');
    T_final=fsolve(@expander_eqs,T_guess,fsolve_options);
end

    function F=expander_eqs(T_final)
    [h_in s_in]=refpropm('HS','T',T_final,'P',P_HP,'helium');
    h_out_ideal=refpropm('H','P',P_LP,'S',s_in,'helium');
    F=(h_in-h_out)-eta*(h_in-h_out_ideal);
    end

end
```

B6. HXode.m

```matlab
function T_f=HXode(UA,m_dot,T,P,para_H2,type);

%INPUT SYNTAX:
%type=1 ---> two way HX, solving from top down.
%type=3 ---> three way HX, solving from top down.
%UA=[UA_total, fraction_H2 (if three way)]
%m_dot=[m_dot_H2,m_dot_HeLP,m_dot_HeHP(if three way)]
%T=[T_H2_start,T_HeLP_start,T_HeHP_start(if three way)]
%P=[P_H2_start,T_HeLP_start,T_HeHP_start(if three way)]
%para_H2=x_para_H2

UA_init=UA;
if length(UA)>1 %test if it is a 3-pass HX
    fract_H2=UA(2);
    UA=UA(1);
end
m_dot_H2=m_dot(1);
m_dot_HeLP=m_dot(2);
T_H2=T(1);
T_HeLP=T(2);
P_H2=P(1);
P_HeLP=P(2);
if type==3||type==4 %test if it is a 3-pass HX
    m_dot_HeHP=m_dot(3);
    T_HeHP=T(3);
    P_HeHP=P(3);
end

switch type
    case 1 %2-pass, top down
        posneg=1;
        options=odeset('Initialstep',1,'MaxStep',2000,'OutputFcn',@odeplot);
        [UA,T]=ode45(@odefun,[0,UA],[T_H2,T_HeLP],options);
    case 2 %2-pass, bottom up
        posneg=-1;
        [UA,T]=ode45(@odefun,[0,UA],[T_H2,T_HeLP]);
    case 3 %3-pass, top down
        posneg=1;
        %-------PLOT ON-------%

options=odeset('Initialstep',1,'MaxStep',2000,'OutputFcn',@odeplot,'Events',@
events);
        %options=odeset('Initialstep',1,'MaxStep',200000,'Events',@events);
        [UA,T]=ode45(@odefun3way,[0,UA],[T_H2,T_HeLP,T_HeHP],options);
        %--------------------%

        %-------PLOT OFF------%
        %[UA,T]=ode45(@odefun3way,[0,UA],[T_H2,T_HeLP,T_HeHP]);
        %--------------------%
```

```matlab
    case 4 %3-pass, bottom up
        posneg=-1;
        %-------PLOT ON-------%

options=odeset('Initialstep',1,'MaxStep',200,'OutputFcn',@odeplot,'Events',@events);
        [UA,T]=ode45(@odefun3way,[0,UA],[T_H2,T_HeLP,T_HeHP],options);
        %--------------------%

        %-------PLOT OFF------%
        %[UA,T]=ode45(@odefun3way,[0,UA],[T_H2,T_HeLP,T_HeHP]);
        %--------------------%

        % UA_tot=UA(end);
    otherwise
        disp('invalid type')

end


if type==4 && UA(end)<UA_init(1)
    %the ODE solver didn't complete
    posneg=1; %change to top-down solving
    if T_H2<50
        T_top_guess=[75 72 75];
        T_max=80;
        T_min=70;
        A_eq=[1 0 -1;0 0 0;0 0 0];
        b_eq=[0;0;0];
        bbb=1
    elseif T_H2<80
        T_top_guess=[115 112 124];
        T_max=125;
        T_min=114;
        aaa=1
        A_eq=[];
        b_eq=[];
    end
    options=optimset('TypicalX',T_top_guess);
    T_top=fmincon(@temp_error,T_top_guess,[],[],A_eq,b_eq,[T_min T_min T_min],[T_max T_max T_max],@mycon)
end


if type==4 & posneg==1
    %the solver used the top-down shooting method
    T_f=T_top;
else
    T_f=T(end,:);
end
%plot(posneg*UA,T)  %this enables plotting if it is uncommented
```

```matlab
%----------------END OF MAIN PROGRAM-------------------%
%---------------SUBFUNCTIONS BELOW--------------------%


%---------------2 way HX, ODE function----------------%
    function dT=odefun(UA_loc,T) %ode function for dT. Each row of T is of
the form: [T_H2,T_HeLP]
        dT=zeros(2,1);
        c_p_H2=c_p_H2mix(T(1),P_H2,para_H2); %T(1) is the H2 temp, at this
step
        c_p_HeLP=refpropm('C','T',T(2),'P',P_HeLP,'helium'); %T(2) is the LP
He temp, at this step
        dT(1)=posneg*(-(T(1)-T(2))*(1/m_dot_H2/c_p_H2));
        dT(2)=m_dot_H2*c_p_H2/m_dot_HeLP/c_p_HeLP*dT(1);
    end
%----------------------------------------------------%


%-------------3 way HX ode function-------------------%
    function dT=odefun3way(UA_loc,T)
        dT=zeros(3,1);
        c_p_H2=c_p_H2mix(T(1),P_H2,para_H2);
        c_p_HeLP=refpropm('C','T',T(2),'P',P_HeLP,'helium');
        c_p_HeHP=refpropm('C','T',T(3),'P',P_HeHP,'helium');
        b=[0;(T(1)-T(2))*fract_H2/m_dot_H2/c_p_H2;(T(3)-T(2))*(1-
fract_H2)/m_dot_HeHP/c_p_HeHP];
        A=[m_dot_H2*c_p_H2, -m_dot_HeLP*c_p_HeLP, m_dot_HeHP*c_p_HeHP;-
posneg,0,0;0,0,-posneg];
        dT=A\b;
    end
%----------------------------------------------------%


%--events function. kills the ODE program if temps cross or if temps get
%--too high or low----------------------------------------------------%
    function [value,isterminal,direction] = events(UA_loc,T)
        if min(T)<20 || max(T)>400 || min(T(1),T(3))<T(2) || T(1)<25 ||
T(2)<18
            %something bad happened - temps outside min/max, or temps
            %crossed middle stream resulting in 2nd law violation
            value=0;
            %stop the ODE solver
        else
            value=1;
            %let the ODE solver keep running
        end
        isterminal=1;
        direction=0;
    end
%----------------------------------------------------------------------%



%---------error calculator for top-down shooting method----------------%
    function errors=temp_error(T_top)
```

```matlab
        %if min(top_temps)<min([T_H2 T_HeLP T_HeHP]) || max(top_temps)>300 ||
min(top_temps(end,1),top_temps(end,3))<top_temps(end,2)
        %    errors=1000
        %else
        clear UA T;

options=odeset('Initialstep',1,'MaxStep',2000,'OutputFcn',@odeplot,'Events',@
events,'NonNegative',[1 1 1]);
        [UA,T]=ode45(@odefun3way,[0,UA_init(1)],T_top,options);

        errors=sum((T(end,:)-[T_H2 T_HeLP T_HeHP]).^2)
        %end

        %this nested subfunction is just a copy of the one above. It's here
        %because the ODE solver is run inside this function
        function [value,isterminal,direction] = events(UA_loc,T)
            if min(T)<20 || max(T)>400 || min(T(1),T(3))<T(2) || T(1)<25 ||
T(2)<18
                value=0;
            else
                value=1;
            end
            isterminal=1;
            direction=0;

        end
    end
%-----------------------------------------------------------------------%

    function [c ceq] = mycon(T_top)
        %nonlinear constraints for fmincon

        %inequality constraints c<=0
        c=[T_top(2)-T_top(1);T_top(2)-T_top(3)];

        %equality constraints ceq=0
        ceq=[UA(end)-UA_init(1)];
    end

%------------hydrogen C_p calculator-------------------%
    function cph2=c_p_H2mix(temp,press,para) %this gives a convenient way of
calculating the cp for the H2 mixture.
        c_p_p=refpropm('C','T',temp,'P',press,'parahyd'); %J/kg-K
        c_p_n=refpropm('C','T',temp,'P',press,'hydrogen'); %J/kg-K
        cph2=c_p_p*(para-(1-para)/3) + 4/3*(1-para)*c_p_n;
    end
%---------------------------------------------------%

end
```

B7. whatisUA.m

```matlab
function UA=whatisUA(T_bottom,T_top,P,m_dot,para_H2)



%this function will estimate the UA for a heat exchanger, based on
%endpoint temperatures
%T_bottom: [T_H2_bottom T_He_LP_bottom T_He_HP_bottom (if 3way)
%T_top: similar
%m_dot: [m_dot_H2 m_dot_He_LP m_dot_He_HP (if 3way)]
% whatisUA([20 19.05],[33 29.01],[2100 250],[.005787 .0193],.9515)


%%%%%%%%%%%%%%auto guess generator section %%%%%%%%%%%%%%%%%%%%%%%%
if length(T_bottom)==2 %two way HX
    %make a quick guess at UA using the LMTD method:
    T_avg=(T_bottom(2)+T_top(2))/2;
    c_p_He=refpropm('C','T',T_avg,'P',P(2),'helium');
    UA_guess=m_dot(2)*c_p_He*(T_top(2)-T_bottom(2))/( ((T_top(1)-T_top(2))-
(T_bottom(1)-T_bottom(2))) / log((T_top(1)-T_top(2))/(T_bottom(1)-
T_bottom(2)))        )
elseif length(T_bottom)==3 %three way HX
    T_avg_H2=(T_bottom(1)+T_top(1))/2;
    T_avg_HeHP=(T_bottom(3)+T_top(3))/2;
    c_p_H2=c_p_H2mix(T_avg_H2,P(1),para_H2);
    c_p_HeHP=refpropm('C','T',T_avg_HeHP,'P',P(3),'helium');
    UA_H2_LPHe=m_dot(1)*c_p_H2*(T_top(1)-T_bottom(1))/( ((T_top(1)-T_top(2))-
(T_bottom(1)-T_bottom(2))) / log((T_top(1)-T_top(2))/(T_bottom(1)-
T_bottom(2))) );
    UA_HPHe_LPHe=m_dot(3)*c_p_HeHP*(T_top(3)-T_bottom(3))/( ((T_top(3)-
T_top(2))-(T_bottom(3)-T_bottom(2))) / log((T_top(3)-T_top(2))/(T_bottom(3)-
T_bottom(2))) );
    UA_guess(1)=UA_H2_LPHe+UA_HPHe_LPHe;
    UA_guess(2)=UA_H2_LPHe/UA_guess(1)
end
%%%%%%%%%%%%%%%%%%%%%%%%%%%%%%%%%%%%%%%%%%%%%%%%%%%%%%%%%%%%%%%%%%%

%%%%manually enter guess here, if auto guess generator fails%%%%
%UA_guess=[3600,.4]

%%%%%%%%%%%%%%%%%%%%%%%%%%%%%%%%%%%%%%%%%%%%%%%%%%%%%%%%%%%%%%%%%%%

if length(T_bottom)==3
    options=optimset('Display','iter','TolFun',.001,'TolX',10);
    UA=fminsearch(@temp_error,UA_guess,options);
else

    options=optimset('Display','iter');
    UA=fminsearch(@temp_error_2st,UA_guess,options);
end


    function errors=temp_error_2st(UA)
```

```matlab
        if UA<=0
            errors=100
        else
            top_temps=HXode(UA,m_dot,T_bottom,P,para_H2,2);
            errors=sum((T_top-top_temps).^2);
        end
    end

%%%%%%%%%%%%%%%solve from top down%%%%%%%%%%%
    function errors=temp_error(UA)
        if UA(1,2)>=1||UA(1,2)<=0
            errors=100;
        else
            bottom_temps=HXode(UA,m_dot,T_top,P,para_H2,3);
            %UA   %this can be uncommented to show the UA at each step
            errors=sum((T_bottom-bottom_temps).^2);
        end
    end

    function cph2=c_p_H2mix(temp,press,para) %this gives a convenient way of
calculating the cp for the H2 mixture.
        if temp<18
            cph2=0
        else
            c_p_p=refpropm('C','T',temp,'P',press,'parahyd'); %J/kg-K
            c_p_n=refpropm('C','T',temp,'P',press,'hydrogen'); %J/kg-K
            cph2=c_p_p*(para-(1-para)/3) + 4/3*(1-para)*c_p_n;
        end
    end
end
```

B8. wet_expander_performance.m

```matlab
%this program is used to determine the relationship between the efficiency
%and the inlet temperature for a liquid hydrogen "single-phase wet
%expander." The high and low H2 pressures and the desired low H2
%temperature (this must be liquid) are entered.
function a=wet_expander_performance(b) %a and b are dummy variables, because
this function has nested functions and MATLAB requires a top-level function
for this.
P_H2_high=1800; %kPa
P_H2_low=100; %kPa. This is the storage tank pressure
T_H2_low=20; %K. This must be a subcooled or saturated liquid
para_H2_low=.951; %parahydrogen content of liquid

[h_H2_low s_H2_low]=H2props(T_H2_low,P_H2_low,para_H2_low);

%find inlet temp for an isentropic process, i.e. a 100% efficient expander
hs=0;
s_100=s_H2_low;
fsolve_options=optimset('display','off');
T_100=fsolve(@eqns_that_equal_zero,T_H2_low,fsolve_options);
h_100=h_in;

%find inlet temp for a constant h process, i.e. a 0% efficient expander
hs=1;
h_0=h_H2_low;
T_0=fsolve(@eqns_that_equal_zero,T_H2_low,fsolve_options);
s_0=s_in;

%now, divide the temperature difference T_100-T_0 into increments
T=linspace(T_0,T_100,100);

%find the efficiency at each point
for i=1:length(T)
[h(i) s(i)]=H2props(T(i),P_H2_high,para_H2_low);
eta(i)=(h(i)-h_H2_low)/(h_100-h_H2_low);
end
clf
plot(eta,T)
xlabel 'Wet Expander Efficiency [-]'
ylabel 'Inlet Temperature [K]'

%---FIT CURVE---%
xdata=eta;
ydata=T;
[estimates,model]=fitcurvedemo(xdata,ydata);
disp 'curve fit: y=Ax^2+Bx+C (T_in=A*eta^2+B*eta+C) estimates=[A,B,C]'
estimates
hold on
[sse,FittedCurve]=model(estimates);
%plot(eta,FittedCurve,'r--')
```

```matlab
function F=eqns_that_equal_zero(T_in)
    [h_in,s_in]=H2props(T_in,P_H2_high,para_H2_low);
    if hs==0
        F=s_100-s_in;
    elseif hs==1
        F=h_0-h_in;
    end
end

function [estimates, model] = fitcurvedemo(xdata, ydata)
% Call fminsearch with a random starting point.
start_point = rand(1, 3);
model = @parabfun;
estimates = fminsearch(model, start_point);
% parabfun accepts curve parameters as inputs, and outputs sse,
% the sum of squares error for A .* xdata.^2 + B.*xdata + C - ydata,
% and the FittedCurve. FMINSEARCH only needs sse, but we want to
% plot the FittedCurve at the end.
    function [sse, FittedCurve] = parabfun(params)
        A = params(1);
        B = params(2);
        C = params(3);
        FittedCurve = A .* xdata.^2 + B.*xdata + C;
        ErrorVector = FittedCurve - ydata;
        sse = sum(ErrorVector .^ 2);
    end
end

end
```